Review of photo(electro)catalytic multi-metallic layered double hydroxides

Chenjun Ning[a], Sha Bai[a], Jikang Wang[a], Zixian Li[a], Zhiyue Han[c], Yufei Zhao[a,*], Dermot O'Hare[b,*], Yu-Fei Song[a,*]

[a]*State Key Laboratory of Chemical Resource Engineering, Beijing Advanced Innovation Center for Soft Matter Science and Engineering, Beijing University of Chemical Technology, Beijing 100029 P. R. China.*

[b]*Chemistry Research Laboratory, Department of Chemistry, University of Oxford, Mansfield Road, Oxford OX1 3TA, United Kingdom*

[c] *State Key Laboratory of Explosion Science and Technology, Beijing Institute of Technology, Beijing, China.*

ABSTRACT

The development of efficient photo(electro)catalysis using sustainable renewable resources to prepare high value-added products is now a major goal to achieve new environmentally friendly technologies. However, existing solutions still offer unsatisfied catalytic efficiency and low energy

Abbreviations: 2D, two-dimensional; 3D, three-dimensional; MOFs, metal organic frameworks; COFs, covalent organic frameworks; LDHs, layered double hydroxides; SA, single atom; NP, nanoparticle; CO_2, carbon dioxide; CO_2ER, carbon dioxide reduction reaction; CORR, carbon monoxide reduction reaction; SACs, single-atom catalysts; OER, oxygen evolution reaction; HER, hydrogen evolution reaction; HMFOR, 5-hydroxymethylfurfural oxidation reaction; ORR, oxygen reduction reaction; HzOR, hydrazine oxidation reaction; CO_2PR, carbon dioxide photocatalytic reduction; MMCT, metal-to-metal charge-transfer; XPS, X-ray photoelectron spectroscopy; XAS, X-ray absorption spectroscopy; XANES, X-ray absorption near edge spectrum; FT-EXAFS, Fourier transform-extended X-ray absorption fine structure; EPR, electron paramagnetic resonance; DFT, density functional theory; UV, ultraviolet; WT, wavelet transform; SEM, scanning electron microscopy; TEM, transmission electron microscopy; 1D, one-dimensional; XRD, X-ray diffraction; HRTEM, high resolution transmission electron microscope; SEAD, selected area electron diffraction; LSV, linear sweep voltammetry; ESR, electron spin resonance; XAFS, X-ray absorption fine structure; PDOS, partial density of states; TON, turnover number; TPR, temperature programmed reduction; MMO, mixed metal oxide; LSHs, layered single metal hydroxides; LMHs, layered metal hydroxides; HEHs, high-entropy hydrotalcites; HEOs, high-entropy oxides; HAADF-STEM, high angle annular dark field scanning transmission electron microscope; EDX, energy dispersive X-ray spectrometer; UTF, ultrathin film; Fe-PP, iron porphyrin; LBL, layer-by-layer; CDs, carbon dots; RTP, room-temperature phosphorescent; TDOS, total density of states; FDCA, 2,5-furandicarboxylic acid; AFM, atomic force microscopy; Eg, band gap energy; SCs, fiber supercapacitors; UPS, ultraviolet photoelectron spectroscopy; CV, cyclic voltammetry; NIR, near-infrared; FT, Fischer–Tropsch; FTIR, Fourier transform infrared spectroscopy; UV-vis, ultraviolet–visible spectroscopy; M-O-M, metal–oxo–metal; PP, pyrophosphate; TPP, triphosphate; SSMS, ultra-stable mineralization structure; ICG, indocyanine green; DOX, doxorubicin hydrochloride; NCs, nanoclusters; PDT, photodynamic therapy; QY, quantum yield; MRI, magnetic resonance imaging; CAs, contrast agents; LMMH, layered multi-metallic hydroxides.

*Corresponding author. Tel.: +86-10-64431832.

Email address: zhaoyufei@mail.buct.edu.cn (Y. Zhao), dermot.ohare@chem.ox.ac.uk and songyf@mail.buct.edu.cn (Y.-F. Song).

utilization. Therefore, it is paramount to develop new strategies to control the morphology and structure of functional materials to improve their photo(electro)catalytic activity. Layered double hydroxides (LDHs), as a kind of two-dimensional (2D) materials, have been largely explored in photo(electro)catalytic reactions due to their extensive tenability of elemental composition and interlayered anions. Furthermore, the intrinsic feature of atomic dispersion has been utilized to introduce more active sites to further improve the reaction performance. Herein, we review strategies that have been developed for introducing more active sites into or onto the LDH layer for the construction of multi-metallic LDHs based photo(electro)catalytic material. The accompanied structure and electronic changes that are pivotal for modulation for catalytic activity are proposed, such as, improving carrier transportation, and optimizing molecular activation energy. We review the catalytic performance of multi-metallic LDHs for photo(electro)catalytic water splitting, CO_2 photoreduction, CO hydrogenation, heavy metal mineralization/reutilization and beyond. We highlight future challenges and opportunities to design multi-metallic LDHs to address future photo(electro)catalysis research challenges.

Keywords: multi-metallic layered double hydroxides; structural regulation, water splitting, CO_2 reduction, heavy metal mineralization

Contents

1. Introduction

The continuous development in societal life styles and the rapid growth of the global population insures ever increasing demands that inevitably lead to energy and resource shortcomings and environmental pollution. We urgently need sustainable developments and environment-friendly strategies to alleviate this situation. By taking advantage of sustainable renewable energy (wind energy, tidal energy, solar energy), photo(electro)catalysis has the potential to convert water and greenhouse gases into hydrogen and other high value-added products (important industrial raw materials for chemicals production). And these issues existing in catalytic activity of current photo(electro)catalysis (such as low conversion, poor energy utilization, and low selectivity) are urgently required to be solved [1-4]. Since the discovery of graphene in 2004, the exploration and application of ultra-thin two-dimensional (2D) nanomaterials has become more and more extensive [5, 6]. In comparison with conventional traditional three-dimensional (3D) materials, 2D materials are widely applied in the field of energy storage and transformation. The unique features of 2D materials, geometric and electronic properties with the super large specific surface and the highly exposed coordination unsaturated sites make them excellent candidates for developing novel catalysts and processes [7, 8]. Furthermore, 2D materials are ideal model catalysts for understanding the real active site and surface reaction mechanism through combining theoretical calculation chemistry and surface science technology [6]. At the same time, researchers have been developing additional approaches such as surface modification and/or doping in order to introduce more active sites and construct more defective structures, thereby bringing about effective enhancements to their inherent characteristics [9]. Today, 2D materials are highly various, including metals, oxides, halides, nitrides, carbides, hydroxides, hydrides, MXenes, metal organic frameworks (MOFs), covalent organic frameworks (COFs), polymers, black phosphorus, silicene, antimonene, and perovskites [10, 11]. Therefore, it would be a significant step forward to develop structure-activity relationships for controllable catalytic active sites on 2D materials for the photo(electro)catalysis.

Among 2D materials, the commonly used formula of layered double hydroxides (LDHs) is $[M_{1-x}^{2+}M_x^{3+}(OH)_2]^{x+}(A^{n-})_{x/n}\cdot mH_2O$, where the M^{2+} are normally Mg^{2+}, Co^{2+}, Ni^{2+}, etc. and the M^{3+} are typically Al^{3+}, V^{3+}, Cr^{3+}, Fe^{3+} in $M(OH)_6$ octahedral coordination. The A^{n-} is the intercalated anion such as NO_3^- and SO_4^{2-}, CO_3^{2-}. The most common MgAl-LDH that based on "double metals" have been widely explored, since it was artificially synthesized for the first time in 1942 which was followed by the confirmation of crystal structure of single-crystalline MgAl-LDH in 1969 [12, 13]. The wide tunability of the nature of either the metal M^{2+} and M^{3+} cations, their molar ratios and the nature of interlayered anions has prompted them to be extensively studied [14-18]. In recent years, researchers have found that the pristine binary (two metal cations) LDHs can be easily transformed into ternary LDHs or multi-metallic LDHs *via* incorporating other metal atoms into the layers, thus

causing the generation of more active sites and modulation of electronic or morphology structure, to further facilitate the catalytic activity [19, 20]. What's more, researchers also tried to adjust the introduction form of the other elements by changing the synthesis method and route to purposefully achieve the structure modulation of multi-metallic LDHs, so as to expect the improvement of catalytic performance.

In this review, we summarize the most recent development in the ingenious design, synthesis, and characterization of multi-metallic LDHs structure and derivatives as catalysts (Scheme 1) in the field of various photo(electro)catalytic reaction systems (Figure 1), such as water oxidation, hydrogen evolution, CO_2 reduction, nitrogen fixation, organic syntheses, and pollutants removal, etc. (Table 1). What's more, the structure-function relationship between multi-metallic LDHs and catalytic reactions are highlighted, which provides valuable visions for the exploration of robust and promising catalysts on LDHs based materials. In addition, we also put forward some prospects about the application of multi-metallic LDHs and derivatives in catalysis and heavy metal mineralization/reutilization as well as photothermal cancer treatment.

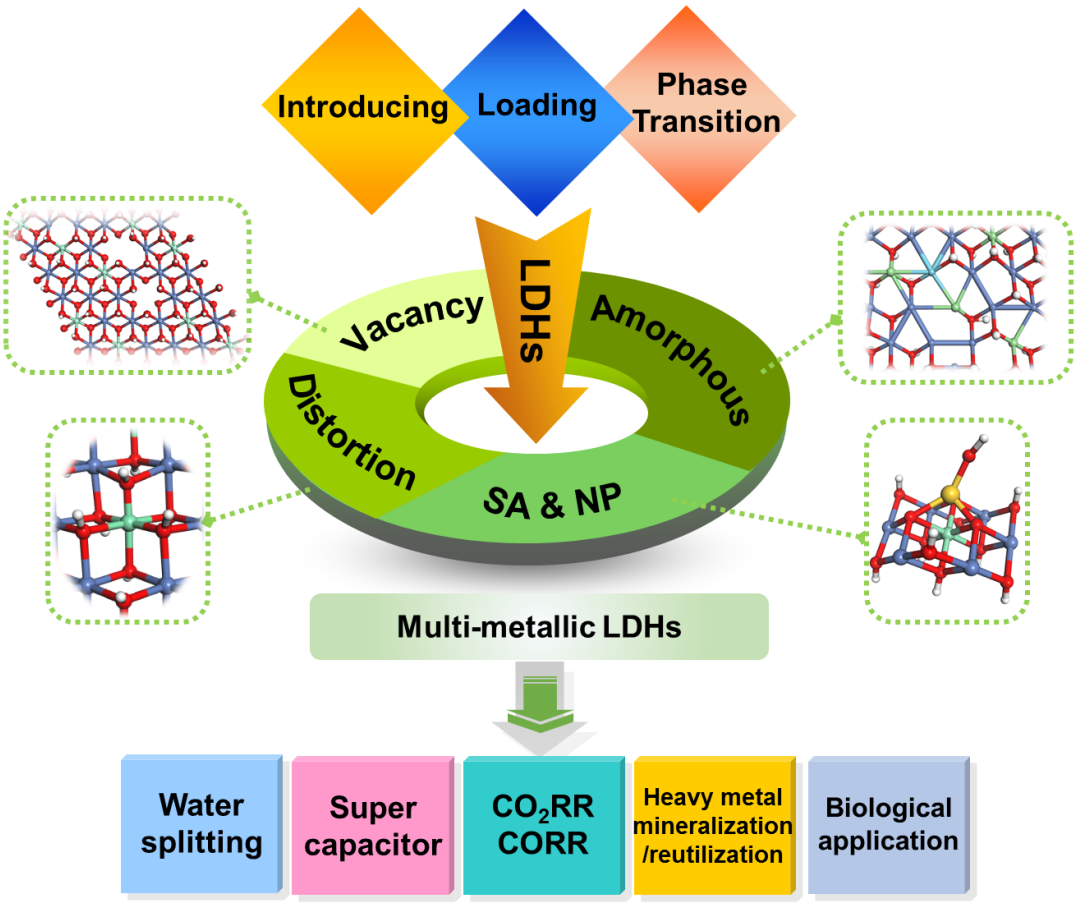

Scheme 1. Design and development of multi-metallic LDHs for various application.

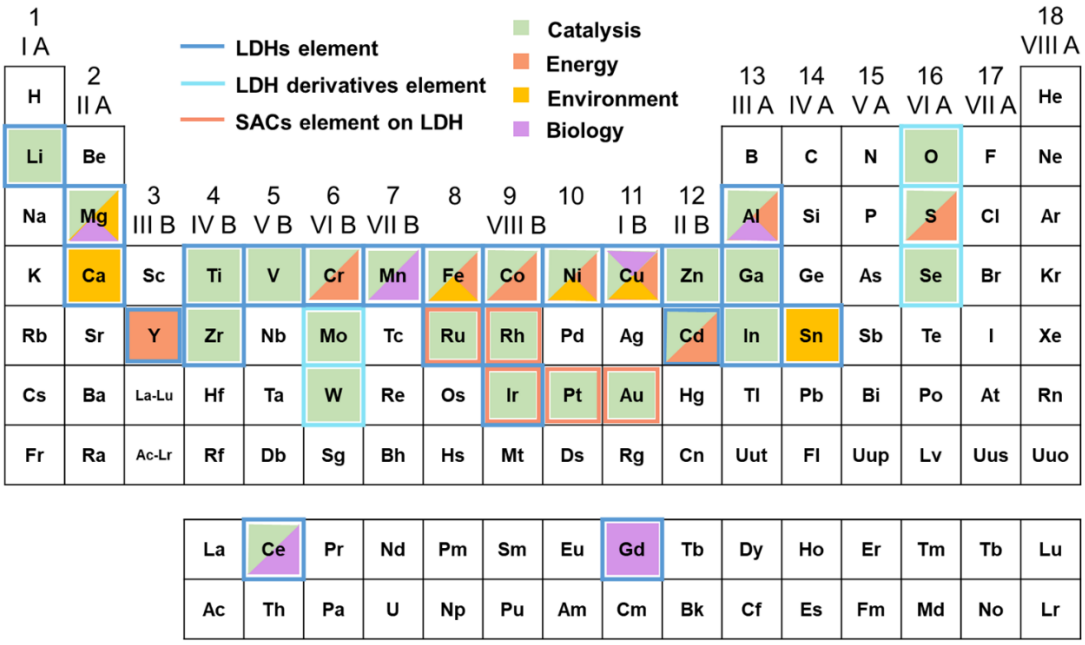

Figure 1. Review of the element composition reported for multi-metallic LDHs and their various catalytic applications and beyond.

	V	NiFeV-LDH	OER	Overpotential 264 mV vs 327 mV (100 mA·cm^{-2})	[23] (2018)
			OER	Overpotential 231 mV vs 278 mV (100 mA·cm^{-2})	[24] (2018)
	Cr	NiFeCr-LDH	OER	Overpotential 280 mV vs 322 mV (10 mA·cm^{-2})	[25] (2018)
			OER	Overpotential 202 mV vs 287 mV (10 mA·cm^{-2})	[26] (2020)
	Mn	NiFeMn-LDH	OER	Overpotential 230 mV vs 335 mV (100 mA·cm^{-2})	[27] (2018)
	Fe	NiFeFe-LDH	OER	Overpotential 249 mV vs 328 mV (100 mA·cm^{-2})	[19] (2018)
NiFe-LDH	Co	NiFeCo-LDH	OER	Overpotential 288 mV vs 303 mV (10 mA·cm^{-2})	[28] (2020)
			HMFOR	Overpotential 300 mV vs 330 mV (10 mA·cm^{-2})	[28] (2020)
			ORR and OER	Overvoltage differences 0.769 V vs 0.840 V	[29] (2017)
	Cu	NiFeCu hydr(oxy)oxide	OER	Overpotential 224 mV vs 266 mV (10 mA·cm^{-2})	[30] (2019)
	Zn	NiFeZn-LDH	OER	Overpotential 200 mV vs 240 mV (20 mA·cm^{-2})	[22] (2018)
	Se	NiFeSe-derived oxide	OER	Overpotential 195 mV vs 244 mV (10 mA·cm^{-2})	[31] (2016)
	Zr	NiFeZr-LDH	OER	Overpotential 257 mV vs 330 mV (100 mA·cm^{-2})	[32] (2019)
	Ru	Ru/NiFe-LDH	HzOR	Potential 1.26 V vs 1.36 V (10 mA·cm^{-2})	[33] (2019)
		NiFeRu-LDH	HER	Overpotential 29 mV vs 269 mV (10 mA·cm^{-2})	[34] (2018)
	Rh	Rh/NiFe-LDH	HzOR	Potential 1.38 V vs 1.46 V (10 mA·cm^{-2})	[35] (2021)
	W	NiFeW-LDH	OER	Overpotential 230 mV vs 255 mV (50 mA·cm^{-2})	[36] (2020)
	Ir	NiFeIr-LDH	HER	Overpotential 34 mV vs 273 mV (10 mA·cm^{-2})	[37] (2018)
	Au	Au/NiFe-LDH	OER	Overpotential 237 mV vs 263 mV (10 mA·cm^{-2})	[38] (2018)
CoFe-LDH	Ni	CoFeNi-LDH	CO_2PR	CH_4 78.9%, H_2 1.7% vs CH_4 0%, H_2 30.5% (λ > 500 nm)	[39] (2020)
	Ru	Ru/CoFe-LDH	OER	Overpotential 198 mV vs 310 mV (10 mA·cm^{-2})	[40] (2019)
	W	CoFeW oxyhydroxide	OER	Overpotential 191 mV vs 279 mV (10 mA·cm^{-2})	[41] (2016)
	Ce	CoFeCe-LDH	HER	Overpotential 73 mV vs 194 mV (10 mA·cm^{-2})	[42] (2020)
MgFe-LDH	Ca	CaMgFe-LDH	Soil adsorption	Removal efficiency 72.5% vs 58.2%	[43] (2017)
CaFe-LDH	Ni	NiCaFe-LDH	CO_2PR	CH_4 31.7%, CO 40.5%, H_2 27.8% vs CH_4 0%, CO 14.7%, H_2	[44] (2021)

CoAl-LDH	Mg	CoMgAl-LDH	CO_2PR	TOF(CO) 11.57 h^{-1} vs 3.4 h^{-1}	[53] (2021)
	S	CoAlS hydroxysulfide	OER	Overpotential 414 mV vs 590 V (10 mA·cm^{-2})	[54] (2017)
	Cu	CoCuAl-LDH	ethylbenzene selective oxidation	Conversion 96.8%, selectivity to acetophenone (95.4%)	[55] (2016)
ZnAl-LDH	Ru	ZnAlRu-LDH	OER	Overpotential 245 mV vs 670 mV (10 mA·cm^{-2})	[56] (2020)
	Ir	ZnAlIr-LDH	OER	Overpotential 345 mV vs 670 mV (10 mA·cm^{-2})	[56] (2020)
	Cu	CuZnAl-LDH	Photocatalytic nitrogen fixation	ammonia production rate 110 μmol g^{-1} h^{-1} vs 17.1μmol g^{-1} h^{-1}	[57] (2020)
	Au	Au/ZnAl−LDH	Hydrogenation	Crotonyl alcohol selectivity 96.0% vs 43.6%	[58] (2018)
	Zr	ZnAlZr-LDH	ethyl levulinate Hydrogenation	Valerolactone formation rate 326 vs 149 (μmol g^{-1} min^{-1}), conversion 49% vs 24%	[59] (2017)
	Ru	Ru/ZnAl-LDH	ethyl levulinate Hydrogenation	Valerolactone formation rate 655 vs 149 (μmol g^{-1} min^{-1}), conversion 78% vs 24%	[59] (2017)
MgAl-LDH	Mn	MgMnAl-LDH	ethylbenzene	Conversion 50.3% vs 0.4%	[60] (2007)
	Ru	Ru/MgAl-LDH	R-alkylation of various nitriles with	α-Ethylated phenylacetonitrile yield 98%	[61] (2004)
	Ru	Ru/MgAl-LDH	CO_2 hydrogenation	turnover frequency (TOF) 19 h^{-1}	[62] (2017)
CoCr-LDH	Ru	CoCrRu LDH	OER	Overpotential 290 mV vs 340 mV (10 mA·cm^{-2})	[63] (2020)
ZnCr-LDH	Au	Au/ZnCr–LDH	Degradation	Removal efficiency 83.6% vs 40.9%	[64] (2018)

2. Strategies for structural regulation

The most reported LDH contain M^{2+} and M^{3+} cations, like Mg^{2+}, Al^{3+}, etc. Besides, metal ions can also be Li^{+}, Ti^{4+}, Zr^{4+}, or Sn^{4+} etc. for some specific LDH such as LiAl-LDH. By changing the combination and ratios of these elements, a range of physical/chemical reactivity can be explored to further modulate the catalytic activity. However, the tunable composition space available using only two elements severely limits the potential to introduce more active sites and induce higher catalytic activity. Furthermore, synergistic effects between multiple metal centers could facilitate the catalytic activity through the interactive mechanisms and/or even changes in morphology and microstructure.

2.1 Introduction of the third metal cation into LDHs

2.1.1 Valence regulation of multiple metal ions in LDHs

It has been deeply exploration that Ni or Fe with high valence in NiFe-based electrocatalysts could be favorable to catalytic performance on oxygen evolution reaction (OER) [65, 66]. The controllability of metal cation composition of LDHs could ensure the existence of metal-to-metal charge-transfer (MMCT) mechanism [67, 68] during reactions. The introduction of other variable valence transition metal cations in order to modify the electronic structure and chemical environment of atoms on the layer has become a common strategy for improving the performance for many catalytic chemistries [25, 32, 46, 69-72].

For instance, the surface electronic structure of LDHs can be modified by introducing Mn^{2+} into NiFe-LDH structure in order to boost OER performance [27]. According to a Bader charge analysis from theoretical calculations, electric charge of Ni^{2+} and Fe^{3+} sites increased after Mn^{2+} incorporating compared with that in pristine NiFe-LDH (Figure 2a). The X-ray photoelectron spectroscopy (XPS) data revealed a negative shift for the Ni 2p and Fe 2p binding energies for NiFeMn-LDH, this was also accompanied by an increase in the valence state of Mn from +2 to +4, supporting the prediction from calculations for electron transfer from Mn^{2+} to neighboring Ni^{2+} and Fe^{3+} sites of NiFeMn-LDH (Figure 2b). The introduction of partially reduced Ni^{2+} and Fe^{3+} sites appeared to facilitate significantly improvement water oxidation performance.

Atom doping can significantly affect the electronic structure, but it can also facilitate activation of intermediates and boost catalytic performance. Electronic structure modification using doping of V^{3+} into the NiFe-LDH forming NiFeV-LDH reduced the onset potential for efficient electrocatalytic water oxidation [20]. The XPS spectra (Figure 2c), indicated there was no change to the Ni^{2+}, whereas the binding energy of the Fe^{3+} decreased after doping and the V^{3+} was observed to be partially oxidized to V^{4+} and V^{5+}. In this case, theory and experiment results demonstrated that OER kinetics could be improved via V^{3+} introduction, contributing to the improvement in electrical conductivity and electrocatalytic activity (Figure 2d) [24].

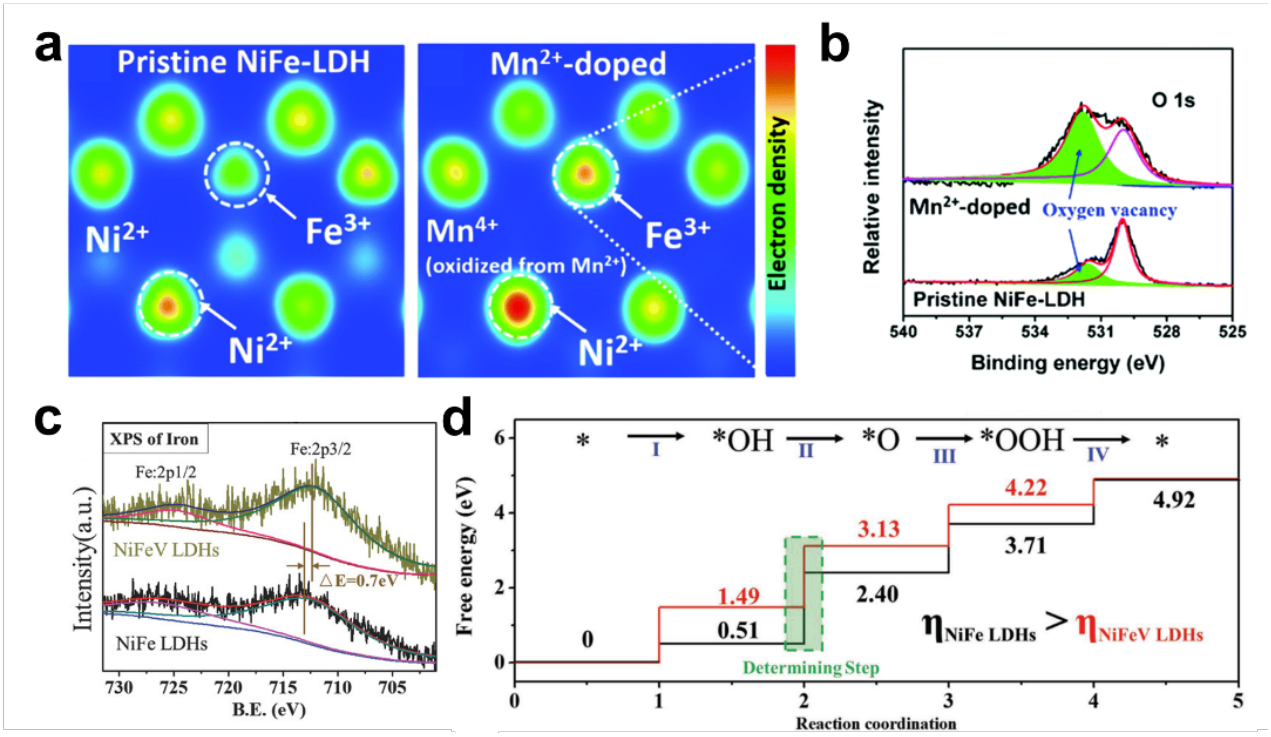

Figure 2. a) Theoretical calculations for the electron density in NiFe-LDH and NiFeMn-LDH, b) O 1S XPS region for NiFe-LDH and N_xFeMn-LDH. Reprinted with permission from [20]. Copyright 2018, Wiley-VCH. c) Fe 2p XPS of NiFe-LDH and NiFeV-LDH, d) Gibbs free energy diagram for OER for NiFe-LDH and NiFeV-LDH. Reprinted with permission from [27]. Copyright 2018, Royal Society of Chemistry.

Introducing heteroatoms also creates new interactions with surrounding atoms. For example, partial substitution of Ni^{2+} with Fe^{2+} introduces new Fe-O-Fe moiety (Figure 3a), Fe^{2+}-doped NiFe-LDH exhibited enhanced OER due to the tuning of the local atomic structure of NiFe-LDH [19]. In-operando X-ray absorption spectroscopy (XAS) has been performed to gain further insights into the relationship between the local structure (Fe-O-Fe) and the enhanced OER activity. Figure 3b showed the variation in the Ni and Fe valence states for Fe^{2+}-doped NiFe-LDH, from Figure 3c the contraction of the Fe-O 1st coordination shell was consistent with oxidation of the Fe centers to generate $Fe^{(3+\delta)+}$ sites. Substitution of Fe^{2+} on the Ni^{2+} sites perturbed the electronic environment and stabled the higher-valence of Fe, improving the OER activity.

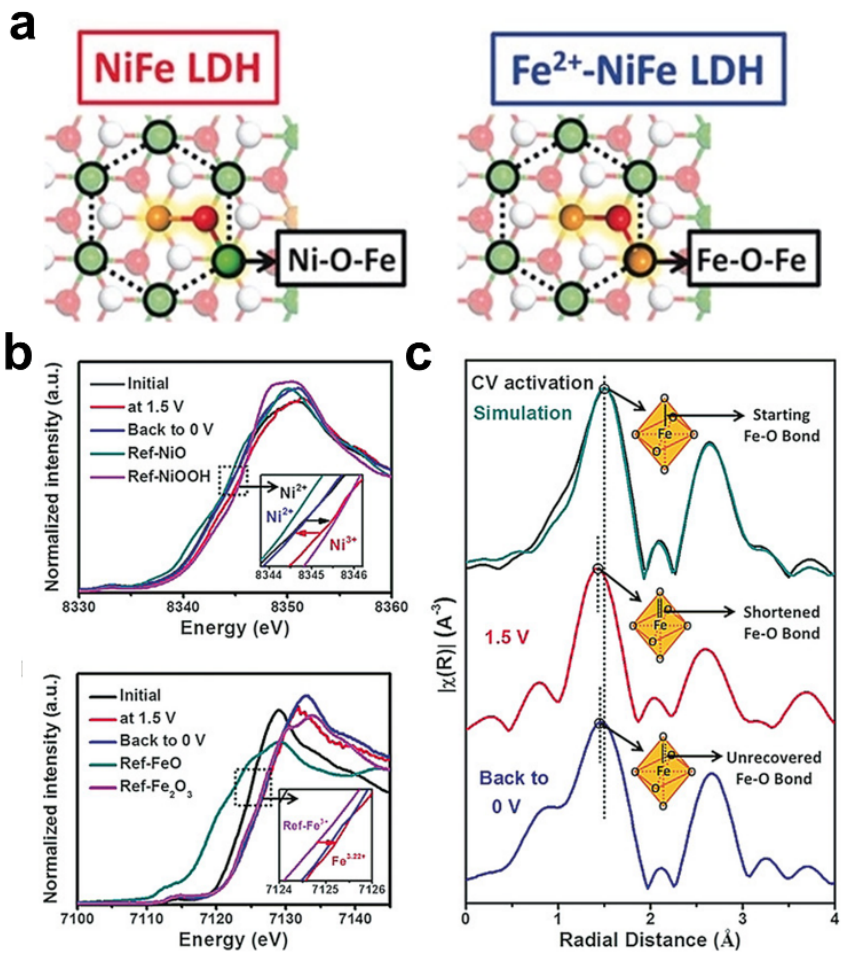

Figure 3. a) Atomic model of NiFe-LDH and Fe^{2+} doped NiFe-LDH, b) *in situ* Ni K-edge and Fe K-edge XANES spectra for Fe^{2+}-doped NiFe-LDH, (c) k^2-weighted Fe FT-EXAFS for a Fe^{2+}-doped NiFe-LDH under OER conditions. Reprinted with permission from [19]. Copyright 2018, Wiley-VCH.

These results suggest that introducing the variable valence metal ions into binary LDH facilitates tuning of the valence states of the metal cations, which in turn promotes electron transfer, generation and stabilization of highly catalytic active sites which is synergistically beneficial for improving performance.

2.1.2 Vacancy engineering of layers

Defect engineering in catalytic materials has been confirmed as a versatile strategy for activity improvement. In these processes, surface defects could be highly beneficial for decreasing molecular activation energies, modulating of electronic structure, and stabling the active intermediates, etc [4, 73]. Due to the higher surface energy of 2D materials compared with the conventional bulk materials, the surface, corner or edge atoms could be more easily migrate from 2D lattice [74, 75], creating a range of surface defects, such as single and/or multiple vacancies, vacancy associates, pits, dislocations, lattice disorders, voids, and distortions [76, 77].

Introducing vacancy defects, which can dramatically affect the coordination environment and valence states of atoms, has been demonstrated to be an effective method of tuning the electronic structure of materials [4]. Jin *et al*. prepared etched ultrathin NiFeAl ternary LDH nanosheets containing low-coordination number Ni and Fe sites and

Al vacancies via etching strategy (Figure 4a) [21]. The ratio of Al of NiFeAl-LDH through electrochemical treatment was largely decreased, indicating the generation of Al^{3+} vacancies. Benefiting from the abundant Al^{3+} vacancies and coordinatively unsaturated Ni^{2+} sites, the electron transfer reactions can be greatly facilitated along with allowing exposure of the active sites, thus V_{Al}-rich ultrathin NiFeAl-LDH nanosheets exhibited enhanced OER performance.

NiFeZn-LDH with Zn vacancy (denoted as D-NiFeZn-LDH) and NiFeAl-LDH with Al vacancy (denoted as D-NiFeAl-LDH) were prepared using an alkaline etching method by introducing Zn^{2+} or Al^{3+} sites into NiFe-LDH thus selectively creating atomic M^{2+}/M^{3+} defects (Figure 4b) [22]. According to XPS of D-NiFeZn-LDH, the decreased valence of Ni and Fe indicated etching of Zn^{2+} sites generated Ni^{2+}–O–Fe^{3+} defects, the lower Ni valence state and unchanged Fe valence state for D-NiFeAl-LDH confirmed the production of Ni^{2+}–O–Fe^{3+} defects was induced by Al^{3+} vacancies. To demonstrate the existence of Zn^{2+} or Al^{3+} vacancies, based on the electron paramagnetic resonance (EPR) spectra (Figure 4c), D-NiFeZn-LDH showed a strong peak that could be ascribed to the more Ni^{2+}–O–Fe^{3+} defect than D-NiFeAl LDHs. And based on the experimental results, it can be confirmed that M^{2+} vacancies were more favorable to improving catalytic activity.

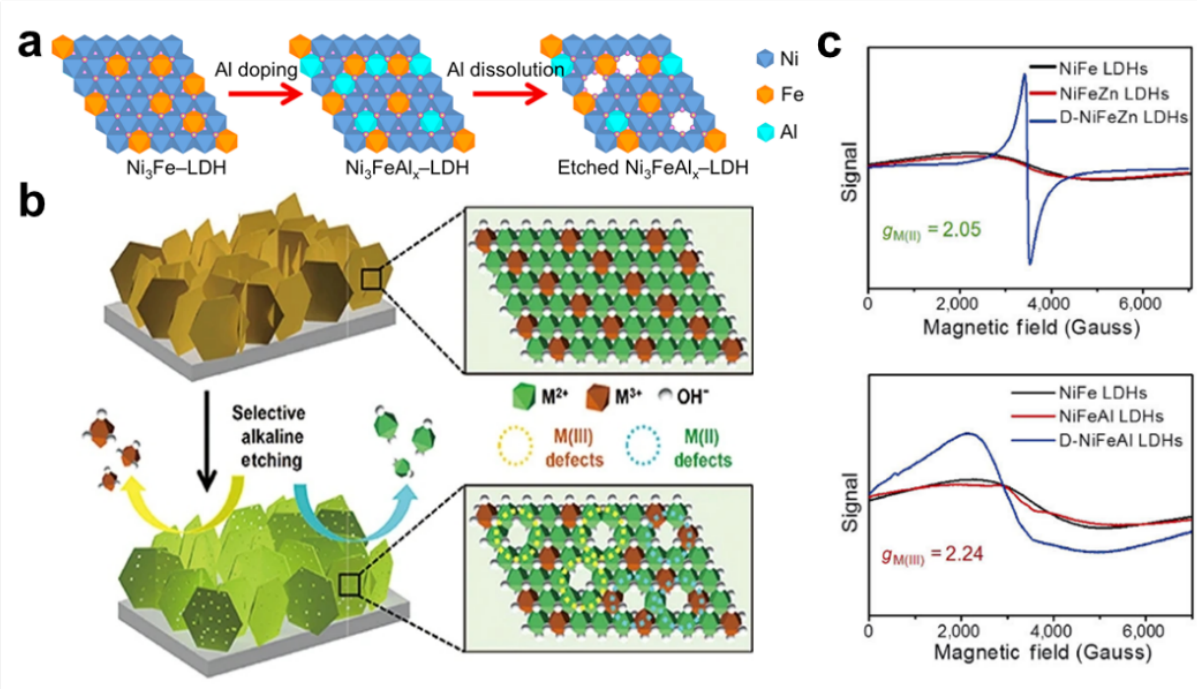

Figure 4. a) Schematic preparation of NiFeAl-LDH. Reprinted with permission from [21]. Copyright 2017, Elsevier. b) schematic illustration of NiFe-LDH via introducing M^{2+}/M^{3+} vacancy defects, c) EPR spectra of NiFe-LDH, NiFeZn-LDH, D-NiFeZn-LDH, NiFeAl-LDH, D-NiFeAl-LDH. Reprinted with permission from [22]. Copyright 2018, Springer-Verlag.

In addition to cation vacancy control, the creation of anion vacancies can also greatly affect electronic structure and further enhance catalytic performance [42, 78]. The introduction of Mn^{2+} into NiFe-LDH could lead to the increase of oxygen vacancies due to the electron transfer from Mn^{2+} to Ni^{2+} and Fe^{3+} [27]. Density functional theory (DFT) calculations supported the existence of oxygen vacancies and low valence Ni^{2+} and Fe^{3+} in the Mn^{2+}-doped NiFe-LDH and this significantly increases the M–O^{d-}H $^{d+}$ binding strength and facilitates deprotonation for significantly improved water oxidation performance. Similarly, Zhang *et al.* successfully synthesized CuZnAl-LDH

containing oxygen vacancies and low valence $Cu^{\delta+}$ ($\delta < 2$) by incorporating Cu atoms into ZnAl-LDH layers [57]. Both experimental studies and calculation showed that oxygen vacancies and coordinatively unsaturated $Cu^{\delta+}$ may improve photoinduced electrons transfer and N_2 activation. As a result, this system exhibited excellent photocatalytic performance for N_2 photoreduction to NH_3. In another case, NiCoFe-LDH nanosheets with O and Fe vacancies could be prepared via partial substitution of Ni on the Co sites in CoFe-LDH [39]. The X-ray absorption fine structure (XAFS) (Figure 5a) demonstrated the O and Fe vacancies after the incorporation of Ni atoms, promoting the photo-induced charge separate and transfer. Consequently, the synergistic effect of Ni doping and vacancies facilitated the CH_4 production and H_2 suppression (Figure 5b, c). Similarly, when a suitable amount of Co is incorporated into MgAl-LDH [53], the CoMgAl-LDH was able to generate more hydroxyl vacancies (Figure 5d-f) due to the lattice distortion ascribed to smaller ionic radius of Co^{2+} than Mg^{2+} which was observed to be beneficial for carrier transport in the photoreaction.

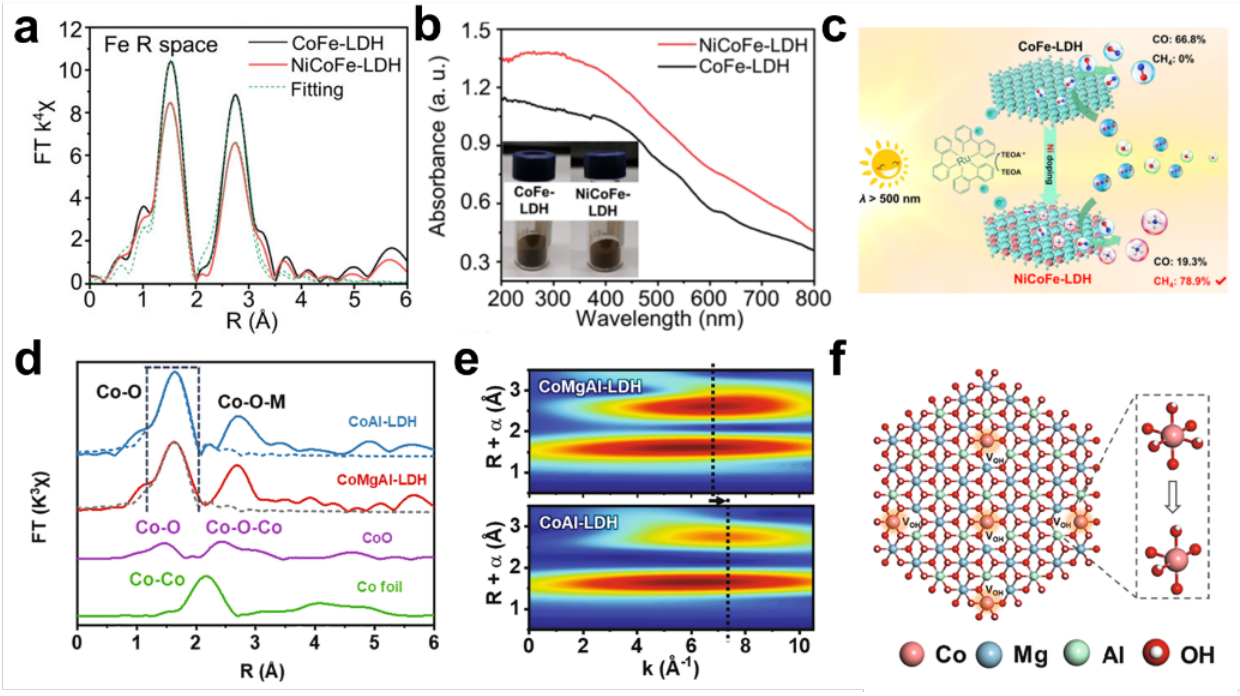

Figure 5. a) FT-EXAFS of Fe K-edge and b) UV−vis spectra, c) schematic illustration of CO_2PR to CH_4 for NiCoFe-LDH and CoFe-LDH. Reprinted with permission from [39]. Copyright 2020, American Chemical Society. d) FT-EXAFS of Co K-edge for CoMgAl-LDH, CoAl-LDH, CoO and Co metal, e) WT plot, f) schematic illustration of a CoMgAl-LDH containing oxygen vacancies. Reprinted with permission from [53]. Copyright 2021, Elsevier.

When ions are introduced into the LDH layers that create large differences in electronegativity, then electron transfer is likely to occur to promote the formation of electron-rich centers that may have high catalytic activity; the introduction of large cations may cause distortions within the layers that may be accompanied by the formation of oxygen vacancies, generating coordinatively unsaturated active sites, that are beneficial to the adsorption of substrates or intermediates and electrons transfer for the efficient catalysis.

There is another question arouse, how can we quantify the defect concentration and may provide a quasi-location site of the defects that formed on the multi-metallic LDHs LDH in order to further map the detail of the defects.

Take monolayer NiAl-LDH catalyst as example[79], through AFM and HRTEM results, the whole concentration of oxygen and metal ions can be clearly calculated, while by virtue of XAFS results, the corresponding coordination number of the first Ni-O shell can be preciously obtained with a number of 5.5 compared with the pure NiAl-LDH with a Ni-O coordination number of 6.0, thus the oxygen defect concentration can be obtained with a number of 8.3%, corresponding to the oxygen defect intensity of 2.14 nm^{-3}, similar though can also fit to calculate metal ions defect concentration. Then a location site description can be defined as material- -defect type- located highly exposed facet-concentration, like LDH-$V_{O\text{-}(001)}$-2.14 nm^{-3}. Such defect quantity location method provides guideline for precisely regulate selectivity of catalytic reaction by accurate defect engineering. The above-mentioned description maybe also suitable for highly active facet exposed NiO, ZnO, TiO_2 systems. Take NiO as an example as obtained from calcination of NiTi-LDH monolayer precursor[80], through combination of AFM, TEM and XAFS results, the synthesized highly exposed (110) facts of NiO have abundant of oxygen defect, and the location site of defects can be regarded as NiO-$V_{O\text{-}(110)}$-2.76 nm^{-3}. Such defect quantitative provide a new and more intuitive view of the defect structure. However, defective quantities are also limited, for instance, the defects of materials will be affected by the reaction environment, thus the defect structure will not maintain a constant state. Therefore, it may need to use more *in situ* characterizations to reflect the change of defect structure in real time for further exploration.

2.2 Lattice modulation of layers

2.2.1 Lattice distortions in the layers

Apart from vacancies, other defects, such as dislocations, disorder of lattice can have influence on the physicochemical properties of materials along with many local atomic arrangement parameters slightly altering, such as bond lengths or angles, atomic distances and coordination numbers [73, 74].

For instance, $Ni^{2+}Ti^{3+}Ti^{4+}$-LDHs containing Ti^{3+} defects was formed by decreasing the thickness of bulk $Ni^{2+}Ti^{4+}$-LDH down to a few layers with the generation of oxygen vacancies (Figure 6a) [81]. Both electron spin resonance (ESR) and XAFS studies showed both an increased concentration of Ti^{3+} defects along with structure distortions and lower coordination number in first Ti–O coordination shell compared with bulk NiTi-LDH (Figure 6b). DFT calculations also revealed that a significantly reduced band gap for NiTi-LDH once incorporated with Ti^{3+} centers, this situation facilitated electron–hole separation for photocatalytic water oxidation. Site-selective incorporation of ruthenium and iridium was found to promote reaction kinetics of self-supported NiV-LDH [52]. According to an XAFS study (Figure 6c-e), Ru (Ir) introduction cause high distortion of octahedral V along with V vacancies for NiVRu-LDH or NiVIr-LDH. DFT calculations verified that the efficient modulation of electronic structures via Ru or Ir introduction would promote both HER and OER activities by reducing the energy barrier of HER and largely improve OER. Similarly, synergistically perturbation to the electronic structure for $Ni(OH)_2$ through Fe and V incorporation can enhance the overall OER performance (Figure 6f) [23]. A severely distorted local coordination for V and a shortening of V–O bond lengths formed under OER conditions was thought to make a crucial contribution to the promoted catalytic activity.

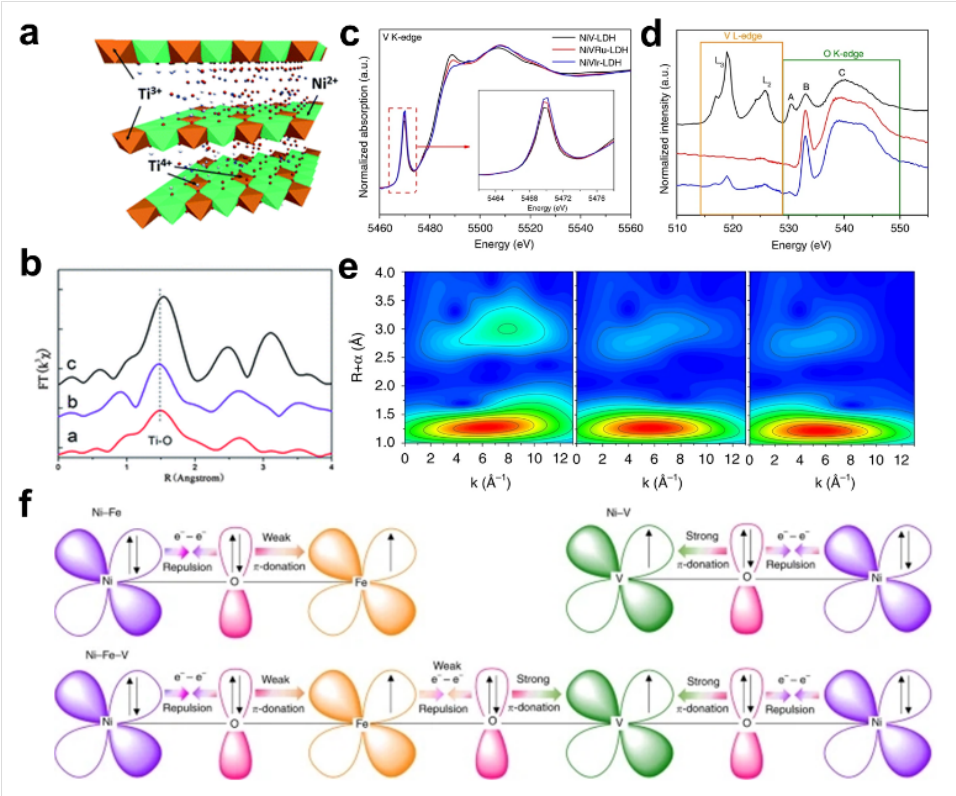

Figure 6. a) Schematic illustration of Ti^{3+} self-doped NiTi-LDH, b) Ti K-edge EXAFS spectra for NiTi-LDH. Reprinted with permission from [81]. Copyright 2014, Royal Society of Chemistry. c) V K-edge and d) V L-edge XANES spectra, e) WT-EXAFS of V for NiV-LDH, NiVRu-LDH and NiVIr-LDH. Reprinted with permission from [52]. Copyright 2019, Springer Nature. f) Schematic representations of NiFeV-LDH. Reprinted with permission from [23]. Copyright 2018, Springer Nature.

Overall introducing heteroatom metals ions can create unsaturated coordination and distortions within the layers that is often accompanied by production of oxygen vacancies. Generation of these highly active configurations can tend to facilitate electron transfer, reduce barrier and overall improve catalytic performance.

2.2.2 Crystal phase transition of the laminar structure

Transition metal ion substitution with multiple valence states (such as Ni^{2+}, Co^{2+}, Fe^{3+}, Mn^{2+}) into LDHs has been confirmed to have influence on modification of electronic structure, on the other hand substitution with cations that offer only a single valence state has received very little attention. Wang *et al.* [82] found the incorporation of Al could largely increase the crystallinity of LDH and improve the reversible electrochemical activity involving both Ni^{2+} and Co^{2+}, ensuring the stable existence of $Ni(OH)_6$ and $Co(OH)_6$. Thus, LDHs can offer improvements of the specific capacitance and cyclic performance for high-performance supercapacitors. As a result, NiCoAl-LDHs were prepared via changing the Al ratio. [45]. The scanning electron microscopy (SEM) and transmission electron microscope (TEM) images showed a transition from one-dimensional (1D) nanowires ($NiCo_2$-OH) to mixed structure with nanowires and nanosheets for $NiCo_2Al_x$-LDHs (Figure 7a, b), indicating that the Al^{3+} ions in $NiCo_2Al_x$-LDHs were benefit for the generation of nanosheets. As shown in the X-ray diffraction (XRD) (Figure 7c), the introduction of Al^{3+} favored a change from the β-phase (NiCo-OH) to α-phase (NiCoAl-LDH) with the increased interlayer spacing for ion transport and improving the

crystallinity. As a result, the observed increase in specific capacitance (Figure 7d) of the $NiCo_2Al_2$-LDH is ascribed to hierarchical structure and morphological stability inducing better ions transport and electrolyte accessibility.

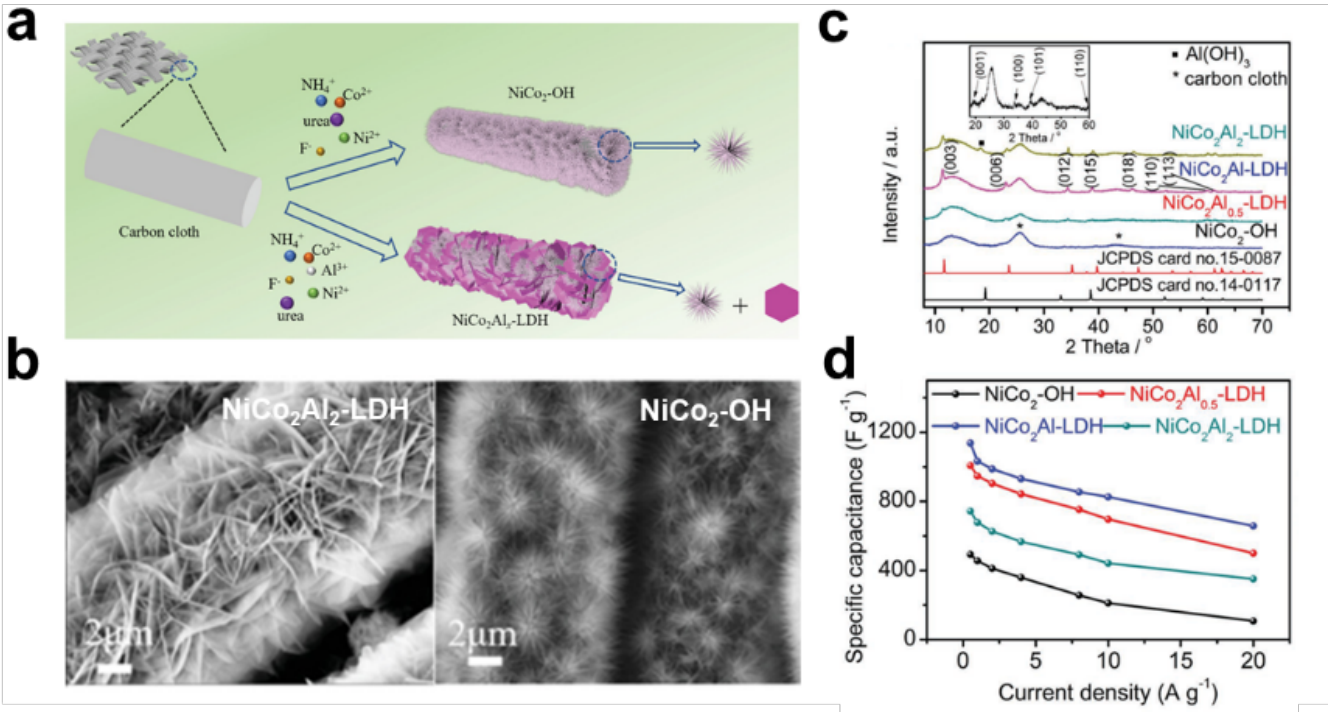

Figure 7. a) Schematic illustration, b) SEM images, c) XRD patterns, d) gravimetric specific capacity CC@$NiCo_2$-OH and CC@$NiCo_2Al_x$-LDH electrodes. Reprinted with permission from [45]. Copyright 2019, Wiley-VCH.

The introduction of Al^{3+} can not only provide a stable framework for the nucleation and growth of LDH phase, but also promote the construction of a lamellar structure and increasing the specific surface of the material, these features are beneficial to the contact between more active sites and reactants to improve performance.

2.2.3 Crystalline vs amorphous phases

In addition to the creation of point defects and lattice distortions, the introduction of higher valence ions or non-metal ions may lead to larger regions of disorder, forming an amorphous structure. Compared with the crystalline counterparts, it has been demonstrated that amorphous phases have a larger ratio of unsaturated coordination sites, which could facilitate reactants adsorption and charge transfer [83]. However, the low conductivity or poor stability of purely amorphous phases may cause their lower catalytic activity [84]. Hence, a potential catalyst construction by integrating advantages of two phases to balance stability and activity. Therefore, the creation of crystalline–amorphous interfaces may be an efficient way to enhance the catalytic performance and stability of catalysts.

The ultrathin tungsten-doped NiFe-LDH nanosheets directly growing on nickel foam (NiFeW-LDH/NF) with many crystalline–amorphous boundaries was prepared as potential catalysts for OER [36]. The oriented crystalline nanoparticles with amorphous phase can be observed by high resolution transmission electron microscope (HRTEM) (Figure 8a), the lattice fringes corresponding to the characteristic (012), (015), and (018) facets of NiFeW-LDH

could be seen in the circles of nanoparticles, confirming the existence of the boundaries, this could promote the generation of active site and efficient reaction. On the other hand, the incorporation of W^{6+} facilitated the modulation of electronic structure for Ni and Fe sites to promote efficient electron transfer, resulting in the excellent catalytic activity for OER (Figure 8b, c). Similarly, CuNiCo-LDH with amorphous edge was prepared via the incorporation of sulfur ions [47]. The HRTEM images showed the crystal internal area with amorphous nanosheets edges (Figure 8d) and elemental mapping EDX analysis confirmed the location of S ions. Besides, based on XPS results, sulfurization was accompanied by the generation of Ni^{3+} ions ascribed to the partially unsaturated coordination Ni amorphous species. Thus, the edge sulfurization of LDH facilitate the high conductivity and highly active sites for the electrocatalytic hydrazine oxidation reaction (HzOR) (Figure 8e). In another example, CoAlS(OH) with poor crystallinity tending to amorphous phase was prepared by immersing CoAl-LDH in S^{2-} solution, in which the S^{2-} replaced OH^- [54]. The SEM and selected area electron diffraction (SEAD) showed that the platelet-shaped structure for CoAl-LDH was preserved (Figure 8f, g). The efficient sulfurization was attributed to preserving an effective morphology, thus CoAlS(OH) hydroxysulfides with such structural regulation and many exposed active sites exhibited excellent bifunctional OER activity (Figure 8h).

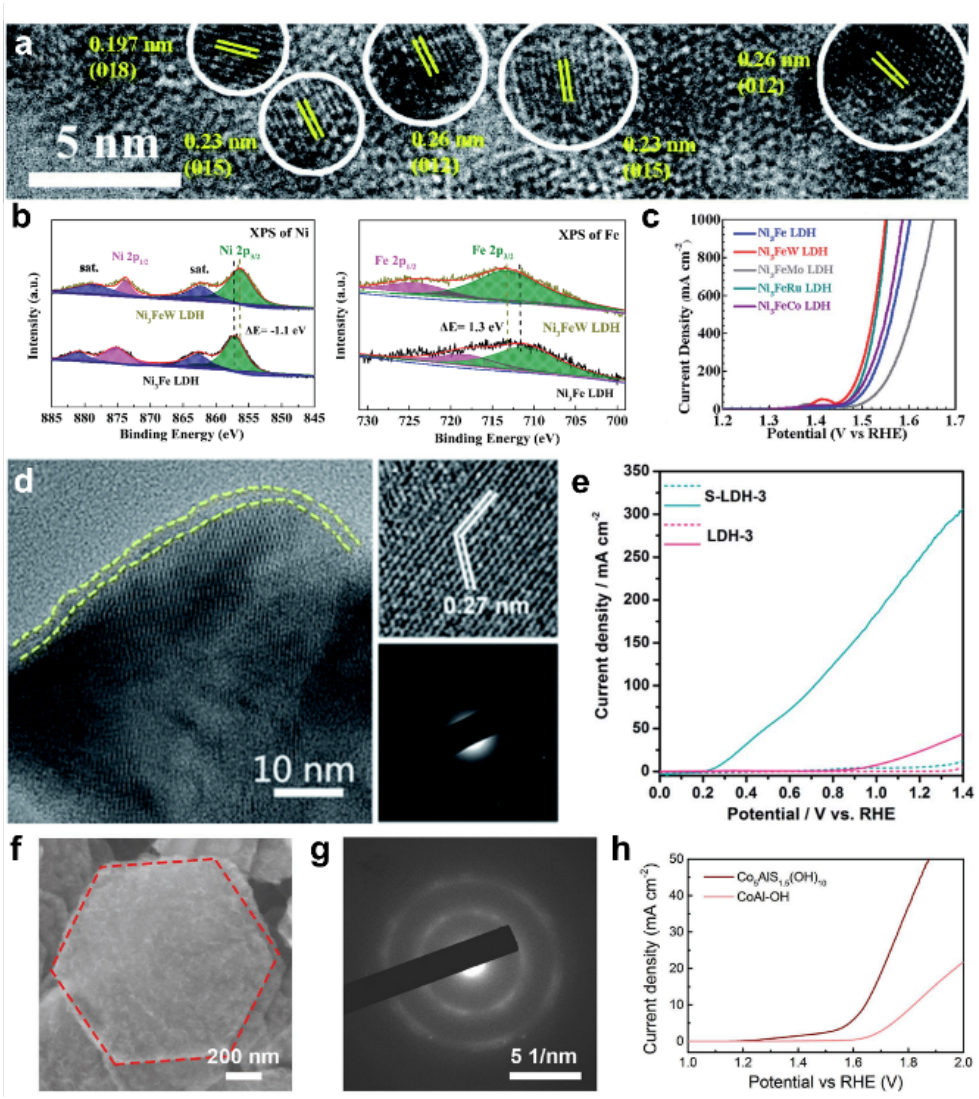

Figure 8. a) HRTEM images of NiFeW-LDH nanosheets, b) XPS for NiFe-LDH and NiFeW-LDH, c) OER LSV curves. Reprinted

with permission from [36]. Copyright 2020, Royal Society of Chemistry. d) HRTEM images and corresponding SAED pattern of S-CuNiCo-LDH; e) LSV curves of S-LDH-3 (S-CuNiCo-LDH) and LDH-3 (CuNiCo-LDH). Reprinted with permission from [47]. Copyright 2019, Royal Society of Chemistry. f) SEM image, g) SAED pattern of CoAlS hydroxysulfides; h) OER and LSV plots of CoAl-OH and CoAlS hydroxysulfides. Reprinted with permission from [54]. Copyright 2017, Wiley-VCH.

Therefore, by controlling the formation of the amorphous structures via adjusting the incorporated ions, the crystalline–amorphous phase boundaries form could be purposefully constructed, the high activity of the amorphous form and the stability of the crystal lattice deliver stable materials with excellent catalytic activity.

2.2.4 Amorphous structure transformation

Metal cations incorporation into LDH layers could adjust coordination and electronic structures [75]. Changing the synthesis methods and synthesis conditions can induce trivalent and bivalent metal cations atomic ratios to go beyond the normal range for LDHs. Thus, multi-metallic oxyhydroxides with amorphous phases along with unsaturated coordination and disordered bonding environments have exhibited huge potential for their enhanced catalytic activity.

Sargent *et al.* prepared an FeCoW oxyhydroxides gel with amorphous phase via a room-temperature sol-gel process [41]. The HRTEM and XRD data demonstrated that the FeCoW gel was an amorphous phase (Figure 9a). According to EXAFS, the distortion of the WO_6 octahedra increased (Figure 9b) along with the generation of CoOOH and FeOOH during the OER. It is thought the metal ion coordination in CoFeW could adjust the electronic structure to facilitate the efficiency of OER. Similarly, amorphous Ni_5Co_3Mo−OH prepared via chloride ion corrosion on a Ni foam exhibited excellent performance toward water splitting [50]. This performance was attributed to the Mo doping significantly boosting the kinetics of NiCo−OH facilitated charge transfer. In another case, Guo *et al.* incorporate Cu into a NiFe hydroxide shell and thereby synthesize homogeneous amorphous nanocages of CuNiFe hydr(oxy)oxide (Figure 9c) [30]. The introduction of Cu improved conductivity of the amorphous material. Furthermore, according to the XPS results, more Ni^{2+} was oxidized to Ni^{3+} along with the introduction of Cu, causing to larger percentage of NiOOH, to further promote OER activity. As a result, the enhanced catalytic activity was ascribed to generation of Ni active species and improved charge transfer in CuNiFe hydr(oxy)oxide (Figure 9d).

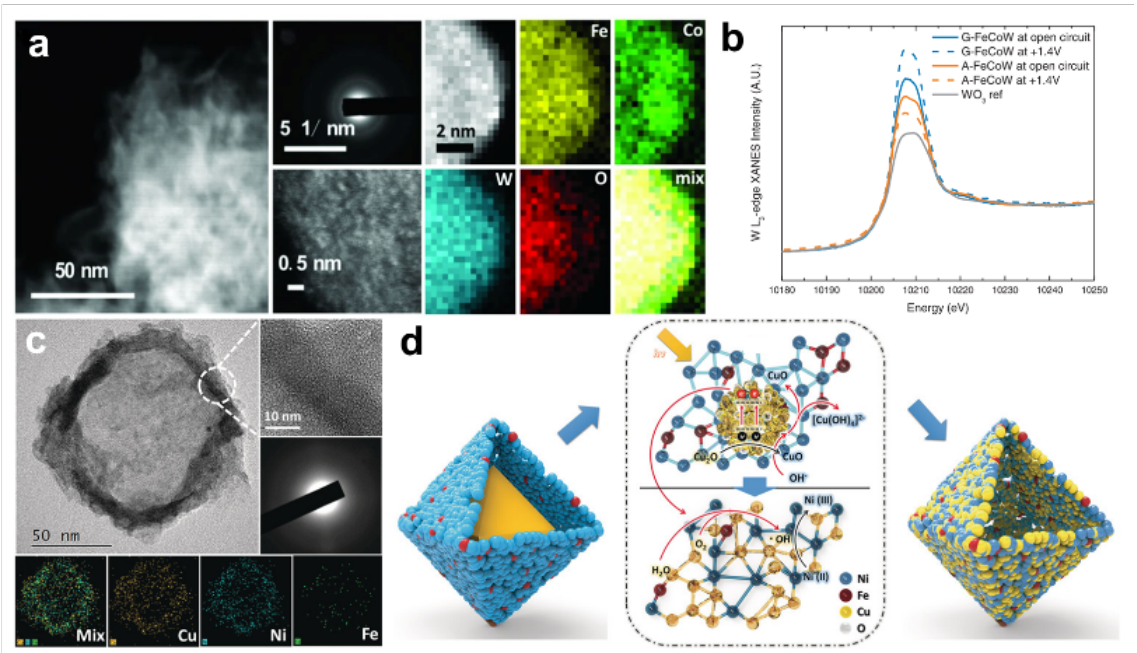

Figure 9. a) HAADF-STEM image, SAED pattern, elemental mapping of G-FeCoW oxyhydroxides, b) bulk W L_3-edge XANES spectra. Reprinted with permission from [41]. Copyright 2016, American Association for the Advancement of Science. c) TEM image, SAED pattern and EDS elemental mapping, d) schematic illustration of OER catalysis enhancement mechanism of AN-CuNiFe. Reprinted with permission from [30]. Copyright 2019, Wiley-VCH.

When incorporating highly charged cations into the octahedal brucite layers of an LDHs, the resultant materials may completely turn into amorphous phases (oxyhydroxides), in which the coordinatively unsaturated highly active sites could facilitate electron transfer and improved reaction kinetics.

2.3 Loading metal atoms/particles on the layers

2.3.1 Single atom anchoring on layers

Single-atom catalysts (SACs) have exhibited huge potential in the research on heterogeneous catalysis. When compared with nanoparticles or bulk of materials, these catalysts may reach the maximum atom-utilization efficiency [85-89]. However, single metallic atoms tends to aggregate attributed to dramatically increased surface energy [90]. Considering the stability of SACs, it is of significance to explore an appropriate support which can serve as a matrix for dispersing/isolating single metallic atom sites to promote the atomic utilization [91]. It has been confirmed that the M^{3+} ions atoms are highly dispersed and ordered in the layer of LDHs (Figure 10), where each M^{3+} ions were surrounded by M^{2+} ions with no M^{3+}-M^{3+} close contacts [67, 92]. Furthermore, compared with other oxides (hydroxides), LDHs have the intrinsic property of tunable element composition, as a result, there has been many explorations on how single metal atoms could be inserted/anchored in an ordered manner on LDHs.

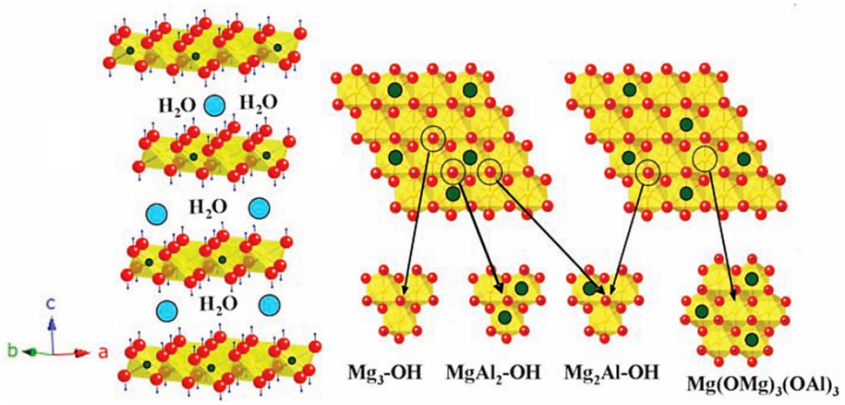

Figure 10. A polyhedral representation of the LDH structure. Reprinted with permission from [67]. Copyright 2008, American Association for the Advancement of Science.

Research on single-atom supported LDH materials could be traced back to 2003. Kaneda *et al.* successfully prepared Ru/MgAl-LDH [61]. According to the XAFS (Figure 11a), the peaks centered at 3.5 Å could not be observed, demonstrating Ru species existed as single atoms. Furthermore, a monomeric Ru^{4+} with one OH and two H_2O was bonded to three O atom in the layer of MgAl-LDH (Figure 11b). Thus, the cooperative catalytic activity between grafted-Ru and LDH base sites facilitated R-alkylation. Besides, Zhang *et al.* prepared Au/NiFe–LDH via electrochemical method [38]. From XAFS analysis, the single Au atoms were adsorbed on oxygen creating Au−O bonds. DFT calculations supported the surface charge transfer from the Au atoms to O, Ni and Fe atoms (Figure 11c) improved the OER. Although this work demonstrated single Au atoms were highly-dispersed on the layer of LDH by Au−O bonding, evidence for the precise location of single metal atoms remained elusive. Song *et al.* reported a facile method for synthesizing Ru SA supported on a monolayer NiFe-LDH [33]. According to WT-EXAFS, the Ru/NiFe-LDH exhibited one peak centered at 4.1 $Å^{-1}$, which could be ascribed to Ru–O shell (Figure 11d, e). With the help of model fitting and energy calculations, the Ru atoms were confirmed to locate on the layer of LDH and possibly vertically above Fe atoms (Figure 11f). In addition, the location of Ru SA may stabilize the intermediates and lower the reaction barriers, and thus enhancing the hydrazine electrooxidation. Further work by this research group successfully prepared NiFe-LDH doped with single-atom Rh [35]. Through comparing XAFS experimental and simulation results (Figure 11g) and in contrast to Ru, the Rh atoms were shown to exist in the layers as RhO_6. Furthermore, the layer distortions and defect sites caused by the Rh doping contributed to the good catalytic performance (Figure 11h). For another case, Ru SA anchoring on the layer of CoFe-LDH (Ru/CoFe-LDH) was synthesized by a dipping method [40]. Through XPS and computational simulation, it was confirmed that there was strong electron effect between single atomic Ru and CoFe-LDH due to electron transportation from the Co and Fe atoms to Ru atoms (Figure 11i). According to *in situ* XAS, compared with irreversible oxidization of Fe and Co, the reversible change of Ru valence state indicated that Ru local structure could re-construct under the reaction conditions (Figure 11j), demonstrating that Ru could stably work as the active site without dissolution into the electrolyte during reaction. Cui *et al.* successfully anchored single Ir atoms on NiFe oxyhydroxides ($Ir_{0.1}/Ni_9Fe$ SAC) by *in situ* cryogenic–photochemical reduction method [93]. XAS analysis and DFT calculations, suggested that a highly oxidized single Ir atom ($Ir^{5.3+}$) is created under operating conditions and this contributed to the exceptional

OER performance.

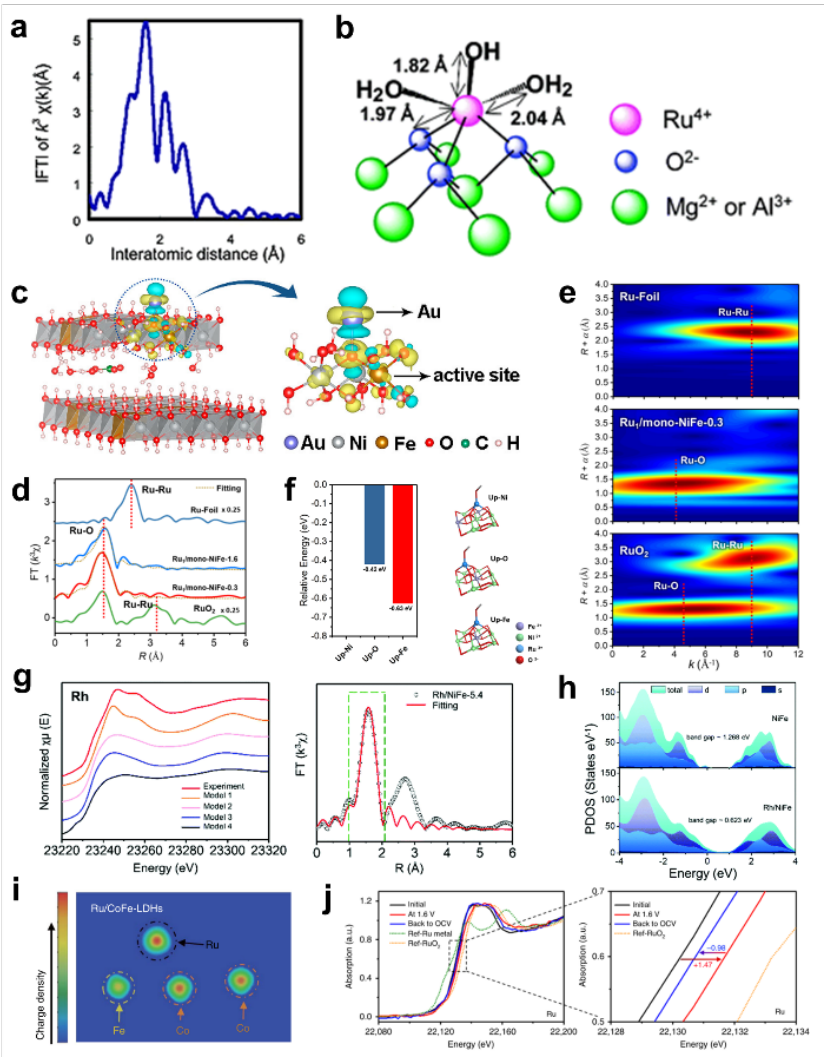

Figure 11. a) FT-EXAFS, b) Surface structure of Ru/MgAl-LDH. Reprinted with permission from [61]. Copyright 2008, American Chemical Society. c) Differential charge densities of NiFe LDH with and without Au atom when one O atom is adsorbed on the Fe site. Reprinted with permission from [38]. Copyright 2018, American Chemical Society. d) FT-EXAFS, e) FT-EXAFS for Ru/NiFe-LDH, f) relative energy of Ru atom upon the O, Ni and Fe of Up-Ni, Up-O, Up-Fe. Reprinted with permission from [33]. Copyright 2019, Royal Society of Chemistry. e) XANES spectra and the corresponding calculation and fitting results for Rh/NiFe-LDH, h) PDOS of DFT calculation for NiFe-LDH and Rh/NiFe-LDH. Reprinted with permission from [35]. Copyright 2021, Royal Society of Chemistry. i) operando XAS and *in situ* XANES measurement under the electrochemical condition, j) charge density from computational simulation of Ru/CoFe-LDHs. Reprinted with permission from [40]. Copyright 2019, Springer Nature.

Single atom noble metal-based catalysts have also been prepared to enhance thermal reactions. Ru SA/MgAl-LDH exhibited the enhanced hydrogenation of CO_2 to HCOOH [62]. Upon the addition of $NaOH_{aq}$, isolated single-atomic Ru species would graft onto O atoms of OH of LDH to form Ru−OH bonds (Figure 12a-c by Ru K-edge XANES and UV-vis spectroscopy. Based on Figure 12d, the electron transfer for OH could be crucial for creating electron-rich Ru centers with high catalytic activity. What's more, when compared with other M^{2+} ions, Ru/MgAl-LDH exhibited the best catalytic performance, indicating that the LDH basicity may promote Ru SA to enhance the

activity.

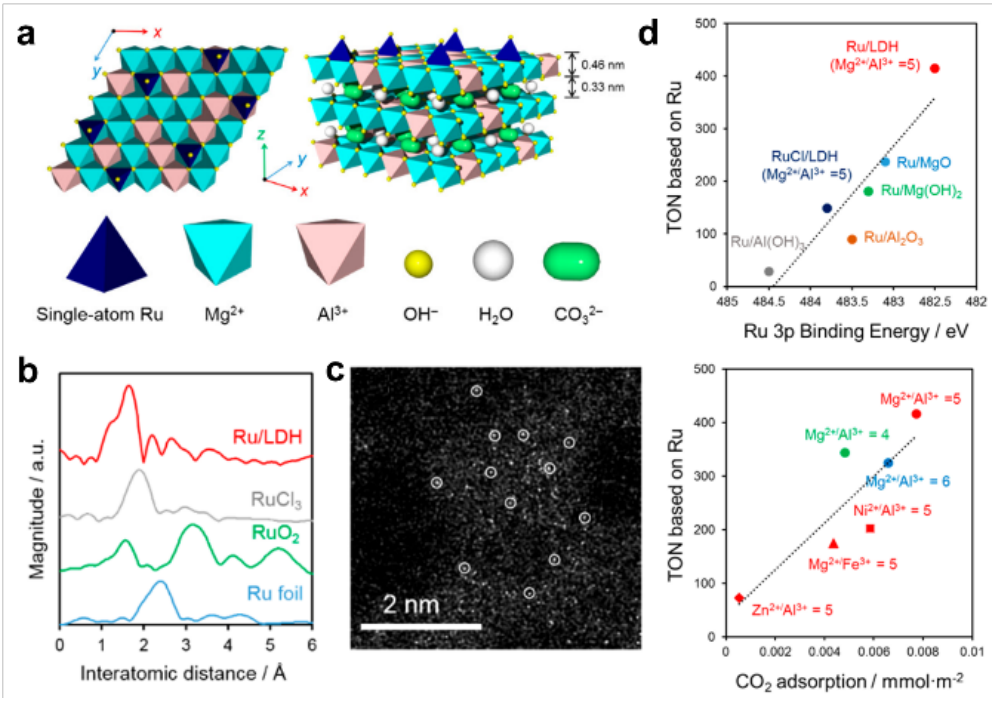

Figure 12. a) Schematic illustration, b) Ru K-edge FT-EXAFS spectra, c) HAADF-STEM image of Ru/MgAl-LDH, d) relationship between the turnover number (TON) based on Ru, Ru 3p binding energy and CO_2 adsorption. Reprinted with permission from [62]. Copyright 2017, American Chemical Society.

The LDH structure in which metal atoms are highly dispersed and ordered can be a benefit for the generation of single-atom catalysts. Single atoms may be stabilized by grafting to the hydroxylated LDH surface, thereby promoting both stability and synergy with the layer atoms.

2.3.2 Nanoparticle loading on the support

Besides, LDHs also exhibited the advantage on preparing highly-dispersed metal and mixed metal oxide nanoparticles attributed to the high dispersion of metal atoms on the layer. Fe-based catalysts show promising potential CO hydrogenation to olefins [94] due to the electronic structure [95, 96]. And Fe atoms can be introduced into the layer of LDH to obtain highly dispersed Fe-based catalysts, therefore, a Fe-based heterostructure photocatalyst was prepared via H_2 reduction from ZnFeAl-LDH (Figure 13a) [97], in which Fe-500 consisted of Fe^0 and FeO_x nanoparticles supported by ZnO and amorphous Al_2O_3. Al_2O_3 could be a thermally stable support to avoid catalyst sintering and aggregation during reduction process. According to Fe K-edge XANES and *in situ* XPS analysis (Figure 13b), with increasing the reduction temperature, more Fe^0 could be generated from FeO_x. DFT calculations indicate that the interfaces between Fe and FeO_x was beneficial for the product selectivity towards olefins and suppressed CO_2 evolution under photoirradiation. Followed by this, through annealing of the ZnCoAl-LDH or MgFeAl-LDH precursor, a novel photothermal catalyst (Co-450) containing metallic Co was synthesized [98], that consisted of Co and Co_3O_4 supported on the ZnO–Al_2O_3. Co-450 exhibited excellent CO hydrogenation activity. Both experiment and theory suggested that the O modulated the electronic structure of Co, leading to modest hydrogenation and excellent selectivity to olefins (Figure 13c). Similarly, via H_2-reduction from CoFeAl-

LDH, the alumina-supported CoFe-alloy NPs was prepared [99]. Due to the photothermal activity of CoFe alloy nanoparticles and low barrier energy of CH_2-CH_2 coupling, CoFe-650 exhibited the enhanced selectivity (≈95%) to hydrocarbons for CO_2 hydrogenation.

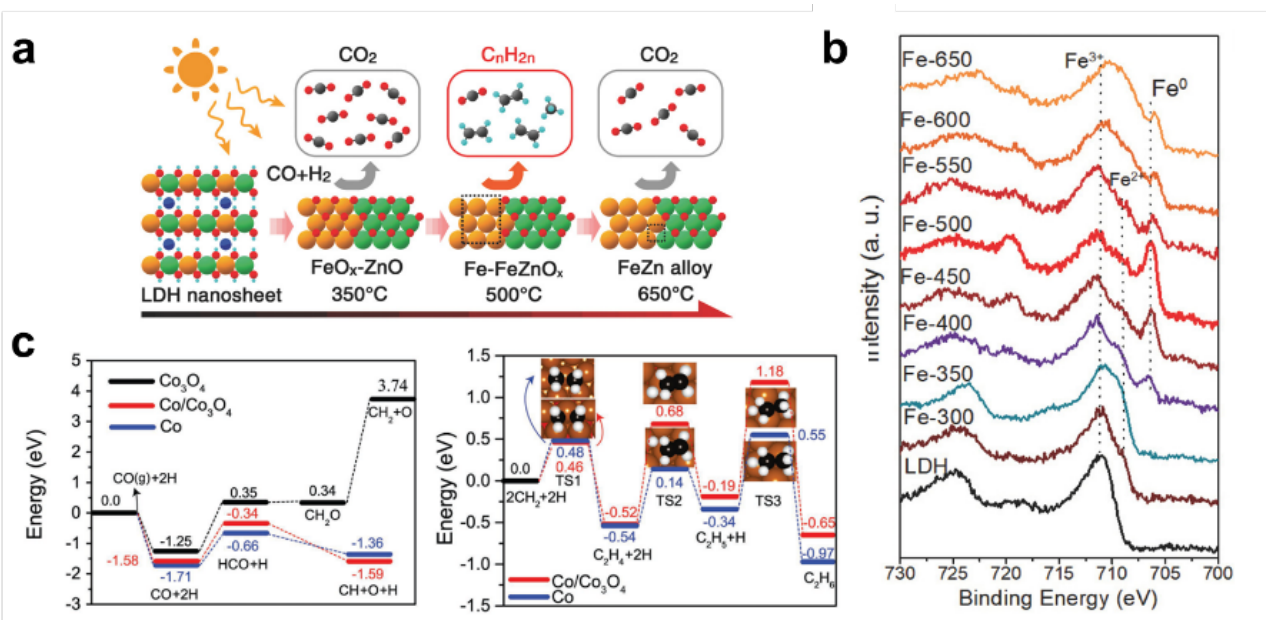

Figure 13. a) The Fe-*x* photocatalysts that were obtained by H_2 reduction of ZnFeAl-LDH, b) *in situ* XPS spectra. Reprinted with permission from [97]. Copyright 2018, Wiley-VCH. c) The potential energy profile of CO dissociation. Reprinted with permission from [98]. Copyright 2018, Wiley-VCH.

In addition, by annealing NiZnAl-LDH, Ni_xZn bimetallic catalysts (Figure 14a) were synthesized [100]. Due to the dilution effect of non-magnetic Zn atoms, a non ferromagnetic Ni_1Zn_1Al alloy could be inferred in which each Ni atom was surrounded by Zn atoms (Figure 14b). Consequently, due to the oxophilicity of Zn and decrease of electron density on the Ni, improving the hydrodeoxygenation (HDO) pathway along with the decarboxylation pathway inhibited. Furthermore, by adjusting the atomic ratio of LDH can not only influence the atomic distribution of the alloy, but also adjust its geometric structure. For example, take CuCoAl-LDH as precursor, Cu@(CuCo-alloy) nanoparticles on Al_2O_3 (Figure 14c) were fabricated [101]. From the TEM (Figure 14d) with EDS line scan, the Cu signal was in the center, the Cu and Co signals were in the shell, indicating that CuO was initially reduced to metallic Cu nanoparticles, followed by the reduction of Co_3O_4. XPS experiments indicate a higher surface Cu/Co ratio (2.88/1.00) than the bulk ratio confirming the Cu migrated to form CuCo alloy. H_2-temperature programmed reduction (TPR) profiles (Figure 14e) and XPS analysis indicated that Cu could promote the generation of Co to form CuCo alloy. The strong interaction of Cu and Co facilitated mass diffusion and transportation and contributes to the enhanced catalytic activity on CO hydrogenation.

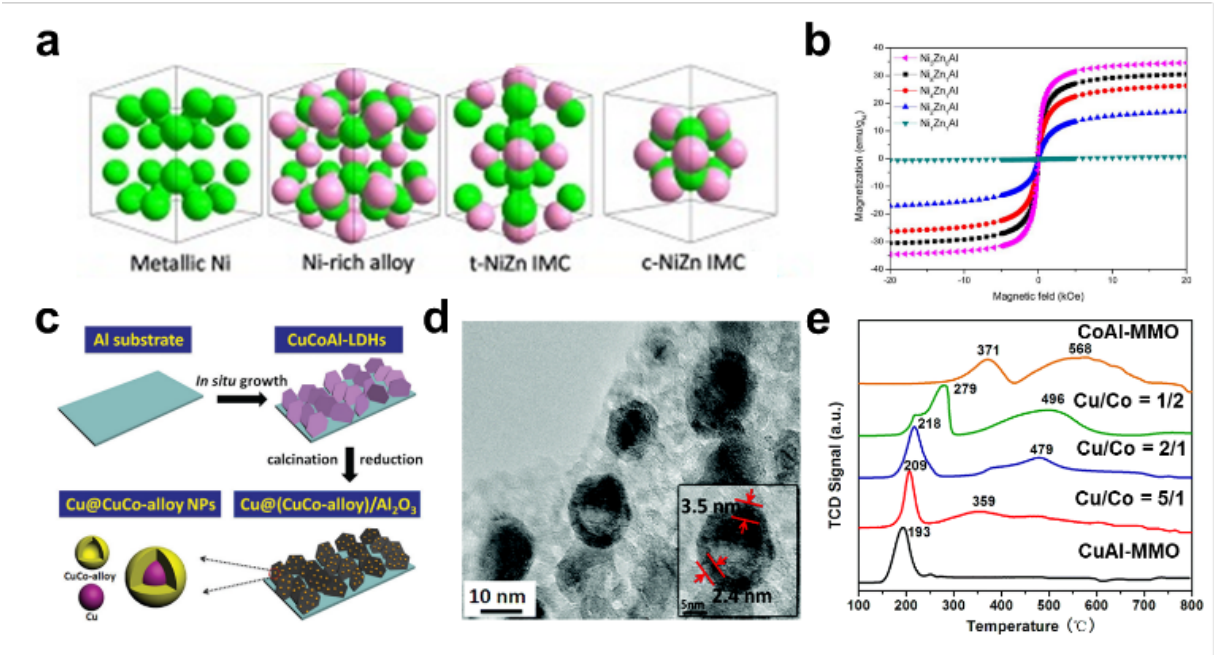

Figure 14. a) Schematic illustration of Ni-Zn bimetallic catalysts, b) magnetic hysteresis loops of NiZnAl samples at 27 °C. Reprinted with permission from [100]. Copyright 2018, Elsevier. c) Illustration of Cu@(CuCo-alloy)/Al_2O_3, d) TEM image of Cu@(CuCo-alloy)/Al_2O_3, e) H_2-TPR profiles. Reprinted with permission from [101]. Copyright 2015, Royal Society of Chemistry.

The characteristics of high dispersion and adjustable atomic ratios for LDHs and that catalytically active elements with varying ratios can be easily introduced and dispersed allows for a logical analysis and determination of the structure-activity relationship.

2.4 Construction of multi-metallic LDHs

2.4.1 Introducing multiple cations into the laminate for high-entropy materials

The origin of LDHs could be traced back to the 1960s, and the general structure has been confirmed based on the structural study of the minerals hydrotalcite and pyroaurite [102, 103], in which $Mg(OH)_2$ with M^{3+} replacing Mg^{2+} on the layer. Subsequently, Yan *et al.* [104] proposed the construction mechanism of LDHs. In addition to the ionic radius criterion, the distortion angle of octahedral coordination of the cations has a huge effect on the formation of LDHs. Recently, Sasaki *et al.* proposed that both layered single metal hydroxides (LSHs) and LDHs can be uniformly classified into layered metal hydroxides (LMHs) due to their similar layered structures [105-108].

Taking advantage of layer element adjustment within LDHs, He *et al.* synthesized successfully a quaternary CoZnGaAl-LDH on the surface of spherical c-Al_2O_3 [109]. Similarly, a series of quaternary CoZnFe^{II}Fe^{III}-LDH and even quinary CuZnMnFeAl-LDH with different ion ratios were prepared by coprecipitation method [110, 111]. However, doping with larger atoms will lead to unsaturation of the octahedral coordination in the laminate and increase the degree of disorder. Due to the individual K_{sp} of the metal ions, pH changes during the nucleation process will also cause successive precipitation leading to the formation of impurities. Therefore, it is difficult to explore a synthesis strategy that can integrate multiple elements into the laminate lattice without impurities. Zou *et al.* reported high-entropy hydrotalcites (HEHs) [51] (Figure 15a) via fast coprecipitation. According to Figure 15b, some lattice

distortions such as defects and dislocation could be observed attributed to introduction of various multi-metallic atoms, and the diffraction peaks of XRD pattern broaden as the metallic elements increase (Figure 15c, d), demonstrating the severe lattice distortion. As a result, the enhanced OER activity of HEHs (Figure 15e) could be attributed to the crystal defects in the HEHs lattice structure. A series of high-entropy oxides (HEOs) derived from HEHs was prepared via a low-temperature plasma strategy (Figure 15f) [112]. EPR experiments on the HEOs from low-temperature plasma treatment (P-HEOs) showed more surface oxygen vacancies than the HEOs from high-temperature calcination (C-HEOs) (Figure 15g). The nanosheet structure, abundant O vacancies, and high specific surface area of P-HEOs promotes catalytic activity on HMF electrooxidation (Figure 15h).

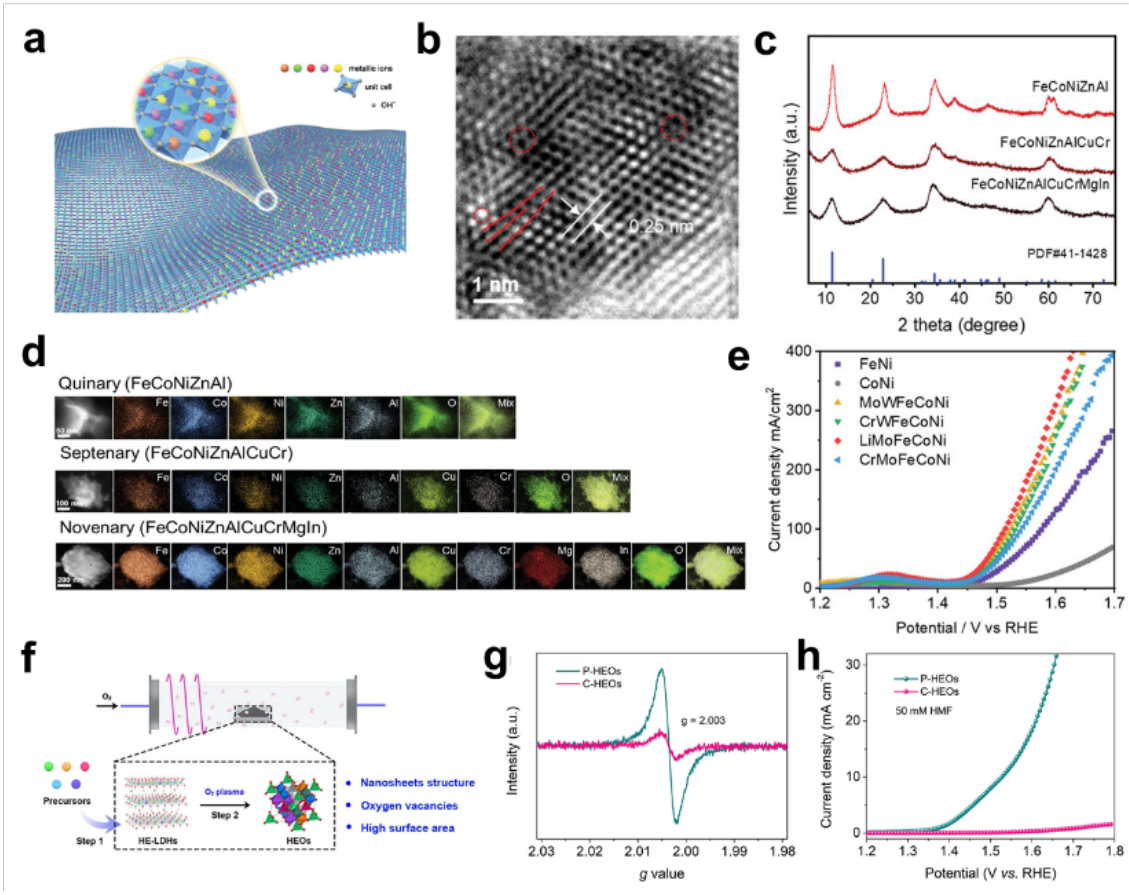

Figure 15. a) Structure of 2D HEH, b) atomic resolution high angle annular dark field scanning transmission electron microscope (HAADF-STEM) of FeCoNiZnAlCuCrMgIn HEH, c) XRD patterns, d) HAADF-STEM and Energy dispersive X-ray spectrometer (EDX) elemental mapping of HEHs, e) LSV curves for HEHs in OER. Reprinted with permission from [51]. Copyright 2021, Wiley-VCH. f) Low-temperature plasma strategy for HEOs, g) EPR spectra, h) LSV curves. Reprinted with permission from [112]. Copyright 2021, Wiley-VCH.

The use of high-entropy LDHs has greatly expanded the possibility of introducing more active sites into the laminates of LDHs. Based on the high dispersion characteristics of LDH itself, various kinds of high-entropy alloys or oxides with uniformly dispersed elements could be prepared via different processing strategies. Further studies into the application of high-entropy materials with high catalytic activity is required.

2.4.2 Introducing multiple species into the interlayer galleries

The nature of the interlayer anions in an LDH galleries is highly flexible [113-116], supramolecular materials prepared by introducing active molecules into the interlayer galleries has been widely investigated [117-124]. For example, the catalytic active metal ions coordinated to the porphyrin or other ligands can be assembled within an LDH to form a composite material [122, 125-127].

Wang *et al.* reported a method to anchor single Pt atoms intercalated in NiFe-LDH (NiFe-CO_3^{2-}-LDH-Pt SA) via space-confined electroreduction (Figure 16a) [128]. XAFS analysis ((Figure 16b), showed single Pt atoms generated through replacing Pt-Cl bonds with Pt-O bonds in LDH laminates along with lattice distortion than NiFe-$PtCl_6^{2-}$-LDH. The interlayer single Pt atoms not only could facilitate the electron transportation of NiFe-LDH for HER, but also changed Ni valence and Ni/Fe–O bond accompanied by the transformation of abundant active phase ($Ni^{2+\zeta}Fe^{3+\zeta}O_xH_y$), optimizing OER intrinsic activity. Wei *et al.* reported the synthesis of ultrathin film (UTF) electrodes [125] based on LDHs and iron porphyrin (Fe-PP) via layer-by-layer (LBL) (Figure 16c), which exhibited good OER activity combining the advantages of LDH and Fe-PP (Figure 16d). In addition, Shi *et al.* [126] constructed Zn-CDs (carbon dots)-LDH system (Figure 16e), which showed ultralong room-temperature phosphorescent (RTP) lifetime (Figure 16f) under ambient conditions and high phosphorescence efficiency. Besides, via exfoliation-assembly strategy, Han *et al.* prepared a serious of transparent ultrathin films of various exfoliated LDHs (CoAl-LDH, MgAl-LDH, NiAl-LDH) assembled alternately with polyanions [129]. The combined functionality of the laminates and interlayer anion indicated that these heterogeneous films could have potential as catalyst, sensors and photovoltaic devices. Moreover, inspired by the LDHs *in situ* transformation from MOFs, the NiCoZn-LDH/Co_9S_8-QDs was prepared on carbon fibers for the application of supercapacitors [130], in which Co_9S_8-QDs were effectively created and embedded within the interlayer of MOFs-derived ternary NiCoZn-LDH via *in situ* selective vulcanization of Co. Due to the abundant active sites from Co_9S_8-QDs, rapid ion/electron transmission from NiCoZn-LDH and enhanced mechanical flexibility of carbon fibers, the hybrid CF@NiCoZn-LDH/Co_9S_8-QDs achieved an outstanding supercapacitor capacity of 2504 F g^{-1} at 1 A g^{-1} and a high capacity retention rate of 62%.

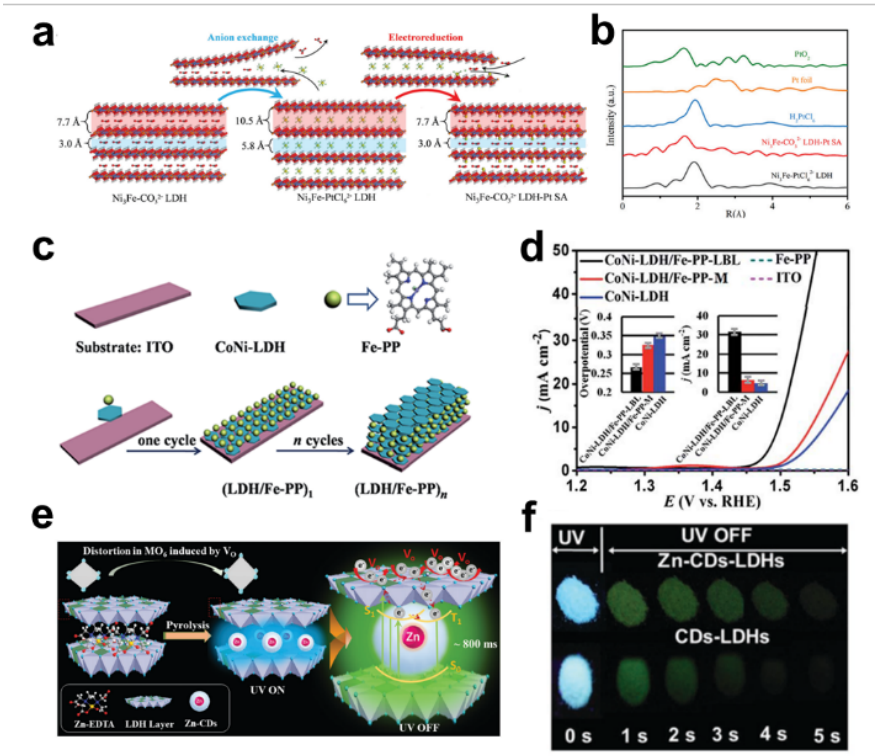

Figure 16. a) Schematic of spatial confinement strategy, b) FT $k^3\chi(k)$-R space curves of Pt L_3-edge XAS for NiFe-CO_3^{2-}-LDH, NiFe-$PtCl_6^{2-}$-LDH, NiFe-CO_3^{2-}-LDH-Pt SA. Reprinted with permission from [128]. Copyright 2021, Royal Society of Chemistry. c) Schematic representation of the LBL assembly of the (CoNi-LDH/Fe-PP)n UTFs, d) LSV curves of CoNi-LDH/Fe-PP-LBL, CoNi-LDH/Fe-PP and CoNi-LDH. Reprinted with permission from [125]. Copyright 2016, Royal Society of Chemistry. e) Schematic representation, f) photographs of the afterglow of CDs-LDH and Zn-CDs-LDH. Reprinted with permission from [126]. Copyright 2018, Wiley-VCH.

The tunable characteristics of LDH interlayer anions through various strategies such as ion exchange or exfoliation recombination is a further dimension. The synergistic interactions of intercalated species and laminates of LDH offer the possibility to improve electron transport capacity, and increases active densities.

3. Applications of multi-metallic LDHs

3.1 Electrocatalysis

3.1.1 Electrocatalytic Water splitting

Electrochemical water splitting has become an important approach to producing hydrogen. However, the overall water-splitting process is severed limited by the poor kinetics of OER. Therefore, it is essential to develop efficient, and highly active OER catalysts using earth abundant elements [131] due to the high price of traditional OER catalysts. Recently, LDHs have been explored as OER electrocatalysts attributed to their excellent catalytic activity [2], like NiX-LDH, CoX-LDH [2, 29, 69, 132-134]. Additionally, binary LDHs can be easily transformed into ternary or multi-metallic LDHs via introduction of other metal cations by taking advantage of cation flexibility within LDH layers. These substitutions may directly or indirectly modulate the electronic structure and so an impact

on catalytic activity.

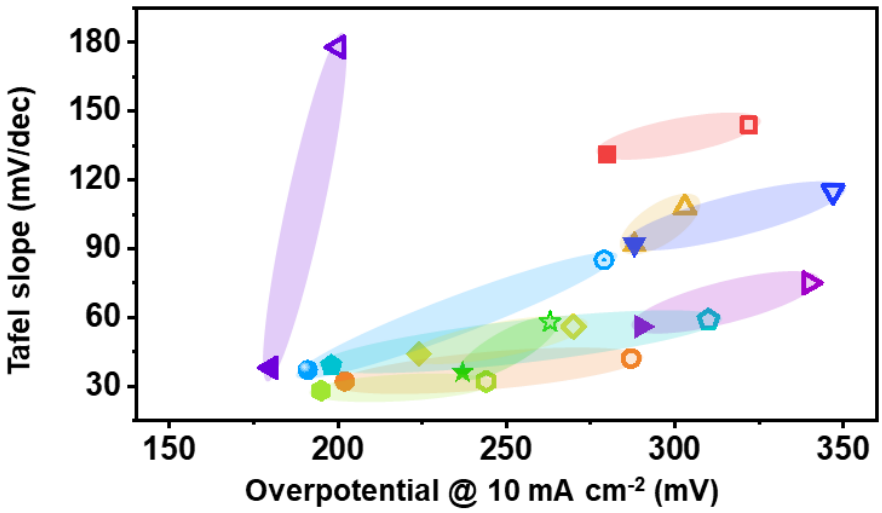

Figure 17. Comparison of the OER performance of multi-metallic LDHs with original binary LDHs from current researches [25, 26, 28, 30, 31, 38, 40, 41, 52, 63], hollow marks represent binary LDHs and solid marks represent multi-metallic LDHs.

For example, Al, Zn are unique amphoteric metals, whose hydroxides are reactive to acidity and alkalinity. The addition of excessive alkali could cause the dissolution of their hydroxide phases. If this process occurs in the LDH, it will lead to the generation of vacancies in the layer. Leaching of base-soluble Zn^{2+} or Al^{3+} sites from D-NiFeZn-LDH and D-NiFeAl-LDH produces selectively M^{2+} or M^{3+} defects that leads to enhancement of the electrocatalytic activity for OER (Figure 18a) [22]. According to the DFT calculations on these systems, Ni^{2+}–Fe^{3+} sites were predicted to offer a lower OER overpotential than Ni^{2+}–Ni^{2+} sites, which was consistent with the experimental results. Therefore, it could be concluded that in this system, M^{2+} defects were more favorable for improving the electrocatalytic activity.

More recently, the substitution of high valence state cations such as Cr, V, Ir and Ru have exhibited huge potentials for OER [34, 49, 56, 135-138]. For example, Li *et al.* explained that the vanadium doping in NiFe-LDH was benefit to enhance OER catalytic activity [20]. The XPS data revealed the average valence state of Fe decreased after V doping. DFT calculations (Figure 18b) predicts a lower over potential in OER for NiFeV-LDH, a narrower bandgap. In order to systematically investigate structure-activity relationship in NiFeM-LDHs for OER [139], various NiFeM-LDHs were prepared and onset potential and corresponded Tafel slope was analyzed during OER (Figure 18c). The incorporation of different atoms could efficiently lower the thermodynamic barrier or accelerate the process. Based on Figure 18d, e, the oxygen species absorption and electron transportation could also be facilitated through different alternatives.

What's more, in view of the outstanding performance of IrO_2 and RuO_2 in OER, introduction of a small amount of these noble metal ions also produces systems with excellent catalytic activity [140]. For example, Ir^{4+}-doped NiFe-LDH exhibited Pt-like HER performance [141]. The binding energies of the Ni and Fe cations in NiFeIr-LDH shifted positively compared to pristine NiFe-LDH, indicating changes to the electronic structure as a result of partial incorporation of Ir. An Ir-doping strategy can significantly enhance the dissociation kinetics on NiFe-LDH. Apart from doping atoms into NiFe-LDH, Ru lattice-doped CoCr-LDH also exhibited enhanced OER activity.[63] In the

HRTEM-STEM images (Figure 18f), the brighter Ru atoms were incorporated in the lattice fringes rather as isolated atomic spots, confirming successful lattice doping. Furthermore, in the Ru EXAFS only Ru-O bonded featured was observed in CoCrRu-LDHs, indicating the atomic dispersion of Ru atom in the LDH layers. Theoretical calculations (Figure 18g) demonstrated that Ru doping can enhance the activity of the Co cations toward OER via getting more electrons from Cr. Furthermore, compared with other MCrRu-LDHs (M = Mg^{2+}, Ni^{2+}, Cu^{2+}, and Zn^{2+}), CoCrRu-LDHs recorded the best activity, confirming the significance of Ru atoms to facilitate OER performance.

Besides, the hierarchical ternary LDHs fabricated from MOFs through a simple self-template strategy have exhibited the superior performance for water splitting and beyonds, which could attributed to that their large surface area and elastic cavity favorable for the promotion of electrical conductivity and mass transfer capability [16]. For instance, a series of hierarchical multi-metal containing LDHs composed of monolayer nanosheets were constructed from oxalate MOFs [142]. Among them, CoNiFe-LDH showed the smaller overpotential of 248 mV at a current density of 10 mA cm^{-2} with a Tafel slope of 38 mV dec^{-1} for OER compared with NiFe-LDH and CoFe-LDH, indicating that the incorporation of Ni or Co had an effect on the modulation of electronic structure for supported LDHs to enhance the reaction kinetics. In addition, *via* changing the Ni/Co ratio, the obtained LDHs with sheet-like morphology achieved a poor OER activity than that of CoNiFe-LDH with octahedral morphology, proving the important role of hierarchical architecture in OER. Similarly, the ternary NiCoFe-LDH hollow polyhedrons *in situ* growth on the surface of ZIF-67 also showed an enhanced OER performance compared with binary NiCo-LDH [143]. Furthermore, a hollow Rh-doped CoFe-LDH (CoFeRh-LDH) structure [144] was constructed by an efficient etching-doping strategy for overall water splitting, achieving a current density of 10 mA cm^{-2} at an overpotential of 28 mV for HER and 100 mA cm^{-2} at 245 mV for OER with cell voltage for overall water splitting of 1.46 V, giving an promising application in water splitting. The promoted performance could be ascribed to the Rh doping and the construction of hollow nano-triangle architecture by virtue of MOFs structure, improving the modulation of electron structure along with the generation of Fe vacancy and explosion of substantial active sites to facilitate the mass transfer and reaction kinetics for overall water splitting.

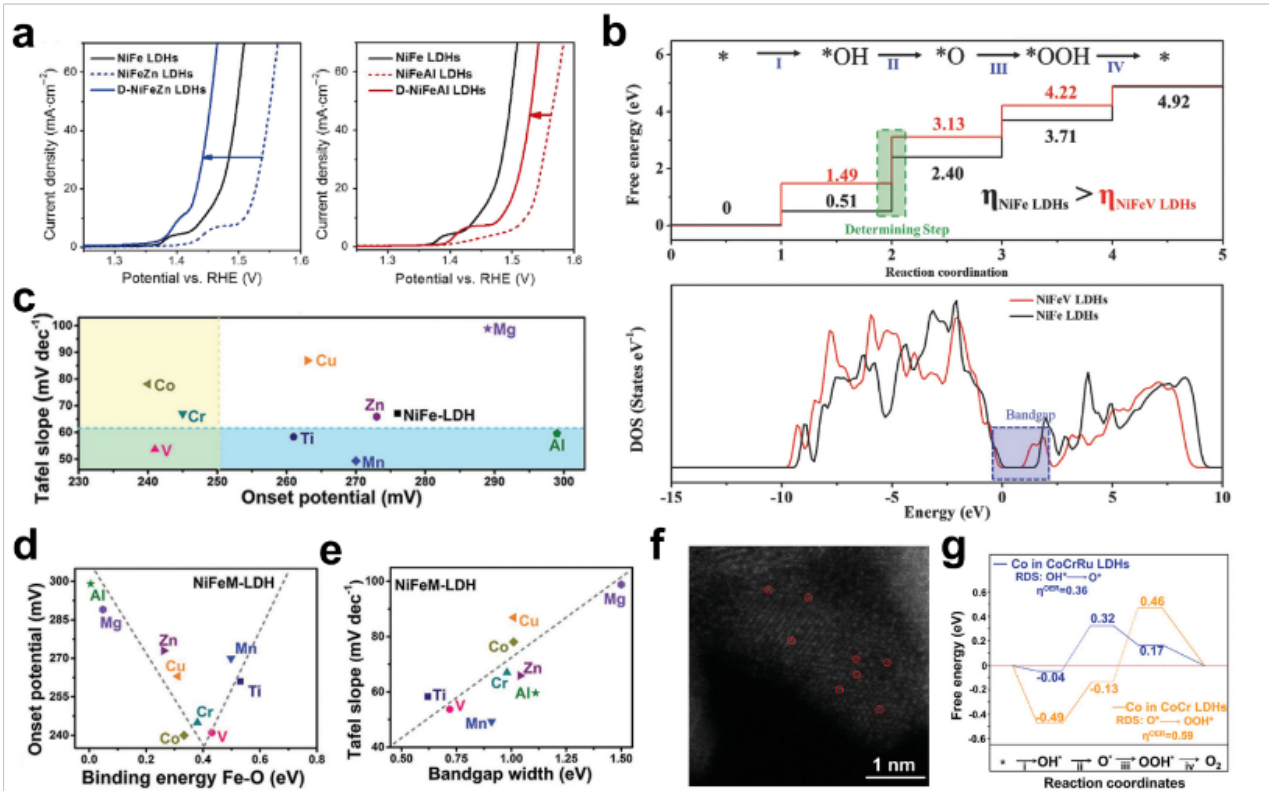

Figure 18. a) OER polarization curves of NiFeZn-LDH, D-NiFeZn-LDH, NiFeAl-LDH and D-NiFeAl-LDH. Reprinted with permission from [22]. Copyright 2018, Springer. b) Gibbs free energy diagram on NiFe-LDH (black line) and NiFeV-LDH (red line) and total density of states (TDOS) curves of NiFeV-LDH and NiFe-LDH. Reprinted with permission from [20]. Copyright 2018, Wiley-VCH. c) the analysis of onset potential and Tafel slope, d) the relationship of onset potential and the binding energy of Fe-O, e) the relationship of Tafel slope and the bandgap width. Reprinted with permission from [139]. Copyright 2021, Wiley-VCH. f) The Cs-corrected STEM image (red circles: bright Ru atoms), g) free energy diagrams of CoCrRu-LDH. Reprinted with permission from [63]. Copyright 2020, Wiley-VCH.

In addition, the doping of high-charge metal cations may lead to a further increase in the disorder of the LDH layer due to local perturbation of the metal coordination environments and electronic structure, in the limit would be the formation of oxyhydroxide-type materials. Zhang *et al.* incorporated W^{6+} in an FeCoW oxyhydroxides gel with amorphous phase via a room-temperature sol-gel process [41]. During the process distortion of WO_6 octahedra increased along with decrease in the average W charge, which then promoted oxidation of Co and Fe ions producing more active sites for OER (Figure 19a). What's more, crystalline–amorphous phase boundaries also enhanced OER activity (Figure 19b, c) by providing highly defective interfaces. Ternary Ni_5Co_3Mo−OH nanosheets was prepared via Mo doping [50]. The presence of Mo^{6+} significantly boosted the kinetics of NiCo−OH by facilitating charge transfer (Figure 19d, e) via O bridges among metal atoms.

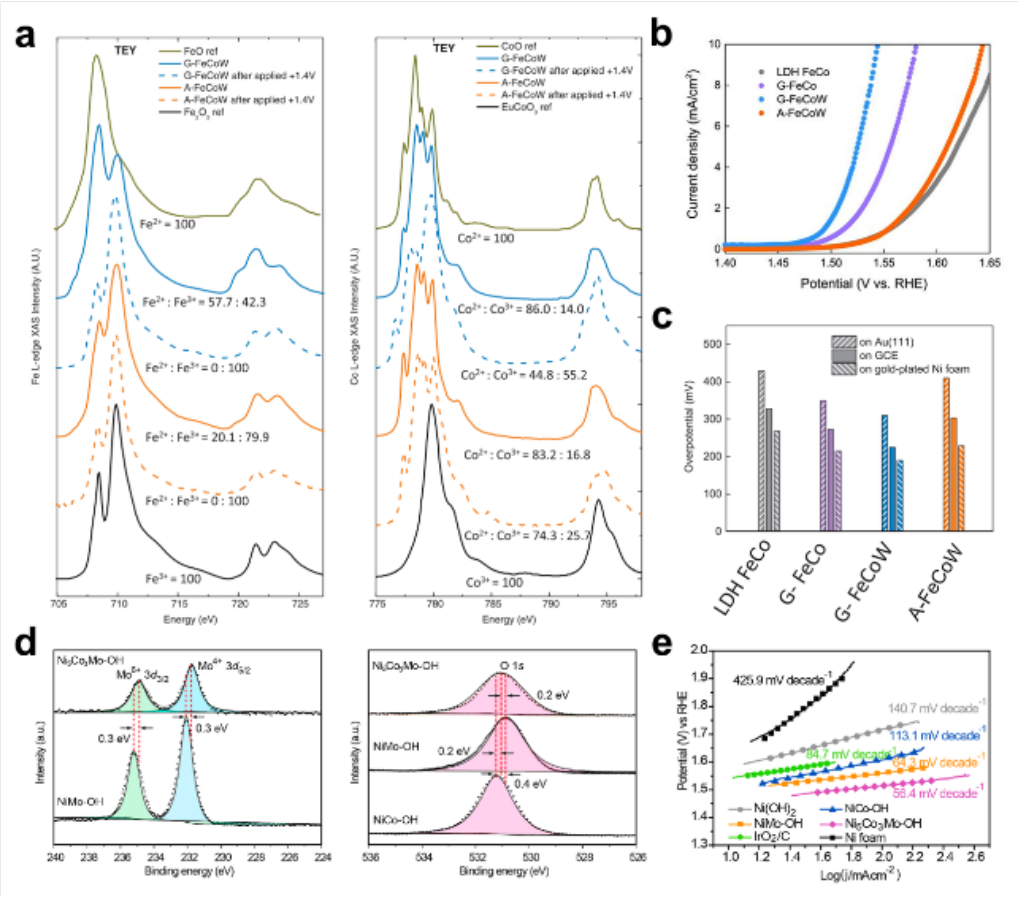

Figure 19. a) Surface-sensitive XAS scans at the Fe and Co L-edge, b) the OER polarization curve, c) overpotentials of FeCo-LDH and FeCoW oxyhydroxides. Reprinted with permission from [41]. Copyright 2016, American Association for the Advancement of Science. d) XPS spectra for Mo 3d and O 1s, e) Tafel plots toward OER of NiCo−OH, NiMo−OH, and Ni_5Co_3Mo−OH. Reprinted with permission from [50]. Copyright 2019, American Chemical Society.

3.1.2 Electrocatalytic organic reactions

In addition to electrolysis of water, electrocatalytic organic synthesis has also received extensive attention [145, 146]. It may provide an alternative, ecofriendly route that avoids high temperature and pressure conditions. In this area, most explorations have mainly focused on binary LDHs or NiX for hydroxymethylfurfural (HMF) conversion, however, multi-metallic LDHs are less researched. Ternary NiCoFe-LDH were observed to be efficient for OER and the conversion of HMF to the product 2,5-Furandicarboxylic acid (FDCA) (Figure 20a) [28]. According to atomic force microscopy (AFM) images, the incorporation of Fe changed the octahedral metal hydroxide layers and decreased the thickness. NiCoFe-LDH exhibited increased active sites, enhanced catalytic kinetics for OER after incorporating Fe into NiCo-LDH (Figure 20b). In addition, NiCoFe-LDHs showed improved performance for HMF conversion into FDCA (Figure 20c, d). The small overpotential and Tafel slope of HMF conversion may be attributed to thinner sheets along with more active sites.

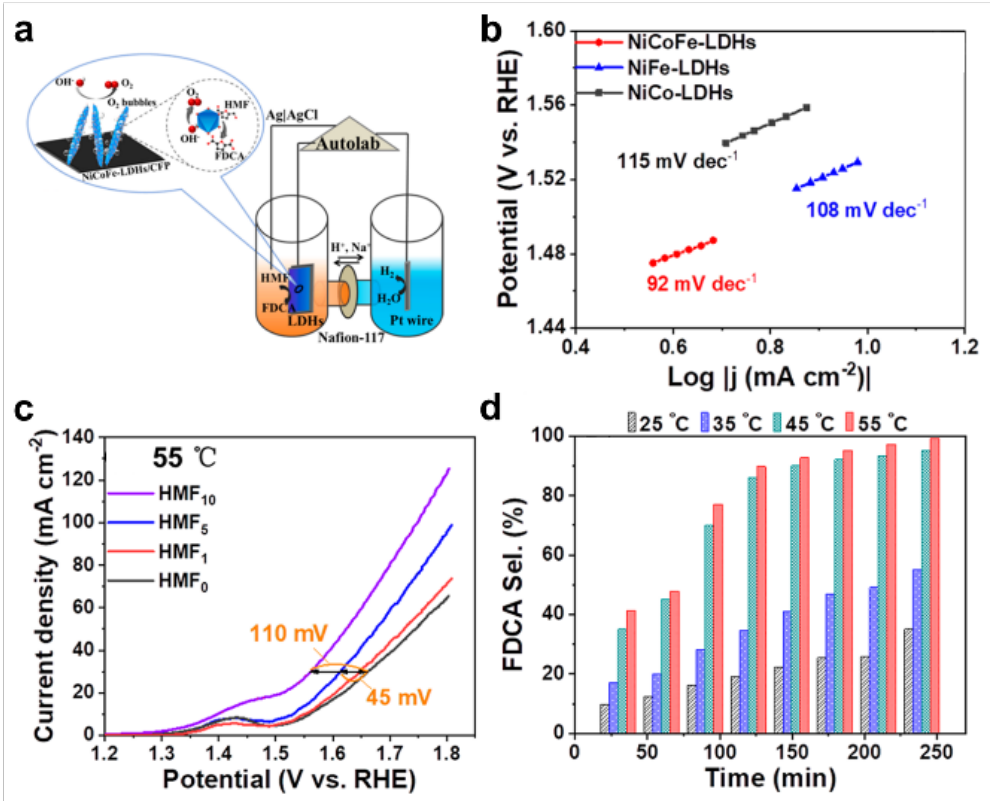

Figure 20. a) Schematic illustration of the electrochemical system of HMFOR, b) Tafel plots of NiCo-LDH, NiFe-LDH and NiCoFe-LDH for OER, c) polarization curves of NiCoFe-LDH, d) HMF conversion performance versus reaction time of NiCoFe-LDH [28]. Reprinted with permission from [28]. Copyright 2020, American Chemical Society.

Besides, hydrazine electrooxidation has been widely explored. Ru SA/NiFe-LDH (Figure 21a) was prepared and exhibited good catalytic activity. [33]. Detailed studies showed that Ru atoms were precisely located above Fe atoms, the loading can reach go up to 7.0 wt% (Figure 21b). Furthermore, DFT calculations demonstrated that Ru SA could efficiently lower the reaction barrier and decrease band gap energy (Eg) for the electron conduction (Figure 21c, d). Similarly, atomically dispersed Rh on NiFe-LDH [35] also exhibited good catalytic performance that may be ascribed to the distortion of layers and introduction of defect sites by the Rh atoms.

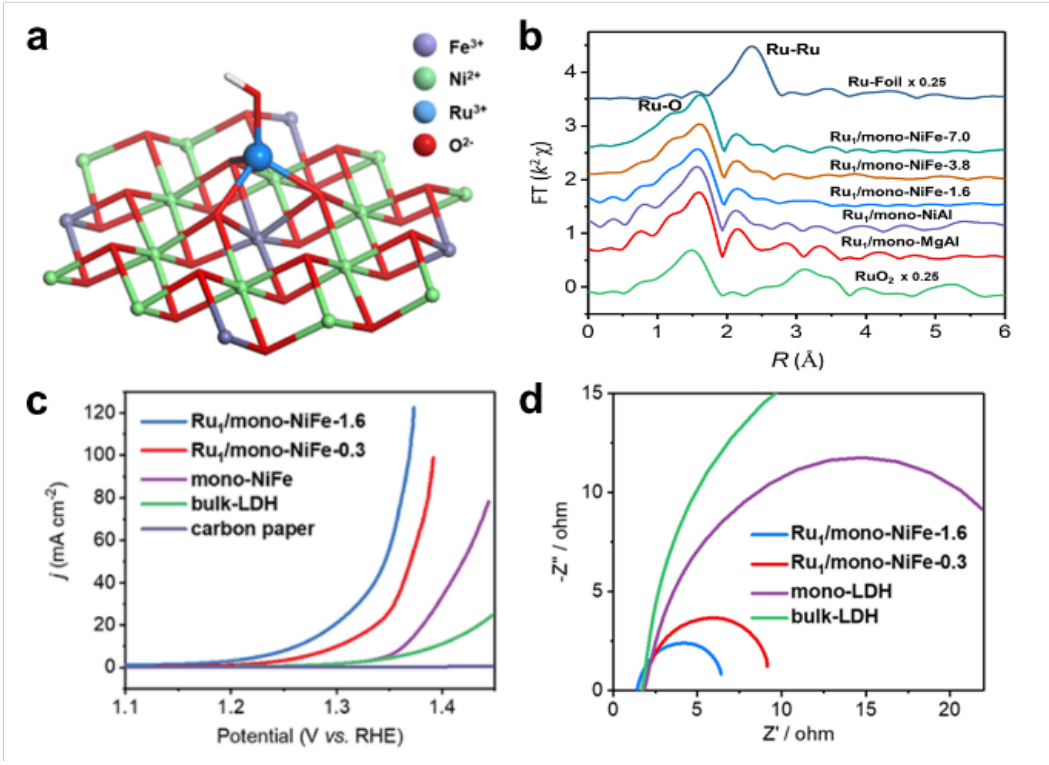

Figure 21. a) Schematic illustration of Ru/mono-NiFe-LDH, b) FT-EXAFS spectra, c) LSV curves of of Ru/mono-NiFe-LDH, mono-NiFe-LDH, bulk-NiFe-LDH and carbon paper, d) EIS of Ru/mono-NiFe-LDH, mono-NiFe-LDH and bulk-NiFe-LDH. Reprinted with permission from [33]. Copyright 2019, Royal Society of Chemistry.

3.2 Supercapacitors

Fiber supercapacitors (SCs) [147, 148] are being extensively researched as energy storage device of various equipment. Cu-doped NiCo-LDH with hierarchical structure (Figure 22a) has been prepared via *in situ* corrosion growth [48]. Both ultraviolet photoelectron spectroscopy (UPS) and Nyquist plots, indicated that Cu introduction could modulate the electronic structure to increased electrical conductivity and faster charge transfer kinetics (Figure 22b, c). The 3D multicomponent structure was also beneficial to allowing adequate electrolyte permeation. This unique structure and *in situ* Cu doping, delivered an electrode with a high specific capacitance and cycling stability (Figure 22d, e). In addition to the electronic structure regulation [149, 150], morphology modulation was also found to promote supercapacitive performance. The changes to the microstructure and morphology of CC@$NiCo_2Al_x$-LDHs by varying the Al stoichiometry has been proven to have a great impact on electrochemical performance [45]. The higher specific capacitance of CC@$NiCo_2Al_x$-LDH over CC@$NiCo_2$-OH was a result of a mixed morphology of nanowires and nanosheets enhancing the exposure of active sites. Faster ion transport, electrolyte accessibility, and morphology stability could be all ascribed to increased crystallinity after the introduction of Al.

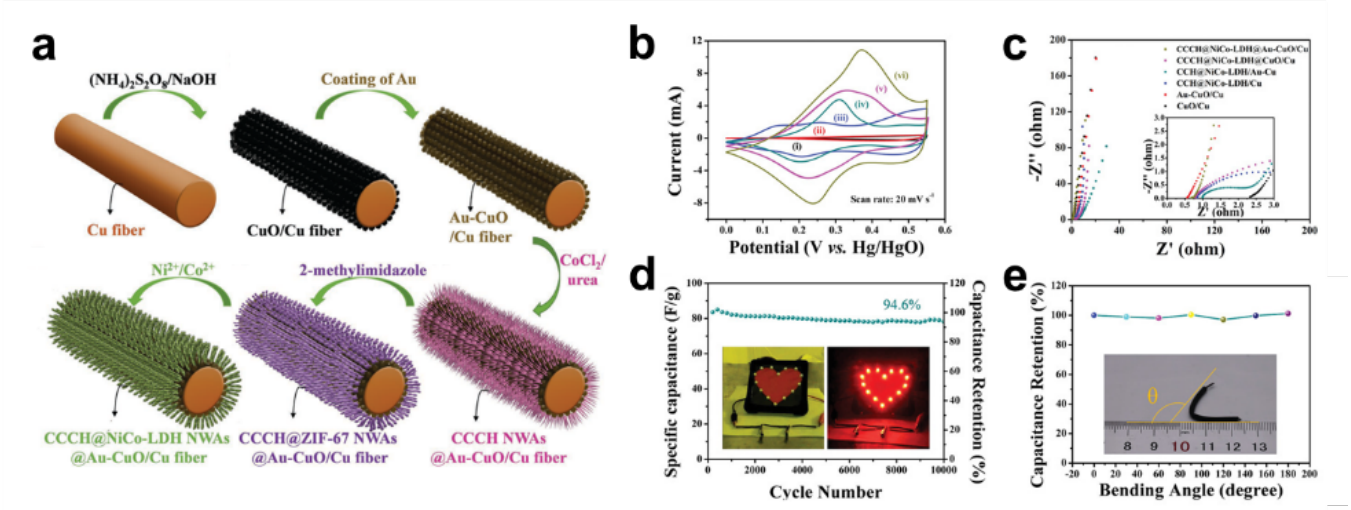

Figure 22. a) Schematic illustration, b) cyclic voltammetry (CV) curves and c) Nyquist plots of the prepared samples, d) long-term cycling performance. e) capacitance retention of hybrid fiber supercapacitor. Reprinted with permission from [48]. Copyright 2019, Wiley-VCH.

3.3 Photocatalysis

Taking inspiration from photosynthesis, the photoreduction of CO_x to hydrocarbons is considered as one of the key strategies for mitigating the energy crisis along with solar energy utilization in order to promote a sustainable future.[14] The traditional photocatalysts exhibits catalytic activity only under UV light irradiation due to the wide bandgap of the active material, this of course significantly limits the utilization of the solar spectrum. Efficient capture of visible–near-infrared (NIR) photons is challenging due to their relatively low energy [151]. Researchers are increasingly making greater use of solar spectrum by expanding the response to visible and infrared light [152, 153].

3.3.1 Photocatalytic CO_2 reduction

Photocatalytic CO_2 reduction to hydrocarbon fuels is an important strategic target that could mitigate energy consumption as well as global warming. However, CO_2 activation is challenging in part due to the strength of the C=O bond. Particularly, CO_2 reduction into CH_4 still difficult, due to the unfavorable kinetics ascribed to a series of multi-electron transfer process [154]. LDHs has been explored as potential photocatalysts [14, 81] attributed to their adjustable band gap and various active sites [39]. Tanaka *et al.* reported the CO_2 photocatalytic conversion on various M^{2+}-M^{3+}-LDHs, they successfully demonstrated the conversion of CO_2 (dissolved in water) into CO and O_2.[155] LDHs was firstly applied on photocatalytic CO_2 reduction by Izumi *et al.* in 2011 [156]. They found the Cu in LDH were the mainly active site. Nickel-based catalysts have high methane activity [157-160], NiCoFe-LDH with various vacancies was applied in CO_2PR and exhibited enhanced activity [39]. DFT study of NiCoFe-LDH highlighted that new defect levels were generated in the middle of the band gap leading to a decreased bandgap and facilitated electrical conductivity of NiCoFe-LDH (Figure 23a), which leading to high CH_4 selectivity (Figure 23b). In a further example, Ru@FL-LDH consisting of ultrathin MgAl-LDH and Ru nanoparticles exhibited improved

catalytic activity for the photothermal reduction of CO_2 [161]. Compared with other Ru-loaded catalysts, Ru@FL-LDH achieved light-absorption across the whole spectral region from the UV–vis–NIR. Ru@FL-LDH maintained a reaction temperature ≈350°C while FL-LDHs reached 67°C, confirming that the Ru nanoparticles was favorable for photo-thermal conversion, dramatically increasing the local temperature under irradiation (Figure 23c). This exfoliated LDHs and Ru nanoparticle system demonstrated highly-efficient catalytic performance recording a 99.3% of selectivity for CH_4 (Figure 23d).

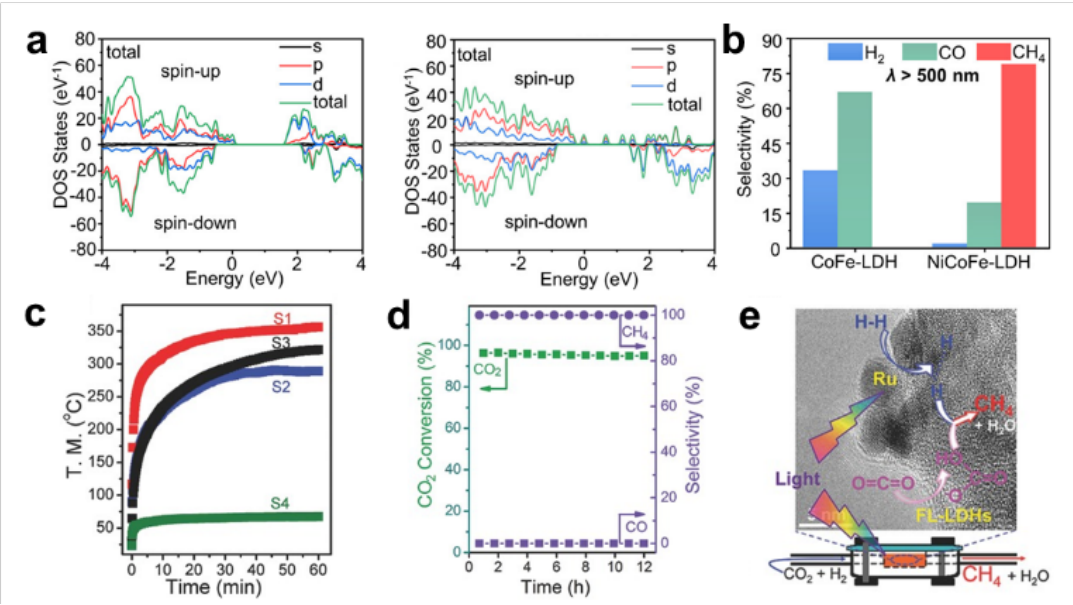

Figure 23. a) The calculated total DOS (TDOS) and partial DOS (PDOS) plots and b) selectivity of CH_4, CO, and H_2. Reprinted with permission from [39]. Copyright 2020, American Chemical Society. c) temperature monitoring (T.M.) of catalysts and FL-LDHs matrix, d) long-term test. Reprinted with permission from [161]. Copyright 2017, Wiley-VCH.

3.3.2 Solar-driven CO hydrogenation

Light olefins are raw materials for production of various chemical products (such as polymers, drugs, etc). Indirect routes of olefin synthesis involve the Fischer–Tropsch (FT) process, which was typically carried out under severe conditions. By contrast, photocatalysis using visible light was promising approach for small molecules conversion to high-valuable products, including hydrocarbons. The photothermal catalyst, Co-450 prepared at 450°C from ZnCoAl-LDH, consisted of Co and Co_3O_4 supported on a $ZnO–Al_2O_3$ (Figure 24a). This material showed remarkable CO hydrogenation activity [98] (Figure 24b). This heterostructure could weaken the hydrogenation activity of Co, causing to high selectivity to olefins (Figure 24c). Similar photothermal CO/CO_2 hydrogenation can be also found in ternary CoFeAl-LDH, ZnFeAl-LDH, and NiFeAl-LDH structure, etc. Another example is Cu@(CuCo-alloy) on Al_2O_3 (denoted as Cu@(CuCo-alloy)/Al_2O_3) that can be fabricated from CuCoAl-LDH [101]. The XPS and *in situ* FTIR data suggested that electron transportation may weaken the C–O bond of the adsorbed CO thus facilitating dissociation and enhancing hydrogenation to alcohols (Figure 24d, e).

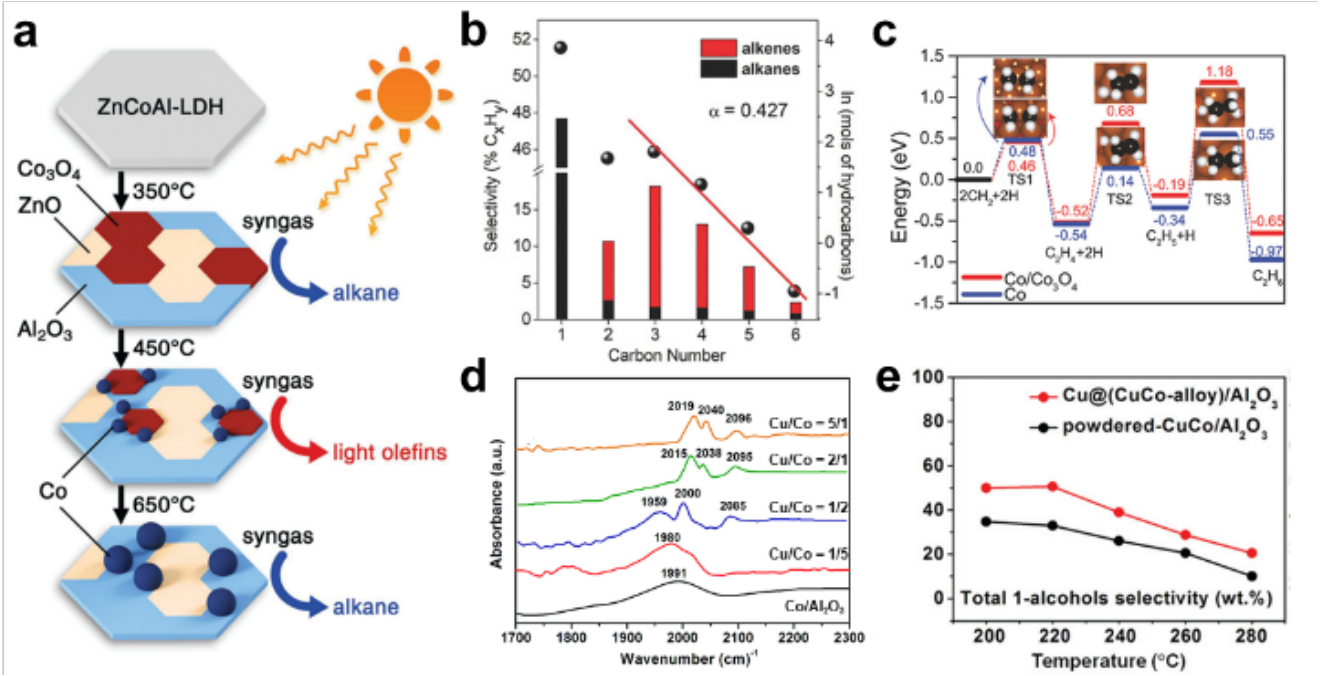

Figure 24. a) Synthesis of Co-x catalysts and their products selectivity for CO hydrogenation under UV–vis irradiation, b) the hydrocarbon product, c) potential energy profile. Reprinted with permission from [98]. Copyright 2018, Wiley-VCH. d) *in situ* FTIR spectra, e) catalytic performances of Cu@(CuCo-alloy)/Al_2O_3 and powdered-CuCo/Al_2O_3. Reprinted with permission from [101]. Copyright 2015, Royal Society of Chemistry.

3.3.3 Organic oxidation reactions

Compared with thermochemical reactions employing high temperatures and pressures, photocatalytic oxidation reaction could drive chemical transformations under mild conditions via highly active radicals, such as hydroxyl (·OH) or superoxide ($\cdot O_2^-$) [162, 163]. The series of Zn_xTi-LDH (x = 1, 2, 3, 4) catalysts were highly selective for the photooxidation of benzene to phenol in water under UV-vis light irradiation (Figure 25a) [164]. XAFS analysis indicated the Ti of ZnTi-LDH may exist with low valence ($Ti^{\delta+}$, $3 < \delta < 4$) than TiO_2 (Figure 25b) which is accompanied by coordinative unsaturation and an abundance of oxygen vacancies. As shown in Figure 25c, ZnTi-LDH exhibited ESR signal at g = 1.996, ascribed to the existence of Ti^{3+} due to the formation of oxygen vacancies. Thus, octahedrally distorted TiO_6 sites and abundant oxygen vacancies facilitated charge carrier separation/transportation the generation of $\cdot O_2^-$ to deliver excellent catalytic performance (Figure 25d).

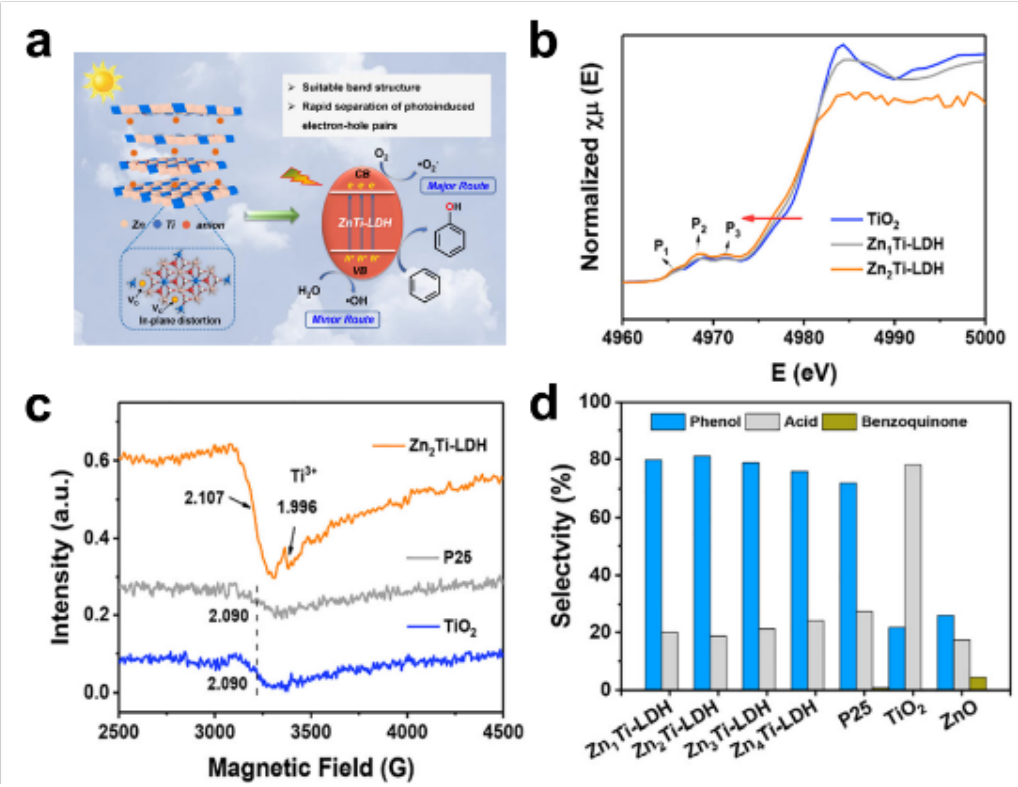

Figure 25. a) Schematic diagram highly selective oxidation of benzene to phenol in water using $ZnTi^{3+}Ti^{4+}$-LDH under UV-vis light irradiation, b) Ti K-edge XANES spectra, c) ESR spectra, d) Selectivity of phenol, oxalic acid, and benzoquinone. Reprinted with permission from [164]. Copyright 2020, Elsevier.

3.4 Environmental and biological applications

In addition, through introducing elements with specific physical/chemical properties, multi-metallic LDHs has also exhibited excellent catalytic activity in the fields of environmental energy and biological anti-cancer, bacteriostatic and other fields.

3.4.1 Wastewater treatment

Water pollution have become a serious environmental issue influencing our health. Today, the Fenton reaction was very effective in wastewater treatment for removing hazardous organics in wastewater. Besides iron-containing species, other transition metals exhibiting at least two oxidation states such as Mn, Cr, Ru and Cu have been proven to be active for Fenton reaction [165-168]. In this study, a series of CuNiSn-LDHs were prepared for phenol degradation [169]. Electron transfer between multivalent metal ions in LDH via metal–oxo–metal (M-O-M) bridges could promote rapid regeneration of highly active Cu^+ ions for superior performance (Figure 26a). Furthermore, with a low Cu/Ni ratio, $Cu(OH)_3Cl_3$ octahedra with a shorter Cu-Cl bonds could be formed, which could further promote electron transfer between Cu and other MO_6 octahedra via Cu-Cl-M linkages (Figure 26b). $Cu_1Ni_2Sn_{0.75}$-LDH could converse 97.8% phenol with better stability.

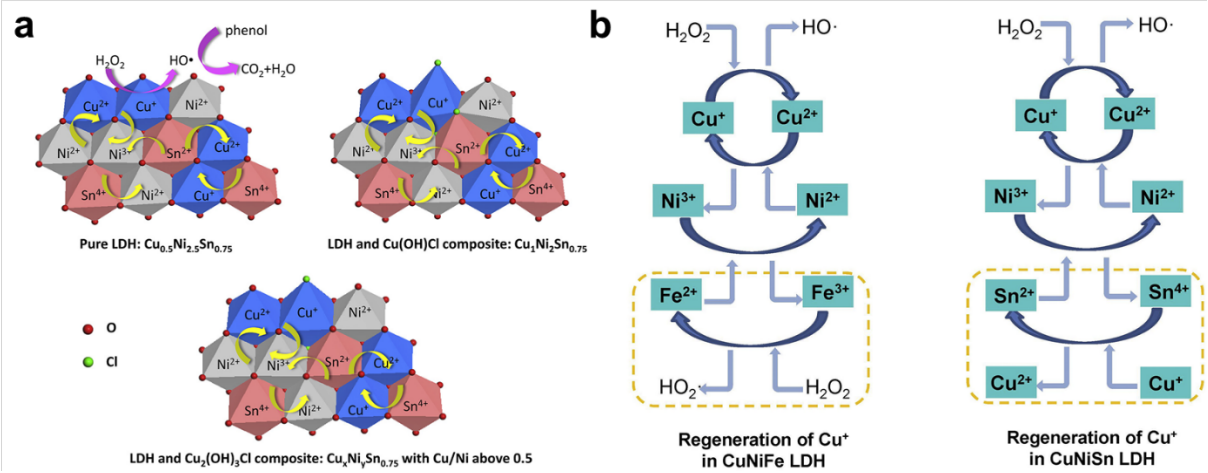

Figure 26. a) Scheme illustration degradation of phenol over CuNiSn-LDH catalyst, b) the regeneration way of Cu^+ active species in conventional Fenton catalysts, CuNiFe-LDH and CuNiSn-LDH. Reprinted with permission from [169]. Copyright 2020, Elsevier.

3.4.2 Heavy metal mineralization/reutilization

Adsorption from soil has become promising strategy to remove arsenic and other anionic heavy metals without by-products [170, 171]. CaMgFe-LDH was applied for arsenic immobilization and showed excellent performance [43].The XRD patterns showed only the diffraction features of MgFe-LDH after As^{3+} removal, indicating no CaFe-LDH produced. It was concluded that the Ca leached from the ternary LDHs to precipitate As^{3+} for efficient removal. What's more, LDHs containing a higher content of Ca exhibited an even higher removal capacity. In addition, the low leaching of Mg from the LDH demonstrated the stability of MgFe-LDH, which favored the $H_2AsO_3^-$ entering the interlayer through anion exchange. Similar to this work, MgCaFe-LDH exhibited good removal of pyrophosphate (PP) and triphosphate (TPP) in water [172]. The Ca release [173] was attributed to the anions precipitation, while anion exchange of MgX-LDH was benefit for immobilization of anions. Besides, $Mo_3S_{13}^{2-}$ intercalated in MgAl-LDH exhibited excellent performance for capture of Ag^+ ions [174]. At low [Ag^+], the interlayered $Mo_3S_{13}^{2-}$ could coordinate with Ag^+ to form $[Ag_x(Mo_3S_{13})_y]^{n-}$ anions which remained in the LDH interlayer galleries, when the [Ag^+] was high the S_2^{2-} and Mo^{4+} in $Mo_3S_{13}^{2-}$ could reduce Ag^+ into Ag^0. A similar adsorption mechanism was observed for low concentrations of Hg^{2+} and Cu^{2+}.

In addition to adsorbing anionic heavy metal pollutants in the interlayer region, LDHs can also immobilize heavy metal cations into the laminate through a unique isomorphous substitution process. Recently, Kong *et al.* discovered this property for LDH in the treatment of heavy metal pollution [175]. The ion exchange between Cd^{2+} and Ca^{2+} in CaAl-LDH causes the topotactic conversion of CaAl-LDH into CdAl-LDH to yield an ultra-stable mineralization structure (SSMS), Cd content in treated soil was below the national standard for three years in field experiments. Following this study, Chi *et al.* reported a detailed exploration on the super-stable mineralization of Ni^{2+} on CaFe-LDH [44]. XRD and XAFS confirmed the occurrence of isomorphous substitution and the formation of super-stable NiCaFe-LDH (Figure 27a). Theoretical calculations verified a super-stable mineralization process and the higher thermodynamics stability of NiCaFe-LDH compared to CaFe-LDH (Figure 27b, c). Therefore, CaFe-LDH can

purify ultra-high concentrations of Ni^{2+} and reduce the concentration of solutions containing trace Ni^{2+} ions in the wastewater to ppb levels. Moreover, NiCaFe-LDH showed excellent catalytic activity in electrocatalytic oxygen evolution and photocatalytic CO_2 reduction (Figure 27d), and has considerable potential for practical application. In short, stable ternary LDH can be formed through a super-stable mineralization process that not only efficiently treat heavy metal pollution, but also yield efficient photo/electrocatalysts.

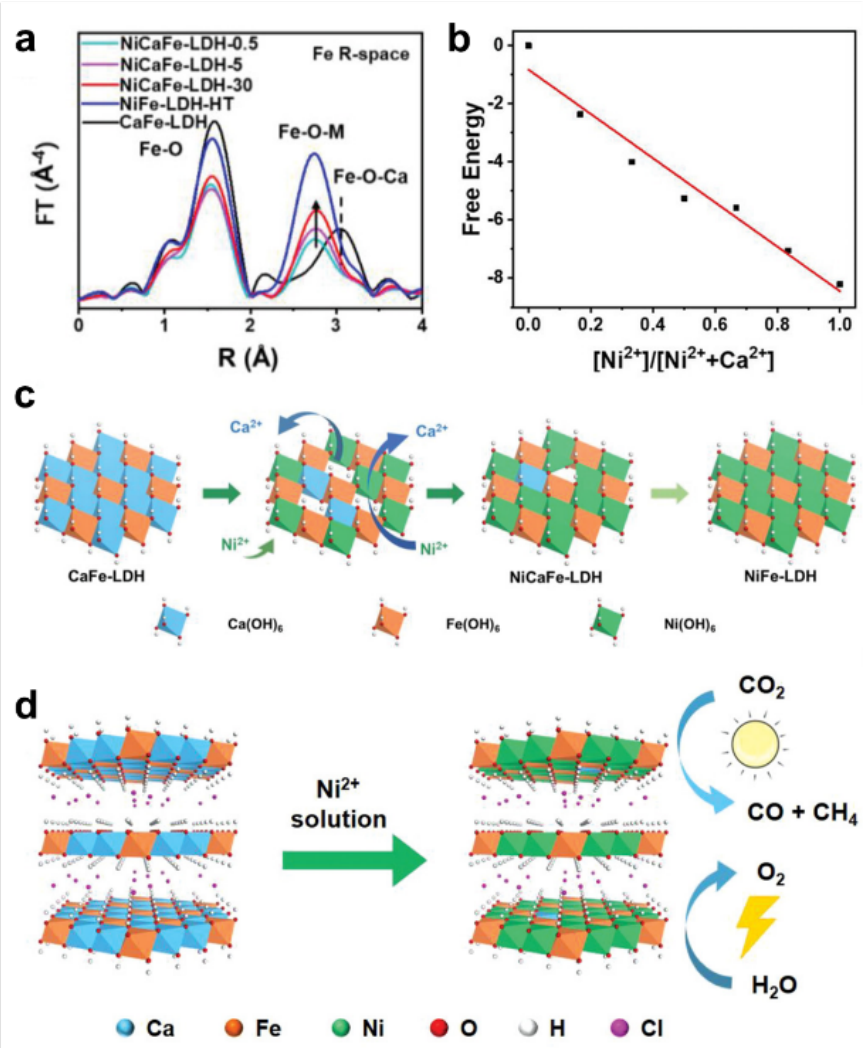

Figure 27. a) FT-EXAFS spectra, b) relationship between the Gibbs free energy and the ratio of $[Ni^{2+}]$ to $[Ni^{2+} + Ca^{2+}]$ in LDH, c) transformation from CaFe-LDH to NiFe-LDH, d) NiCaFe-LDH for OER and CO_2 reduction. Reprinted with permission from [44]. Copyright 2021, Wiley-VCH.

3.4.3 Cancer treatment

LDHs are currently attracting attention as nano-carriers for delivering various drugs and bio-active molecules attributed to low toxicity, good biocompatibility, and excellent anionic exchange capacity [13]. Recently, Gd^{3+} has been widely used in the application of clinical contrast agents for cancer diagnosis, since Gd^{3+} is an f^7 cation which is highly effective at shortening proton longitudinal relaxation times [176]. The ICG-DOX/Gd-LDH was prepared via intercalation of photothermal agent (indocyanine green, ICG) and chemotherapeutic drug (doxorubicin

hydrochloride, DOX) into the interlayer of Gd^{3+}doped LDH to create a chemo-photothermal synergistic therapeutic agent [177]. According the characterization experiments, the high-spin Gd^{3+} on the laminate significantly improved the NMR imaging, but also facilitated photogenerated electron-hole separation and transformation, leading to the generation of more reactive oxygen species under irradiation, facilitating photothermal therapeutic efficiency. In another case, a novel theragnostic system was formed by Au nanoclusters along with photosensitizer Chlorin e6 supported Gd-incorporated LDH [178]. The prepared Ce&AuNCs/Gd-LDH (Figure 28a) exhibited enhanced magnetic resonance/fluorescence dual-modal imaging and excellent photodynamic therapy (PDT) activity on cancer treatment. And the electron transfer from AuNCs to LDHs was favorable for the improvement of fluorescence quantum yield (QY) from 3.1% to 18.5%, thus prompting magnetic resonance imaging (MRI) as well as fluorescence imaging activity.

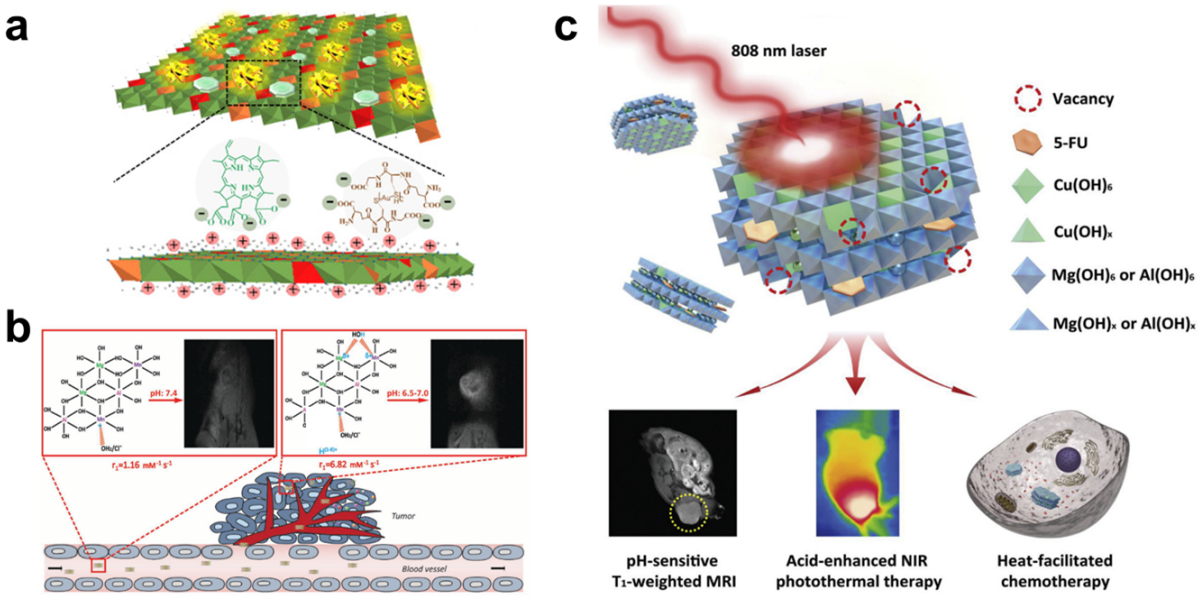

Figure 28. a) Schematic illustration for the structure. Reprinted with permission from [178]. Copyright 2018, Elsevier. b) Structure related multifunctional properties of Mn-containing MgAl-LDH nanoparticles. Reprinted with permission from [179]. Copyright 2017, Wiley-VCH. c) Schematic representation. Reprinted with permission from [180]. Copyright 2018, Elsevier.

Furthermore, Mn has been found to be an essential micronutrient for some enzymes and physiological processes, Mn^{2+}-based materials have been widely applied as an attractive alternative to Gd^{3+}-based T_1-weighted MRI contrast agents (CAs) [179, 180]. By incorporating Mn^{2+} into MgAl-LDH, Mn-LDH was prepared along with ultrasensitive pH response and ^1H relativity and showed enhanced MR imaging for tumor tissues at least 2 d *in vivo* (Figure 28b) [181]. According to the *in situ* EXAFS analysis, special microstructure of Mn was benefit for T_1 relaxation of protons, attributed to a pH-ultra-sensitivity in the T_1-weighted MRI. Similarly, defect-rich multifunctional Cu-doped LDH were synthesized by introducing Cu into MgAl-LDH [182]. The thermal images showed the photothermal conversion was dependent on Cu ratio. The photothermal transduction efficiency could be further promoted in acidic buffers (81.9%) compared to deionized water (53.1%) which is accompanied by more OH defects generation, which could be favorable for specifically improving the photothermal therapy in the acidic environment. The anticancer

drug 5-FU could be intercalated into Cu-LDH, enhancing the synergistic effect of chemotherapy and photothermal therapy to kill more cancer cells (Figure 28c).

3.4.4 Antibacterial application

Recently, LDHs have been indicated as potential inorganic building blocks to produce films and coatings on anti-corrosion, sensing as well as optical applications. For MgAl-LDH, silver ions can be easily converse to Ag NPs in aqueous solution without any reducing agents [172]. The prepared coatings showed enhanced antimicrobial activity against bacteria and efficiently prevent the biofilm generation of nutrient solutions when compared with control glass, which highlighted the high hydrophilicity of prepared Ag-LDH coatings. Similarly to this case, Ag-LDH coating was synthesized on Mg alloy for promoting antibacterial and degrading performance [183]. The prepared Ag-LDH coating could significantly inhibit bacterial proliferation to suppress the degradation of magnesium alloy. What's more, the calcined Ag-LDH showed stronger antibacterial performance over LDH [184]. During the test of simulating bacterial culture up to 5 days, any microbial growth could not be seen in the block of calcined Ag-LDH compared with pristine LDH, indicating the better antibacterial activity of calcined Ag-LDH, which may be further applied in the field of ceramics. Besides, Ti^{3+}doped ZnTi-LDH ($ZnTi^{3+}Ti^{4+}$-LDH) exhibited excellent visible light induced antibacterial activity in the antimicrobial studies of bacteria S. cerevisiae and S. aureus [185], which could be attributed to that $ZnTi^{3+}Ti^{4+}$-LDH with Ti^{3+} and oxygen vacancies was favorable for producing superoxide anion radicals, thus achieving the higher photocatalytic oxidation activity.

4. Summary and Outlook

In the review, we summarize the construction strategies for multi-metallic LDHs over recent years and their application for a range of functions and reactions. We focus on the influence of introducing the heteroatom on the modulation of morphology, electronic structure, lattice, crystal phase of the multi-metallic LDHs formed. The pivotal roles of structural modulation to deliver catalytic activity improvement are proposed, such as, creation of active sites to directly participate in reactions, improving electronic conductivity, lower molecular activation energy, and optimizing reaction pathways. We highlight the use of these materials to as catalysts for water splitting, CO_2 photoreduction, CO hydrogenation, heavy metal mineralization/reutilization etc. Although promising progress in the application of multi-metallic LDHs has been made, there still exist several pressing challenges, which on the other hand serve as huge opportunities for the future research. These challenges include:

(1) How to realize the controllable defect concentration of multi-metallic LDHs to facilitate the catalytic activity when introducing more active sites into layers of binary LDHs. As discussed above, defect sites (vacancy or amorphous phases) are more conducive to carrier transport, band gap adjustment, active intermediate species generation, and further facilitate catalytic performance in many processes. However, how to we accurately quantify and locate the defect sites is still a very demanding and significant task, and which will facilitate the controllable adjustment of active site-driven reaction selectivity and provide clear ideas for the design of high-efficiency catalysts.

(2) How to clearly reveal the reaction mechanism with the help of advanced characterization techniques. Compared with *ex situ* experiments, *in situ* experiments, such as XAS, XPS, FTIR, and Raman, have some real

advantages in revealing in the catalyst structure evolution and observing the reaction processes via analysis of the captured reaction intermediate active species due to the real-time and precise monitoring property. This will provide a more intuitive and clearer insight and understanding of the reaction mechanisms and provide stronger evidence to develop the structure-activity relationships.

(3) How can we take advantage of theoretical calculations to rationally design catalysts and predict reaction results. Though machine learning for algorithm, theoretical calculations could be applied to perform experimental simulation and results prediction. This would provide huge assistance in catalyst design.

(4) How can we design heterojunction structures to expand the application of LDHs. Rather than reaching the limitations of single material; heterojunction structures could realize multiple characteristics of each component through the assembly of different materials, thus driving efficient opto-electronic and photothermal coupling and the leap from homogeneous to heterogeneous reaction.

(5) How to define and understand multi-metallic LDHs more accurately. The deeper exploration and development of LDH-based materials have made the types and combinations of laminate metals more and more diversified, which means that the "D" of LDH (layered double hydroxide) have been derived from the original "double" to "multiple", these multi-metallic LDHs can be named as LMMH (layered multi-metallic hydroxides) for preciously describing the recent development of LDH. Therefore, this will require more understanding and summary from researchers to get a broader and more appropriate description or definition, which may be benefit for the more detailed and deeper exploration of LDHs.

In summary, despite numerous challenges discussed here, it can be expected that continued research on multi-metallic LDHs would further unlock the potential of industrial application of LDHs-based materials in photo(electro)catalytic reactions in the future.

Author contributions

Chenjun Ning: Investigation, Writing - original draft. Sha Bai: Investigation, Data curation, Validation. Jikang Wang: Investigation, Data curation, Formal analysis. Zixian Li: Data curation, Formal analysis. Zhiyue Han: Formal analysis. Yufei Zhao: Conceptualization, Administration, Formal analysis, Writing – review. Dermot O'Hare: Conceptualization, Formal analysis, Writing – review. Yu-Fei Song: Conceptualization, Administration, Formal analysis, Review & editing.

Declaration of Competing Interest

The authors declare that they have no known competing financial interests or personal relationships that could have appeared to influence the work reported in this paper.

Acknowledgements

This research was supported by the National Nature Science Foundation of China (22090032, 22090030, 22288102, 22278030, 21922801, 22011530162) and Major Program of Qingyuan Innovation Laboratory (Grant No. 001220005).

Reference

[1] Z.J. Wang, H. Song, H. Liu, J. Ye, Coupling of solar energy and thermal energy for carbon dioxide reduction: status and prospects, Angew. Chem. Int. Ed. 59 (2020) 8016-8035. https://doi.org/10.1002/anie.201907443.

[2] L. Lv, Z. Yang, K. Chen, C. Wang, Y. Xiong, 2D layered double hydroxides for oxygen evolution reaction: from fundamental design to application, Adv. Energy Mater. 9 (2019) 1803358. https://doi.org/10.1002/aenm.201803358.

[3] X. Chang, T. Wang, P. Yang, G. Zhang, J. Gong, The development of cocatalysts for photoelectrochemical CO_2 reduction, Adv. Mater. 31 (2019) 1804710. https://doi.org/10.1002/adma.201804710.

[4] D. Yan, Y. Li, J. Huo, R. Chen, L. Dai, S. Wang, Defect chemistry of nonprecious-metal electrocatalysts for oxygen reactions, Adv. Mater. 29 (2017) 1606459. https://doi.org/10.1002/adma.201606459.

[5] K.S. Novoselov, A.K. Geim, S.V. Morozov, D. Jiang, Y. Zhang, S.V. Dubonos, I.V. Grigorieva, A.A. Firsov, Electric field effect in atomically thin carbon films, Science 306 (2004) 666-669. https://doi.org/10.1126/science.1102896.

[6] C. Tan, X. Cao, X.J. Wu, Q. He, J. Yang, X. Zhang, J. Chen, W. Zhao, S. Han, G.H. Nam, M. Sindoro, H. Zhang, Recent advances in ultrathin two-dimensional nanomaterials, Chem. Rev. 117 (2017) 6225-6331. https://doi.org/10.1021/acs.chemrev.6b00558.

[7] Y. Sun, S. Gao, F. Lei, C. Xiao, Y. Xie, Ultrathin two-dimensional inorganic materials: new opportunities for solid state nanochemistry, Acc. Chem. Res. 48 (2015) 3-12. https://doi.org/10.1021/ar500164g.

[8] J. Wang, M. Li, M. Xu, J. Li, Y. Zhao, H. Duan, Chapter 1. Recent developments and perspectives on solar-driven fine chemicals synthesis: from the reaction system to 2D photocatalysts, Photocatalysis Using 2D Nanomaterials, (2022) 1-64. https://doi.org/10.1039/9781839164620-00001.

[9] Y. Guo, K. Xu, C. Wu, J. Zhao, Y. Xie, Surface chemical-modification for engineering the intrinsic physical properties of inorganic two-dimensional nanomaterials, Chem. Soc. Rev. 44 (2015) 637-646. https://doi.org/10.1039/c4cs00302k.

[10] D. Deng, K.S. Novoselov, Q. Fu, N. Zheng, Z. Tian, X. Bao, Catalysis with two-dimensional materials and their heterostructures, Nat. Nanotechnol. 11 (2016) 218-230. https://doi.org/10.1038/nnano.2015.340.

[11] A. Gupta, T. Sakthivel, S. Seal, Recent development in 2D materials beyond graphene, Prog. Mater. Sci. 73 (2015) 44-126. https://doi.org/10.1016/j.pmatsci.2015.02.002.

[12] W. Feitknecht, M. Gerber, Regarding double hydroxides and alkaline double salts III. About magnesium aluminum double hydroxide, Helv. Chim. Acta 25 (1942) 131-137. https://doi.org/10.1002/hlca.19420250115.

[13] T. Hu, Z. Gu, G.R. Williams, M. Strimaite, J. Zha, Z. Zhou, X. Zhang, C. Tan, R. Liang, Layered double hydroxide-based nanomaterials for biomedical applications, Chem. Soc. Rev. 51 (2022) 6126-6176. https://doi.org/10.1039/d2cs00236a.

[14] Y. Zhao, G.I.N. Waterhouse, G. Chen, X. Xiong, L.-Z. Wu, C.-H. Tung, T. Zhang, Two-dimensional-related catalytic materials for solar-driven conversion of CO_x into valuable chemical feedstocks, Chem. Soc. Rev. 48 (2019) 1972-2010. https://doi.org/10.1039/c8cs00607e.

[15] Z.-Z. Yang, C. Zhang, G.-M. Zeng, X.-F. Tan, D.-L. Huang, J.-W. Zhou, Q.-Z. Fang, K.-H. Yang, H. Wang, J. Wei, K. Nie, State-of-the-art progress in the rational design of layered double hydroxide based photocatalysts for photocatalytic and photoelectrochemical H_2/O_2 production, Coord. Chem. Rev. 446 (2021) 214103-214129. https://doi.org/10.1016/j.ccr.2021.214103.

[16] G. Wang, D. Huang, M. Cheng, S. Chen, G. Zhang, L. Lei, Y. Chen, L. Du, R. Li, Y. Liu, Metal-organic frameworks template-directed growth of layered double hydroxides: A fantastic conversion of functional materials, Coord. Chem. Rev. 460 (2022) 214467-214488. https://doi.org/10.1016/j.ccr.2022.214467.

[17] H. Ye, S. Liu, D. Yu, X. Zhou, L. Qin, C. Lai, F. Qin, M. Zhang, W. Chen, W. Chen, L. Xiang, Regeneration mechanism, modification strategy, and environment application of layered double hydroxides: Insights based on memory effect, Coord. Chem. Rev. 450 (2022) 214253-214274. https://doi.org/10.1016/j.ccr.2021.214253.

[18] Q. Yu, C. Li, D. Ma, J. Zhao, X. Liu, C. Liang, Y. Zhu, Z. Zhang, K. Yang, Layered double hydroxides-based materials as novel catalysts for gaseous VOCs abatement: Recent advances and mechanisms, Coord. Chem. Rev. 471 (2022) 214738-214759. https://doi.org/10.1016/j.ccr.2022.214738.
[19] Z. Cai, D. Zhou, M. Wang, S.M. Bak, Y. Wu, Z. Wu, Y. Tian, X. Xiong, Y. Li, W. Liu, S. Siahrostami, Y. Kuang, X.Q. Yang, H. Duan, Z. Feng, H. Wang, X. Sun, Introducing Fe^{2+} into nickel-iron layered double hydroxide: local structure modulated water oxidation activity, Angew. Chem. Int. Ed. 57 (2018) 9392-9396. https://doi.org/10.1002/anie.201804881.
[20] P. Li, X. Duan, Y. Kuang, Y. Li, G. Zhang, W. Liu, X. Sun, Tuning electronic structure of NiFe layered double hydroxides with vanadium doping toward high efficient electrocatalytic water oxidation, Adv. Energy Mater. 8 (2018) 1703341-1703347. https://doi.org/10.1002/aenm.201703341.
[21] H. Liu, Y. Wang, X. Lu, Y. Hu, G. Zhu, R. Chen, L. Ma, H. Zhu, Z. Tie, J. Liu, Z. Jin, The effects of Al substitution and partial dissolution on ultrathin NiFeAl trinary layered double hydroxide nanosheets for oxygen evolution reaction in alkaline solution, Nano Energy 35 (2017) 350-357. https://doi.org/10.1016/j.nanoen.2017.04.011.
[22] Q. Xie, Z. Cai, P. Li, D. Zhou, Y. Bi, X. Xiong, E. Hu, Y. Li, Y. Kuang, X. Sun, Layered double hydroxides with atomic-scale defects for superior electrocatalysis, Nano Res. 11 (2018) 4524-4534. https://doi.org/10.1007/s12274-018-2033-9.
[23] J. Jiang, F. Sun, S. Zhou, W. Hu, H. Zhang, J. Dong, Z. Jiang, J. Zhao, J. Li, W. Yan, M. Wang, Atomic-level insight into super-efficient electrocatalytic oxygen evolution on iron and vanadium co-doped nickel (oxy)hydroxide, Nat. Commun. 9 (2018) 2885-2896. https://doi.org/10.1038/s41467-018-05341-y.
[24] K.N. Dinh, P. Zheng, Z. Dai, Y. Zhang, R. Dangol, Y. Zheng, B. Li, Y. Zong, Q. Yan, Ultrathin porous NiFeV ternary layer hydroxide nanosheets as a highly efficient bifunctional electrocatalyst for overall water splitting, Small 14 (2018) 1703257. https://doi.org/10.1002/smll.201703257.
[25] Y. Yang, L. Dang, M.J. Shearer, H. Sheng, W. Li, J. Chen, P. Xiao, Y. Zhang, R.J. Hamers, S. Jin, Highly active trimetallic NiFeCr layered double hydroxide electrocatalysts for oxygen evolution reaction, Adv. Energy Mater. 8 (2018) 1703189. https://doi.org/10.1002/aenm.201703189.
[26] X. Xie, C. Cao, W. Wei, S. Zhou, X.T. Wu, Q.L. Zhu, Ligand-assisted capping growth of self-supporting ultrathin FeNi-LDH nanosheet arrays with atomically dispersed chromium atoms for efficient electrocatalytic water oxidation, Nanoscale 12 (2020) 5817-5823. https://doi.org/10.1039/c9nr10781a.
[27] D. Zhou, Z. Cai, Y. Jia, X. Xiong, Q. Xie, S. Wang, Y. Zhang, W. Liu, H. Duan, X. Sun, Activating basal plane in NiFe layered double hydroxide by Mn^{2+} doping for efficient and durable oxygen evolution reaction, Nanoscale Horiz. 3 (2018) 532-537. https://doi.org/10.1039/c8nh00121a.
[28] M. Zhang, Y. Liu, B. Liu, Z. Chen, H. Xu, K. Yan, Trimetallic NiCoFe-layered double hydroxides nanosheets efficient for oxygen evolution and highly selective oxidation of biomass-derived 5-hydroxymethylfurfural, ACS Catal. 10 (2020) 5179-5189. https://doi.org/10.1021/acscatal.0c00007.
[29] D. Zhou, Z. Cai, X. Lei, W. Tian, Y. Bi, Y. Jia, N. Han, T. Gao, Q. Zhang, Y. Kuang, J. Pan, X. Sun, X. Duan, NiCoFe-layered double hydroxides/N-doped graphene oxide array colloid composite as an efficient bifunctional catalyst for oxygen electrocatalytic reactions, Adv. Energy Mater. 8 (2018) 1701905. https://doi.org/10.1002/aenm.201701905.
[30] Z. Cai, L. Li, Y. Zhang, Z. Yang, J. Yang, Y. Guo, L. Guo, Amorphous nanocages of Cu-Ni-Fe hydr(oxy)oxide prepared by photocorrosion For highly efficient oxygen evolution, Angew. Chem. Int. Ed. 58 (2019) 4189-4194. https://doi.org/10.1002/anie.201812601.
[31] X. Xu, F. Song, X. Hu, A nickel iron diselenide-derived efficient oxygen-evolution catalyst, Nat. Commun. 7 (2016) 12324-12330. https://doi.org/10.1038/ncomms12324.
[32] R. Li, Y. Wang, W. Li, S. Zhou, P. Tian, H. Gao, X. Liu, J. Zang, Ternary NiFeZr layered double hydroxides: a highly efficient catalyst for the oxygen evolution reaction, Chem. Commun. 55 (2019) 13370-13373. https://doi.org/10.1039/c9cc06219j.
[33] Z. Wang, S.-M. Xu, Y. Xu, L. Tan, X. Wang, Y. Zhao, H. Duan, Y.-F. Song, Single Ru atoms with precise coordination on a monolayer layered double hydroxide for efficient electrooxidation catalysis, Chem. Sci. 10 (2019) 378-384.

https://doi.org/10.1039/c8sc04480e.
[34] G. Chen, T. Wang, J. Zhang, P. Liu, H. Sun, X. Zhuang, M. Chen, X. Feng, Accelerated hydrogen evolution kinetics on NiFe-layered double hydroxide electrocatalysts by tailoring water dissociation active sites, Adv. Mater. 30 (2018) 1706279. https://doi.org/10.1002/adma.201706279.
[35] G. Liu, Z. Wang, T. Shen, X. Zheng, Y. Zhao, Y.F. Song, Atomically dispersed Rh-doped NiFe layered double hydroxides: precise location of Rh and promoting hydrazine electrooxidation properties, Nanoscale 13 (2021) 1869-1874. https://doi.org/10.1039/d0nr07157a.
[36] L. Wu, L. Yu, F. Zhang, D. Wang, D. Luo, S. Song, C. Yuan, A. Karim, S. Chen, Z. Ren, Facile synthesis of nanoparticle-stacked tungsten-doped nickel iron layered double hydroxide nanosheets for boosting oxygen evolution reaction, J. Mater. Chem. A 8 (2020) 8096-8103. https://doi.org/10.1039/d0ta00691b.
[37] Q.Q. Chen, C.C. Hou, C.J. Wang, X. Yang, R. Shi, Y. Chen, Ir^{4+}-doped NiFe LDH to expedite hydrogen evolution kinetics as a Pt-like electrocatalyst for water splitting, Chem. Commun. 54 (2018) 6400-6403. https://doi.org/10.1039/c8cc02872a.
[38] J. Zhang, J. Liu, L. Xi, Y. Yu, N. Chen, S. Sun, W. Wang, K.M. Lange, B. Zhang, Single-atom Au/NiFe layered double hydroxide electrocatalyst: probing the origin of activity for oxygen evolution reaction, J. Am. Chem. Soc. 140 (2018) 3876-3879. https://doi.org/10.1021/jacs.8b00752.
[39] X. Hao, L. Tan, Y. Xu, Z. Wang, X. Wang, S. Bai, C. Ning, J. Zhao, Y. Zhao, Y.-F. Song, Engineering active Ni sites in ternary layered double hydroxide nanosheets for a highly selective photoreduction of CO_2 to CH_4 under Irradiation above 500 nm, Ind. Eng. Chem. Res. 59 (2020) 3008-3015. https://doi.org/10.1021/acs.iecr.9b06464.
[40] P. Li, M. Wang, X. Duan, L. Zheng, X. Cheng, Y. Zhang, Y. Kuang, Y. Li, Q. Ma, Z. Feng, W. Liu, X. Sun, Boosting oxygen evolution of single-atomic ruthenium through electronic coupling with cobalt-iron layered double hydroxides, Nat. Commun. 10 (2019) 1711-1721. https://doi.org/10.1038/s41467-019-09666-0.
[41] B. Zhang, X. Zheng, O. Voznyy, R. Comin, M. Bajdich, M. Garcia-Melchor, L. Han, J. Xu, M. Liu, L. Zheng, F.P. Garcia de Arquer, C.T. Dinh, F. Fan, M. Yuan, E. Yassitepe, N. Chen, T. Regier, P. Liu, Y. Li, P. De Luna, A. Janmohamed, H.L. Xin, H. Yang, A. Vojvodic, E.H. Sargent, FeCoW-homogeneously dispersed, multimetal oxygen-evolving catalysts, Science 352 (2016) 333-337. https://doi.org/10.1126/science.aaf1525.
[42] S. Liu, J. Zhu, M. Sun, Z. Ma, K. Hu, T. Nakajima, X. Liu, P. Schmuki, L. Wang, Promoting the hydrogen evolution reaction through oxygen vacancies and phase transformation engineering on layered double hydroxide nanosheets, J. Mater. Chem. A 8 (2020) 2490-2497. https://doi.org/10.1039/c9ta12768b.
[43] J. Zhou, W. Shu, Y. Gao, Z. Cao, J. Zhang, H. Hou, J. Zhao, X. Chen, Y. Pan, G. Qian, Enhanced arsenite immobilization via ternary layered double hydroxides and application to paddy soil remediation, RSC Adv. 7 (2017) 20320-20326. https://doi.org/10.1039/c6ra28116h.
[44] H. Chi, J. Wang, H. Wang, S. Li, M. Yang, S. Bai, C. Li, X. Sun, Y. Zhao, Y.F. Song, Super-stable mineralization of Ni^{2+} ions from wastewater using CaFe layered double hydroxide, Adv. Funct. Mater. 32 (2021) 2106645. https://doi.org/10.1002/adfm.202106645.
[45] X. Gao, X. Liu, D. Wu, B. Qian, Z. Kou, Z. Pan, Y. Pang, L. Miao, J. Wang, Significant role of Al in ternary layered double hydroxides for enhancing electrochemical performance of flexible asymmetric supercapacitor, Adv. Funct. Mater. 29 (2019) 1903879. https://doi.org/10.1002/adfm.201903879.
[46] Q. Ma, B. Li, F. Huang, Q. Pang, Y. Chen, J.Z. Zhang, Incorporating iron in nickel cobalt layered double hydroxide nanosheet arrays as efficient oxygen evolution electrocatalyst, Electrochim. Acta 317 (2019) 684-693. https://doi.org/10.1016/j.electacta.2019.06.019.
[47] W. Liu, J. Xie, Y. Guo, S. Lou, L. Gao, B. Tang, Sulfurization-induced edge amorphization in copper–nickel–cobalt layered double hydroxide nanosheets promoting hydrazine electro-oxidation, J. Mater. Chem. A 7 (2019) 24437-24444. https://doi.org/10.1039/c9ta07857f.
[48] Y. Guo, X. Hong, Y. Wang, Q. Li, J. Meng, R. Dai, X. Liu, L. He, L. Mai, Multicomponent hierarchical Cu-doped NiCo-LDH/CuO double arrays for ultralong-life hybrid fiber supercapacitor, Adv. Funct. Mater. 29 (2019) 1809004.

https://doi.org/10.1002/adfm.201809004.
[49] S. Hao, G. Zheng, S. Gao, L. Qiu, N. Xu, Y. He, L. Lei, X. Zhang, *In situ* synthesis of ternary NiCoRu-based layered double hydroxide by chlorine corrosion toward electrocatalytic water oxidation, ACS Sustain. Chem. Eng. 7 (2019) 14361-14367. https://doi.org/10.1021/acssuschemeng.9b03830.
[50] S. Hao, L. Chen, C. Yu, B. Yang, Z. Li, Y. Hou, L. Lei, X. Zhang, NiCoMo hydroxide nanosheet arrays synthesized via chloride corrosion for overall water splitting, ACS Energy Lett. 4 (2019) 952-959. https://doi.org/10.1021/acsenergylett.9b00333.
[51] X. Yu, B. Wang, C. Wang, C. Zhuang, Y. Yao, Z. Li, C. Wu, J. Feng, Z. Zou, 2D high-entropy hydrotalcites, Small 17 (2021) 2103412. https://doi.org/10.1002/smll.202103412.
[52] D. Wang, Q. Li, C. Han, Q. Lu, Z. Xing, X. Yang, Atomic and electronic modulation of self-supported nickel-vanadium layered double hydroxide to accelerate water splitting kinetics, Nat. Commun. 10 (2019) 3899-3910. https://doi.org/10.1038/s41467-019-11765-x.
[53] C. Ning, Z. Wang, S. Bai, L. Tan, H. Dong, Y. Xu, X. Hao, T. Shen, J. Zhao, P. Zhao, Z. Li, Y. Zhao, Y.-F. Song, 650 nm-driven syngas evolution from photocatalytic CO_2 reduction over Co-containing ternary layered double hydroxide nanosheets, Chem. Eng. J. 412 (2021) 128362-128370. https://doi.org/10.1016/j.cej.2020.128362.
[54] H.F. Wang, C. Tang, B. Wang, B.Q. Li, Q. Zhang, Bifunctional transition metal hydroxysulfides: room-temperature sulfurization and their applications in Zn-air batteries, Adv. Mater. 29 (2017) 702327. https://doi.org/10.1002/adma.201702327.
[55] R. Xie, G. Fan, L. Yang, F. Li, Highly efficient hybrid cobalt-copper-aluminum layered double hydroxide/graphene nanocomposites as catalysts for the oxidation of alkylaromatics, ChemCatChem 8 (2016) 363-371. https://doi.org/10.1002/cctc.201500890.
[56] L. Fagiolari, F. Zaccaria, F. Costantino, R. Vivani, C.K. Mavrokefalos, G.R. Patzke, A. Macchioni, Ir- and Ru-doped layered double hydroxides as affordable heterogeneous catalysts for electrochemical water oxidation, Dalton Trans. 49 (2020) 2468-2476. https://doi.org/10.1039/c9dt04306c.
[57] S. Zhang, Y. Zhao, R. Shi, C. Zhou, G.I.N. Waterhouse, L.Z. Wu, C.H. Tung, T. Zhang, Efficient photocatalytic nitrogen fixation over $Cu^{\delta+}$-modified defective ZnAl-layered double hydroxide nanosheets, Adv. Energy Mater. 10 (2020) 1901973. https://doi.org/10.1002/aenm.201901973.
[58] L. Fang, W. Luo, Y. Meng, X. Zhou, G. Pan, Z. Ni, S. Xia, Visible-light-promoted selective hydrogenation of crotonaldehyde by Au supported ZnAl-layered double hydroxides: catalytic property, kinetics, and mechanism investigation, J. Phys. Chem. C 122 (2018) 17358-17369. https://doi.org/10.1021/acs.jpcc.8b05463.
[59] Z. Gao, G. Fan, L. Yang, F. Li, Double-active sites cooperatively catalyzed transfer hydrogenation of ethyl levulinate over a ruthenium-based catalyst, Molecular Catalysis 442 (2017) 181-190. https://doi.org/10.1016/j.mcat.2017.09.026.
[60] S. Jana, Y. Kubota, T. Tatsumi, High activity of Mn-MgAl hydrotalcite in heterogeneously catalyzed liquid-phase selective oxidation of alkylaromatics to benzylic ketones with 1 atm of molecular oxygen, J. Catal. 247 (2007) 214-222. https://doi.org/10.1016/j.jcat.2007.02.004.
[61] K. Motokura, D. Nishimura, K. Mori, T. Mizugaki, K. Ebitani, K. Kaneda, A ruthenium-grafted hydrotalcite as a multifunctional catalyst for direct r-alkylation of nitriles with primary alcohols, J. Am. Chem. Soc. 126 (2004) 5662-5663. https://doi.org/10.1021/ja0491811.
[62] K. Mori, T. Taga, H. Yamashita, Isolated single-atomic Ru catalyst bound on a layered double hydroxide for hydrogenation of CO_2 to formic acid, ACS Catal. 7 (2017) 3147-3151. https://doi.org/10.1021/acscatal.7b00312.
[63] C. Dong, X. Zhang, J. Xu, R. Si, J. Sheng, J. Luo, S. Zhang, W. Dong, G. Li, W. Wang, F. Huang, Ruthenium-doped cobalt-chromium layered double hydroxides for enhancing oxygen evolution through regulating charge transfer, Small 16 (2020) 1905328. https://doi.org/10.1002/smll.201905328.
[64] S. Fu, Y. Zheng, X. Zhou, Z. Ni, S. Xia, Visible light promoted degradation of gaseous volatile organic compounds catalyzed by Au supported layered double hydroxides: Influencing factors, kinetics and mechanism, J. Hazard. Mater. 363 (2019) 41-54. https://doi.org/10.1016/j.jhazmat.2018.10.009.

[65] F. Song, X. Hu, Exfoliation of layered double hydroxides for enhanced oxygen evolution catalysis, Nat. Commun. 5 (2014) 4477-4485. https://doi.org/10.1038/ncomms5477.
[66] D. Friebel, M.W. Louie, M. Bajdich, K.E. Sanwald, Y. Cai, A.M. Wise, M.J. Cheng, D. Sokaras, T.C. Weng, R. Alonso-Mori, R.C. Davis, J.R. Bargar, J.K. Norskov, A. Nilsson, A.T. Bell, Identification of highly active Fe sites in (Ni, Fe)OOH for electrocatalytic water splitting, J. Am. Chem. Soc. 137 (2015) 1305-1313. https://doi.org/10.1021/ja511559d.
[67] P.J. Sideris, U.G. Nielsen, Z. Gan, C.P. Grey, Mg/Al ordering in layered double hydroxides revealed by multinuclear NMR spectroscopy, Science 321 (2008) 113-117. https://doi.org/10.1126/science.1157581.
[68] X. Long, Z. Wang, S. Xiao, Y. An, S. Yang, Transition metal based layered double hydroxides tailored for energy conversion and storage, Mater. Today 19 (2016) 213-226. https://doi.org/10.1016/j.mattod.2015.10.006.
[69] L. Qian, Z. Lu, T. Xu, X. Wu, Y. Tian, Y. Li, Z. Huo, X. Sun, X. Duan, Trinary layered double hydroxides as high-performance bifunctional materials for oxygen electrocatalysis, Adv. Energy Mater. 5 (2015) 1500245. https://doi.org/10.1002/aenm.201500245.
[70] X. Tao, C. Yang, L. Huang, S. Shang, Novel plasma assisted preparation of ZnCuFeCr layered double hydroxides with improved photocatalytic performance of methyl orange degradation, Appl. Surf. Sci. 507 (2020) 145053-145062. https://doi.org/10.1016/j.apsusc.2019.145053.
[71] G. Wang, B. Wang, C. Su, D. Li, L. Zhang, R. Chong, Z. Chang, Enhancing and stabilizing α-Fe_2O_3 photoanode towards neutral water oxidation: Introducing a dual-functional NiCoAl layered double hydroxide overlayer, J. Catal. 359 (2018) 287-295. https://doi.org/10.1016/j.jcat.2018.01.011.
[72] Y. Zhao, Q. Wang, T. Bian, H. Yu, H. Fan, C. Zhou, L.Z. Wu, C.H. Tung, D. O'Hare, T. Zhang, Ni^{3+} doped monolayer layered double hydroxide nanosheets as efficient electrodes for supercapacitors, Nanoscale 7 (2015) 7168-7173. https://doi.org/10.1039/c5nr01320h.
[73] S. Bai, N. Zhang, C. Gao, Y. Xiong, Defect engineering in photocatalytic materials, Nano Energy 53 (2018) 296-336. https://doi.org/10.1016/j.nanoen.2018.08.058.
[74] J. Xiong, J. Di, J. Xia, W. Zhu, H. Li, Surface defect engineering in 2D nanomaterials for photocatalysis, Adv. Funct. Mater. 28 (2018) 1801983. https://doi.org/10.1002/adfm.201801983.
[75] N. Zhang, C. Gao, Y. Xiong, Defect engineering: A versatile tool for tuning the activation of key molecules in photocatalytic reactions, J. Energy Chem. 37 (2019) 43-57. https://doi.org/10.1016/j.jechem.2018.09.010.
[76] K.S. Novoselov, A. Mishchenko, A. Carvalho, A.H. Castro Neto, 2D materials and van der Waals heterostructures, Science 353 (2016) 461-473. https://doi.org/10.1126/science.aac9439.
[77] S. Bai, T. Li, H. Wang, L. Tan, Y. Zhao, Y.-F. Song, Scale-up synthesis of monolayer layered double hydroxide nanosheets via separate nucleation and aging steps method for efficient CO_2 photoreduction, Chem. Eng, J. 419 (2021) 129390-129398. https://doi.org/10.1016/j.cej.2021.129390.
[78] Z. Gao, L. Yang, G. Fan, F. Li, Promotional role of surface defects on carbon-supported ruthenium-based catalysts in the transfer hydrogenation of furfural, ChemCatChem 8 (2016) 3769-3779. https://doi.org/10.1002/cctc.201601070.
[79] L. Tan, S.-M. Xu, Z. Wang, Y. Xu, X. Wang, X. Hao, S. Bai, C. Ning, Y. Wang, W. Zhang, Y.K. Jo, S.-J. Hwang, X. Cao, X. Zheng, H. Yan, Y. Zhao, H. Duan, Y.-F. Song, Highly selective photoreduction of CO_2 with suppressing H_2 evolution over monolayer layered double hydroxide under irradiation above 600 nm, Angew. Chem. Int. Ed. 58 (2019) 11860-11867. https://doi.org/10.1002/anie.201904246.
[80] Y. Zhao, X. Jia, G. Chen, L. Shang, G.I. Waterhouse, L.Z. Wu, C.H. Tung, D. O'Hare, T. Zhang, Ultrafine NiO nanosheets stabilized by TiO_2 from monolayer NiTi-LDH precursors: an active water oxidation electrocatalyst, J. Am. Chem. Soc. 138 (2016) 6517-6524. https://doi.org/10.1021/jacs.6b01606.
[81] Y. Zhao, B. Li, Q. Wang, W. Gao, C.J. Wang, M. Wei, D.G. Evans, X. Duan, D. O'Hare, NiTi-layered double hydroxides nanosheets as efficient photocatalysts for oxygen evolution from water using visible light, Chem. Sci. 5 (2014) 951-958. https://doi.org/10.1039/c3sc52546e.
[82] X. Wang, Y. Lin, Y. Su, B. Zhang, C. Li, H. Wang, L. Wang, Design and synthesis of ternary-component layered double hydroxides for high-performance supercapacitors: understanding the role of trivalent metal ions, Electrochim.

Acta 225 (2017) 263-271. https://doi.org/10.1016/j.electacta.2016.12.160.
[83] H. Han, H. Choi, S. Mhin, Y.-R. Hong, K.M. Kim, J. Kwon, G. Ali, K.Y. Chung, M. Je, H.N. Umh, D.-H. Lim, K. Davey, S.-Z. Qiao, U. Paik, T. Song, Advantageous crystalline–amorphous phase boundary for enhanced electrochemical water oxidation, Energy Environ. Sci. 12 (2019) 2443-2454. https://doi.org/10.1039/c9ee00950g.
[84] H. Xu, B. Fei, G. Cai, Y. Ha, J. Liu, H. Jia, J. Zhang, M. Liu, R. Wu, Boronization-induced ultrathin 2D nanosheets with abundant crystalline-amorphous phase boundary supported on nickel foam toward efficient water splitting, Adv. Energy Mater. 10 (2019) 1902714. https://doi.org/10.1002/aenm.201902714.
[85] B. Qiao, A. Wang, X. Yang, L.F. Allard, Z. Jiang, Y. Cui, J. Liu, J. Li, T. Zhang, Single-atom catalysis of CO oxidation using Pt_1/FeO_x, Nat. Chem. 3 (2011) 634-641. https://doi.org/10.1038/nchem.1095.
[86] H. Zhang, J. Wei, J. Dong, G. Liu, L. Shi, P. An, G. Zhao, J. Kong, X. Wang, X. Meng, J. Zhang, J. Ye, Efficient visible-light-driven carbon dioxide reduction by a single-atom implanted metal-organic framework, Angew. Chem. Int. Ed. 55 (2016) 14310-14314. https://doi.org/10.1002/anie.201608597.
[87] W. Chen, J. Pei, C.T. He, J. Wan, H. Ren, Y. Zhu, Y. Wang, J. Dong, S. Tian, W.C. Cheong, S. Lu, L. Zheng, X. Zheng, W. Yan, Z. Zhuang, C. Chen, Q. Peng, D. Wang, Y. Li, Rational design of single molybdenum atoms anchored on N-doped carbon for effective hydrogen evolution reaction, Angew. Chem. Int. Ed. 56 (2017) 16086-16090. https://doi.org/10.1002/anie.201710599.
[88] A. Wang, J. Li, T. Zhang, Heterogeneous single-atom catalysis, Nat. Rev. Chem. 2 (2018) 65-81. https://doi.org/10.1038/s41570-018-0010-1.
[89] Y. Wang, J. Mao, X. Meng, L. Yu, D. Deng, X. Bao, Catalysis with two-dimensional materials confining single atoms: concept, design, and applications, Chem. Rev. 119 (2019) 1806-1854. https://doi.org/10.1021/acs.chemrev.8b00501.
[90] X.-F. Yang, A. Wang, B. Qiao, J. Li, J. Liu, T. Zhang, Single-atom catalysts: a new frontier in heterogeneous catalysis, Acc. Chem. Res. 46 (2013) 1740-1748. https://doi.org/10.1021/ar300361m.
[91] R. Qin, P. Liu, G. Fu, N. Zheng, Strategies for stabilizing atomically dispersed metal catalysts, Small Methods 2 (2018) 1700286. https://doi.org/10.1002/smtd.201700286.
[92] L. Mohapatra, K. Parida, A review on the recent progress, challenges and perspective of layered double hydroxides as promising photocatalysts, J. Mater. Chem. A 4 (2016) 10744-10766. https://doi.org/10.1039/c6ta01668e.
[93] X. Zheng, J. Tang, A. Gallo, J.A. Garrido Torres, X. Yu, C.J. Athanitis, E.M. Been, P. Ercius, H. Mao, S.C. Fakra, C. Song, R.C. Davis, J.A. Reimer, J. Vinson, M. Bajdich, Y. Cui, Origin of enhanced water oxidation activity in an iridium single atom anchored on NiFe oxyhydroxide catalyst, P. Natl. Acad. Sci. USA 118 (2021) 2101817118. https://doi.org/10.1073/pnas.2101817118.
[94] S. Xie, W. Ma, X. Wu, H. Zhang, Q. Zhang, Y. Wang, Y. Wang, Photocatalytic and electrocatalytic transformations of C1 molecules involving C–C coupling, Energy Environ. Sci. 14 (2021) 37-89. https://doi.org/10.1039/d0ee01860k.
[95] A.Y. Khodakov, W. Chu, P. Fongarland, Advances in the development of novel cobalt fischer−tropsch catalysts for synthesis of long-chain hydrocarbons and clean fuels, Chem. Rev. 107 (2007) 1692-1744. https://doi.org/10.1021/cr050972v.
[96] H.M.T. Galvis, J.H. Bitter, C.B. Khare, M. Ruitenbeek, A.I. Dugulan, K.P.d. Jong, Supported iron nanoparticles as catalysts for sustainable production of lower olefins, Science 335 (2012) 835-838. https://doi.org/10.1126/science.1215614.
[97] Y. Zhao, Z. Li, M. Li, J. Liu, X. Liu, G.I.N. Waterhouse, Y. Wang, J. Zhao, W. Gao, Z. Zhang, R. Long, Q. Zhang, L. Gu, X. Liu, X. Wen, D. Ma, L.Z. Wu, C.H. Tung, T. Zhang, Reductive transformation of layered-double-hydroxide nanosheets to Fe-based heterostructures for efficient visible-light photocatalytic hydrogenation of CO, Adv. Mater. 30 (2018) 1803127. https://doi.org/10.1002/adma.201803127.
[98] Z. Li, J. Liu, Y. Zhao, G.I.N. Waterhouse, G. Chen, R. Shi, X. Zhang, X. Liu, Y. Wei, X.D. Wen, L.Z. Wu, C.H. Tung, T. Zhang, Co-based catalysts derived from layered-double-hydroxide nanosheets for the photothermal production of light olefins, Adv. Mater. 30 (2018) 1800527. https://doi.org/10.1002/adma.201800527.
[99] G. Chen, R. Gao, Y. Zhao, Z. Li, G.I.N. Waterhouse, R. Shi, J. Zhao, M. Zhang, L. Shang, G. Sheng, X. Zhang, X.

Wen, L.Z. Wu, C.H. Tung, T. Zhang, Alumina-supported CoFe alloy catalysts derived from layered-double-hydroxide nanosheets for efficient photothermal CO_2 hydrogenation to hydrocarbons, Adv. Mater. 30 (2018) 1704663. https://doi.org/10.1002/adma.201704663.

[100] Z. Pan, R. Wang, J. Chen, Deoxygenation of methyl laurate as a model compound on Ni-Zn alloy and intermetallic compound catalysts: Geometric and electronic effects of oxophilic Zn, Applied Catalysis B: Environmental 224 (2018) 88-100. https://doi.org/10.1016/j.apcatb.2017.10.040.

[101] W. Gao, Y. Zhao, H. Chen, H. Chen, Y. Li, S. He, Y. Zhang, M. Wei, D.G. Evans, X. Duan, Core–shell Cu@(CuCo-alloy)/Al_2O_3 catalysts for the synthesis of higher alcohols from syngas, Green Chem. 17 (2015) 1525-1534. https://doi.org/10.1039/c4gc01633e.

[102] R. Allmann, The crystal structure of pyroaurite, Acta Crystallographica Section B-Structural Science Crystal Engineering and Materials 24 (1968) 972-977. https://doi.org/10.1107/S2052520622008095.

[103] K.J. Martin, T.J. Pinnavaia, LDHs as supported anionic reagents halide ion reactivity in $Zn_2Cr(OH)_6X{\cdot}nH_2O$, J. Am. Chem. Soc. 108 (1986) 541-542. https://doi.org/10.1021/ja00263a049.

[104] H. Yan, J. Lu, M. Wei, J. Ma, H. Li, J. He, D.G. Evans, X. Duan, Theoretical study of the hexahydrated metal cations for the understanding of their template effects in the construction of layered double hydroxides, J. Mol. Struc.-THEOCHEM 866 (2008) 34-45. https://doi.org/10.1016/j.theochem.2008.06.031.

[105] X. Liu, R. Ma, Y. Bando, T. Sasaki, A general strategy to layered transition-metal hydroxide nanocones: tuning the composition for high electrochemical performance, Adv. Mater. 24 (2012) 2148-2153. https://doi.org/10.1002/adma.201104753.

[106] R. Ma, T. Sasaki, Two-dimensional oxide and hydroxide nanosheets: controllable high-quality exfoliation, molecular assembly, and exploration of functionality, Acc. Chem. Res. 48 (2015) 136-143. https://doi.org/10.1021/ar500311w.

[107] H. Yin, Z. Tang, Ultrathin two-dimensional layered metal hydroxides: an emerging platform for advanced catalysis, energy conversion and storage, Chem. Soc. Rev. 45 (2016) 4873-4891. https://doi.org/10.1039/c6cs00343e.

[108] G. Chen, H. Wan, W. Ma, N. Zhang, Y. Cao, X. Liu, J. Wang, R. Ma, Layered metal hydroxides and their derivatives: controllable synthesis, chemical exfoliation, and electrocatalytic applications, Adv. Energy Mater. 10 (2019) 1902535. https://doi.org/10.1002/aenm.201902535.

[109] X. Ning, Z. An, J. He, Remarkably efficient CoGa catalyst with uniformly dispersed and trapped structure for ethanol and higher alcohol synthesis from syngas, J. Catal. 340 (2016) 236-247. https://doi.org/10.1016/j.jcat.2016.05.014.

[110] F. Li, L. Zhang, D.G. Evans, X. Duan, Structure and surface chemistry of manganese-doped copper-based mixed metal oxides derived from layered double hydroxides, Colloid. Surface. A 244 (2004) 169-177. https://doi.org/10.1016/j.colsurfa.2004.06.022.

[111] J. Zhao, L. Yang, T. Chen, F. Li, Magnetic $Co_{1-x}Zn_xFe_2O_4$ granular films fabricated via layered double hydroxide precursors, J. Phys. Chem. Solids 73 (2012) 1500-1504. https://doi.org/10.1016/j.jpcs.2011.10.040.

[112] K. Gu, D. Wang, C. Xie, T. Wang, G. Huang, Y. Liu, Y. Zou, L. Tao, S. Wang, Defect-rich high-entropy oxide nanosheets for efficient 5-hydroxymethylfurfural electrooxidation, Angew. Chem. Int. Ed. 60 (2021) 20253-20258. https://doi.org/10.1002/anie.202107390.

[113] Z. Liu, R. Ma, M. Osada, N. Iyi, Y. Ebina, K. Takada, T. Sasaki, Synthesis, anion exchange, and delamination of Co-Al layered double hydroxide: assembly of the exfoliated nanosheet/polyanion composite films and magneto-optical studies, J. Am. Chem. Soc. 128 (2005) 4872-4880. https://doi.org/10.1021/ja0584471.

[114] J. Liang, R. Ma, N. Iyi, Y. Ebina, K. Takada, T. Sasaki, Topochemical synthesis, anion exchange, and exfoliation of Co−Ni layered double hydroxides: a route to positively charged Co−Ni hydroxide nanosheets with tunable composition, Chem. Mater. 22 (2009) 371-378. https://doi.org/10.1021/cm902787u.

[115] Y. Kuroda, Y. Miyamoto, M. Hibino, K. Yamaguchi, N. Mizuno, Tripodal ligand-stabilized layered double hydroxide nanoparticles with highly exchangeable CO_3^{2-}, Chem. Mater. 25 (2013) 2291-2296. https://doi.org/10.1021/cm400846k.

[116] J.L. Gunjakar, T.W. Kim, H.N. Kim, I.Y. Kim, S.J. Hwang, Mesoporous layer-by-layer ordered nanohybrids of layered double hydroxide and layered metal oxide: highly active visible light photocatalysts with improved chemical stability, J. Am. Chem. Soc. 133 (2011) 14998-15007. https://doi.org/10.1021/ja203388r.
[117] Q. Wang, D. O'Hare, Large-scale synthesis of highly dispersed layered double hydroxide powders containing delaminated single layer nanosheets, Chem. Commun. 49 (2013) 6301-6303. https://doi.org/10.1039/c3cc42918k.
[118] W. Liu, R. Liang, Y. Lin, Confined synthesis of carbon dots with tunable long-wavelength emission in a 2-dimensional layered double hydroxide matrix, Nanoscale 12 (2020) 7888-7894. https://doi.org/10.1039/d0nr00272k.
[119] J. Romero, M. Varela, M. Assebban, V. Oestreicher, A. Guedeja-Marrón, J.L. Jordá, G. Abellán, E. Coronado, Insights into the formation of metal carbon nanocomposites for energy storage using hybrid NiFe layered double hydroxides as precursors, Chem. Sci. 11 (2020) 7626-7633. https://doi.org/10.1039/d0sc00697a.
[120] W. Chang, B. Qi, Y.-F. Song, Step-by-step assembly of 2D confined chiral space endowing achiral clusters with asymmetric catalytic activity for epoxidation of allylic alcohols, ACS Appl. Mater. Inter. 12 (2020) 36389-36397. https://doi.org/10.1021/acsami.0c10207.
[121] T. Li, Z. Wang, W. Chen, H.N. Miras, Y.-F. Song, Rational design of a polyoxometalate intercalated layered double hydroxide: highly efficient catalytic epoxidation of allylic alcohols under mild and solvent-free conditions, Chem. Eur. J. 23 (2017) 1069-1077. https://doi.org/10.1002/chem.201604180.
[122] J. Ma, L. Liu, S. Li, Y. Chen, M. Zhuo, F. Shao, J. Gong, Z. Tong, Facile assembly for fast construction of intercalation hybrids of layered double hydroxides with anionic metalloporphyrin, Dalton Trans. 43 (2014) 9909-9915. https://doi.org/10.1039/c4dt00967c.
[123] R. Gao, X. Mei, D. Yan, R. Liang, M. Wei, Nano-photosensitizer based on layered double hydroxide and isophthalic acid for singlet oxygenation and photodynamic therapy, Nat. Commun. 9 (2018) 2798-2807. https://doi.org/10.1038/s41467-018-05223-3.
[124] D. Yan, J. Lu, M. Wei, J. Han, J. Ma, F. Li, D.G. Evans, X. Duan, Ordered poly(p-phenylene)/layered double hydroxide ultrathin films with blue luminescence by layer-by-layer assembly, Angew. Chem. Int. Ed. 48 (2009) 3073-3076. https://doi.org/10.1002/anie.200900178.
[125] C. Zhang, J. Zhao, L. Zhou, Z. Li, M. Shao, M. Wei, Layer-by-layer assembly of exfoliated layered double hydroxide nanosheets for enhanced electrochemical oxidation of water, J. Mater. Chem. A 4 (2016) 11516-11523. https://doi.org/10.1039/c6ta02537d.
[126] W. Shi, J. Yao, L. Bai, C. Lu, Defect-stabilized triplet state excitons: toward ultralong organic room-temperature phosphorescence, Adv. Funct. Mater. 28 (2018) 1804961. https://doi.org/10.1002/adfm.201804961.
[127] K. Teramura, H. Tsuneoka, K. Ogura, T. Sugimoto, T. Shishido, T. Tanaka, Photoactivation of molecular oxygen by an iron(III) porphyrin with a magnesium aluminum layered double hydroxide for the aerobic epoxidation of cyclohexene, ChemCatChem 6 (2014) 2276-2281. https://doi.org/10.1002/cctc.201402131.
[128] W. Chen, B. Wu, Y. Wang, W. Zhou, Y. Li, T. Liu, C. Xie, L. Xu, S. Du, M. Song, D. Wang, Y. liu, Y. Li, J. Liu, Y. Zou, R. Chen, C. Chen, J. Zheng, Y. Li, J. Chen, S. Wang, Deciphering the alternating synergy between interlayer Pt single-atom and NiFe layered double hydroxide for overall water splitting, Energy Environ. Sci. 14 (2021) 6428-6440. https://doi.org/10.1039/d1ee01395e.
[129] J.B. Han, J. Lu, M. Wei, Z.L. Wang, X. Duan, Heterogeneous ultrathin films fabricated by alternate assembly of exfoliated LDHs and polyanion, Chem. Commun. (2008) 5188-5190. https://doi.org/10.1039/B807479H.
[130] Q. Yang, Q. Wang, Y. Long, F. Wang, L. Wu, J. Pan, J. Han, Y. Lei, W. Shi, S. Song, *In situ* formation of Co_9S_8 quantum dots in MOF-derived ternary metal layered double hydroxide nanoarrays for high-performance hybrid supercapacitors, Adv. Energy Mater. 10 (2020) 1903193. https://doi.org/10.1002/aenm.201903193.
[131] Y. Jiao, Y. Zheng, M. Jaroniec, S.Z. Qiao, Design of electrocatalysts for oxygen- and hydrogen-involving energy conversion reactions, Chem. Soc. Rev. 44 (2015) 2060-2086. https://doi.org/10.1039/c4cs00470a.
[132] Z. Zhao, H. Wu, H. He, X. Xu, Y. Jin, A high-performance binary Ni-Co hydroxide-based water oxidation electrode with three-dimensional coaxial nanotube array structure, Adv. Funct. Mater. 24 (2014) 4698-4705.

https://doi.org/10.1002/adfm.201400118.
[133] K. Qin, L. Wang, S. Wen, L. Diao, P. Liu, J. Li, L. Ma, C. Shi, C. Zhong, W. Hu, E. Liu, N. Zhao, Designed synthesis of NiCo-LDH and derived sulfide on heteroatom-doped edge-enriched 3D rivet graphene films for high-performance asymmetric supercapacitor and efficient OER, J. Mater. Chem. A 6 (2018) 8109-8119. https://doi.org/10.1039/c8ta01832d.
[134] R. Yang, Y. Zhou, Y. Xing, D. Li, D. Jiang, M. Chen, W. Shi, S. Yuan, Synergistic coupling of CoFe-LDH arrays with NiFe-LDH nanosheet for highly efficient overall water splitting in alkaline media, Appl. Catal. B: Environ. 253 (2019) 131-139. https://doi.org/10.1016/j.apcatb.2019.04.054.
[135] E. Enkhtuvshin, K.M. Kim, Y.-K. Kim, S. Mihn, S.J. Kim, S.Y. Jung, N.T. Thu Thao, G. Ali, M. Akbar, K.Y. Chung, K.H. Chae, S. Kang, T.W. Lee, H.G. Kim, S. Choi, H. Han, Stabilizing oxygen intermediates on redox-flexible active sites in multimetallic Ni-Fe-Al-Co layered double hydroxide anodes for excellent alkaline and seawater electrolysis, J. Mater. Chem. A 9 (2021) 27332-27346. https://doi.org/10.1039/d1ta07126b.
[136] J. Lee, H. Jung, Y.S. Park, N. Kwon, S. Woo, N.C.S. Selvam, G.S. Han, H.S. Jung, P.J. Yoo, S.M. Choi, J.W. Han, B. Lim, Chemical transformation approach for high-performance ternary NiFeCo metal compound-based water splitting electrodes, Appl. Catal. B: Environ. 294 (2021). https://doi.org/10.1016/j.apcatb.2021.120246.
[137] J. Lee, H. Jung, Y.S. Park, S. Woo, J. Yang, M.J. Jang, J. Jeong, N. Kwon, B. Lim, J.W. Han, S.M. Choi, High-efficiency anion-exchange membrane water electrolyzer enabled by ternary layered double hydroxide anode, Small 17 (2021) 2100639. https://doi.org/10.1002/smll.202100639.
[138] Y.S. Park, J.-Y. Jeong, M.J. Jang, C.-Y. Kwon, G.H. Kim, J. Jeong, J.-h. Lee, J. Lee, S.M. Choi, Ternary layered double hydroxide oxygen evolution reaction electrocatalyst for anion exchange membrane alkaline seawater electrolysis, J. Energy Chem. 75 (2022) 127-134. https://doi.org/10.1016/j.jechem.2022.08.011.
[139] L. Zhou, C. Zhang, Y. Zhang, Z. Li, M. Shao, Host modification of layered double hydroxide electrocatalyst to boost the thermodynamic and kinetic activity of oxygen evolution reaction, Adv. Funct. Mater. 31 (2021) 2009743. https://doi.org/10.1002/adfm.202009743.
[140] F. Zaccaria, L. Fagiolari, A. Macchioni, Optimizing noble metals exploitation in water oxidation catalysis by their incorporation in layered double hydroxides, Inorg. Chim. Acta 516 (2021) 120161-120171. https://doi.org/10.1016/j.ica.2020.120161.
[141] Q.Q. Chen, C.C. Hou, C.J. Wang, X. Yang, R. Shi, Y. Chen, Ir($^{4+}$)-doped NiFe LDH to expedite hydrogen evolution kinetics as a Pt-like electrocatalyst for water splitting, Chem. Commun. 54 (2018) 6400-6403. https://doi.org/10.1039/c8cc02872a.
[142] W.-D. Zhang, H. Yu, T. Li, Q.-T. Hu, Y. Gong, D.-Y. Zhang, Y. Liu, Q.-T. Fu, H.-Y. Zhu, X. Yan, Z.-G. Gu, Hierarchical trimetallic layered double hydroxide nanosheets derived from 2D metal-organic frameworks for enhanced oxygen evolution reaction, Applied Catalysis B: Environmental 264 (2020) 118532-118539. https://doi.org/10.1016/j.apcatb.2019.118532.
[143] Y. Qin, F. Wang, J. Shang, M. Iqbal, A. Han, X. Sun, H. Xu, J. Liu, Ternary NiCoFe-layered double hydroxide hollow polyhedrons as highly efficient electrocatalysts for oxygen evolution reaction, J. Energy Chem. 43 (2020) 104-107. https://doi.org/10.1016/j.jechem.2019.08.014.
[144] K. Zhu, J. Chen, W. Wang, J. Liao, J. Dong, M.O.L. Chee, N. Wang, P. Dong, P.M. Ajayan, S. Gao, J. Shen, M. Ye, Etching-doping sedimentation equilibrium strategy: Accelerating kinetics on hollow Rh-doped CoFe-layered double hydroxides for water splitting, Adv. Funct. Mater. 30 (2020) 2003556. https://doi.org/10.1002/adfm.202003556.
[145] L. Gao, X. Wen, S. Liu, D. Qu, Y. Ma, J. Feng, Z. Zhong, H. Guan, L. Niu, Nickel-vanadium-cobalt ternary layered double hydroxide for efficient electrocatalytic upgrading of 5-hydroxymethylfurfural to 2,5-furancarboxylic acid at low potential, J. Mater. Chem. A (2022). https://doi.org/10.1039/d2ta03016k.
[146] Z. Wang, W. Liu, J. Bao, Y. Song, X. She, Y. Hua, G. Lv, J. Yuan, H. Li, H. Xu, Modulating electronic structure of ternary NiMoV LDH nanosheet array induced by doping engineering to promote urea oxidation reaction, Chem. Eng. J. 430 (2022). https://doi.org/10.1016/j.cej.2021.133100.
[147] S.C. Sekhar, G. Nagaraju, B. Ramulu, S.J. Arbaz, D. Narsimulu, S.K. Hussain, J.S. Yu, An eco-friendly hot-water

therapy towards ternary layered double hydroxides laminated flexible fabrics for wearable supercapatteries, Nano Energy 76 (2020). https://doi.org/10.1016/j.nanoen.2020.105016.
[148] M.B. Poudel, H.J. Kim, Confinement of Zn-Mg-Al-layered double hydroxide and α-Fe_2O_3 nanorods on hollow porous carbon nanofibers: A free-standing electrode for solid-state symmetric supercapacitors, Chem. Eng. J. 429 (2022). https://doi.org/10.1016/j.cej.2021.132345.
[149] J. Xu, S. Gai, F. He, N. Niu, P. Gao, Y. Chen, P. Yang, Reduced graphene oxide/$Ni_{1-x}Co_xAl$-layered double hydroxide composites: preparation and high supercapacitor performance, Dalton Trans. 43 (2014) 11667-11675. https://doi.org/10.1039/c4dt00686k.
[150] S. Singh, N.M. Shinde, Q.X. Xia, C. Gopi, J.M. Yun, R.S. Mane, K.H. Kim, Tailoring the morphology followed by the electrochemical performance of NiMn-LDH nanosheet arrays through controlled Co-doping for high-energy and power asymmetric supercapacitors, Dalton Trans. 46 (2017) 12876-12883. https://doi.org/10.1039/c7dt01863k.
[151] X. Li, L. Liang, Y. Sun, J. Xu, X. Jiao, X. Xu, H. Ju, Y. Pan, J. Zhu, Y. Xie, Ultrathin conductor enabling efficient IR light CO_2 reduction, J. Am. Chem. Soc. 141 (2019) 423-430. https://doi.org/10.1021/jacs.8b10692.
[152] X. Jiao, K. Zheng, Z. Hu, Y. Sun, Y. Xie, Broad-spectral-response photocatalysts for CO_2 reduction, ACS Cent. Sci. 6 (2020) 653-660. https://doi.org/10.1021/acscentsci.0c00325.
[153] L. Tan, Z. Wang, Y. Zhao, Y.F. Song, Recent progress on nanostructured layered double hydroxides for visible-light-induced photoreduction of CO_2, Chem. Asian J. 15 (2020) 3380-3389. https://doi.org/10.1002/asia.202000963.
[154] X. Li, Y. Sun, J. Xu, Y. Shao, J. Wu, X. Xu, Y. Pan, H. Ju, J. Zhu, Y. Xie, Selective visible-light-driven photocatalytic CO_2 reduction to CH_4 mediated by atomically thin $CuIn_5S_8$ layers, Nat. Energy 4 (2019) 690-699. https://doi.org/10.1038/s41560-019-0431-1.
[155] K. Teramura, S. Iguchi, Y. Mizuno, T. Shishido, T. Tanaka, Photocatalytic conversion of CO_2 in water over layered double hydroxides, Angew. Chem. Int. Ed. 51 (2012) 8008-8011. https://doi.org/10.1002/anie.201201847.
[156] N. Ahmed, Y. Shibata, T. Taniguchi, Y. Izumi, Photocatalytic conversion of carbon dioxide into methanol using zinc–copper–M(III) (M=aluminum, gallium) layered double hydroxides, J. Catal. 279 (2011) 123-135. https://doi.org/10.1016/j.jcat.2011.01.004.
[157] Y. Li, J. Hao, H. Song, F. Zhang, X. Bai, X. Meng, H. Zhang, S. Wang, Y. Hu, J. Ye, Selective light absorber-assisted single nickel atom catalysts for ambient sunlight-driven CO_2 methanation, Nat. Commun. 10 (2019) 2359-2367. https://doi.org/10.1038/s41467-019-10304-y.
[158] L. Tan, S.M. Xu, Z. Wang, Y. Xu, X. Wang, X. Hao, S. Bai, C. Ning, Y. Wang, W. Zhang, Y.K. Jo, S.J. Hwang, X. Cao, X. Zheng, H. Yan, Y. Zhao, H. Duan, Y.F. Song, Highly selective photoreduction of CO_2 with suppressing H_2 evolution over monolayer layered double hydroxide under irradiation above 600 nm, Angew. Chem. Int. Ed. 58 (2019) 11860-11867. https://doi.org/10.1002/anie.201904246.
[159] L. Tan, S.-M. Xu, Z. Wang, X. Hao, T. Li, H. Yan, W. Zhang, Y. Zhao, Y.-F. Song, 600 nm induced nearly 99% selectivity of CH_4 from CO_2 photoreduction using defect-rich monolayer structures, Cell Rep. Phys. Sci. 2 (2021) 100322. https://doi.org/10.1016/j.xcrp.2021.100322.
[160] Z. Wang, S.-M. Xu, L. Tan, G. Liu, T. Shen, C. Yu, H. Wang, Y. Tao, X. Cao, Y. Zhao, Y.-F. Song, 600 nm-driven photoreduction of CO_2 through the topological transformation of layered double hydroxides nanosheets, Appl. Catal. B: Environ. 270 (2020) 118884-118894. https://doi.org/10.1016/j.apcatb.2020.118884.
[161] J. Ren, S. Ouyang, H. Xu, X. Meng, T. Wang, D. Wang, J. Ye, Targeting activation of CO_2 and H_2 over Ru-loaded ultrathin layered double hydroxides to achieve efficient photothermal CO_2 methanation in flow-type system, Adv. Energy Mater. 7 (2017) 1601657. https://doi.org/10.1002/aenm.201601657.
[162] Y. Ide, M. Torii, T. Sano, Layered silicate as an excellent partner of a TiO_2 photocatalyst for efficient and selective green fine-chemical synthesis, J. Am. Chem. Soc. 135 (2013) 11784-11786. https://doi.org/10.1021/ja406855e.
[163] Y.W. Zheng, B. Chen, P. Ye, K. Feng, W. Wang, Q.Y. Meng, L.Z. Wu, C.H. Tung, Photocatalytic hydrogen-evolution cross-couplings: benzene C-H amination and hydroxylation, J. Am. Chem. Soc. 138 (2016) 10080-10083. https://doi.org/10.1021/jacs.6b05498.

[164] J. Li, Y. Xu, Z. Ding, A.H. Mahadi, Y. Zhao, Y.-F. Song, Photocatalytic selective oxidation of benzene to phenol in water over layered double hydroxide: A thermodynamic and kinetic perspective, Chem. Eng. J. 388 (2020) 124248-124255. https://doi.org/10.1016/j.cej.2020.124248.

[165] Y. Wang, D. Chen, Y. Wang, F. Huang, Q. Hu, Z. Lin, Tunable surface charge of ZnS:Cu nano-adsorbent induced the selective preconcentration of cationic dyes from wastewater, Nanoscale 4 (2012) 3665-3668. https://doi.org/10.1039/c2nr30689a.

[166] X. Liang, Y. Zhong, H. He, P. Yuan, J. Zhu, S. Zhu, Z. Jiang, The application of chromium substituted magnetite as heterogeneous Fenton catalyst for the degradation of aqueous cationic and anionic dyes, Chem. Eng. J. 191 (2012) 177-184. https://doi.org/10.1016/j.cej.2012.03.001.

[167] T.-H. Cheng, C.-P. Huang, Y.-H. Huang, Y.-J. Shih, Kinetic study and optimization of electro-Fenton process for dissolution and mineralization of ion exchange resins, Chem. Eng. J. 308 (2017) 954-962. https://doi.org/10.1016/j.cej.2016.09.142.

[168] A.D. Bokare, W. Choi, Review of iron-free Fenton-like systems for activating H_2O_2 in advanced oxidation processes, J. Hazard. Mater. 275 (2014) 121-135. https://doi.org/10.1016/j.jhazmat.2014.04.054.

[169] H. Wang, Z. Zhang, M. Jing, S. Tang, Y. Wu, W. Liu, Synthesis of CuNiSn LDHs as highly efficient Fenton catalysts for degradation of phenol, Appl. Clay Sci. 186 (2020) 105433-105443. https://doi.org/10.1016/j.clay.2019.105433.

[170] K. Li, S. Li, Q. Li, H. Liu, W. Yao, Q. Wang, L. Chai, Design of a high-performance ternary LDHs containing Ni, Co and Mn for arsenate removal, J. Hazard. Mater. 427 (2022) 127865-127875. https://doi.org/10.1016/j.jhazmat.2021.127865.

[171] P. Lyu, L. Li, X. Huang, J. Xie, J. Ye, Y. Tian, J. Huang, C. Zhu, Ternary Ca-Mg-Al layered double-hydroxides for synergistic remediation of As, Cd, and Pb from both contaminated soil and groundwater: Characteristics, effectiveness, and immobilization mechanisms, J. Hazard. Mater. 442 (2022) 130030-130049. https://doi.org/10.1016/j.jhazmat.2022.130030.

[172] C. Chen, P. Gunawan, X.W.D. Lou, R. Xu, Silver nanoparticles deposited layered double hydroxide nanoporous coatings with excellent antimicrobial activities, Adv. Funct. Mater. 22 (2012) 780-787. https://doi.org/10.1002/adfm.201102333.

[173] J. Zhou, Y. Su, J. Zhang, X. Xu, J. Zhao, G. Qian, Y. Xu, Distribution of OH bond to metal-oxide in $Mg_{3-x}Ca_xFe$-layered double hydroxide (x= 0–1.5): Its role in adsorption of selenate and chromate, Chem. Eng. J. 262 (2015) 383-389. https://doi.org/10.1016/j.cej.2014.10.010.

[174] L. Yang, L. Xie, M. Chu, H. Wang, M. Yuan, Z. Yu, C. Wang, H. Yao, S.M. Islam, K. Shi, D. Yan, S. Ma, M.G. Kanatzidis, $Mo_3S_{13}^{2-}$ intercalated layered double hydroxide: highly selective removal of heavy metals and simultaneous reduction of Ag^+ ions to metallic Ag^0 ribbons, Angew. Chem. Int. Ed. 61 (2021) e202112511. https://doi.org/10.1002/anie.202112511.

[175] X. Kong, R. Ge, T. Liu, S. Xu, P. Hao, X. Zhao, Z. Li, X. Lei, H. Duan, Super-stable mineralization of cadmium by calcium-aluminum layered double hydroxide and its large-scale application in agriculture soil remediation, Chem. Eng, J. 407 (2021) 127178-127185. https://doi.org/10.1016/j.cej.2020.127178.

[176] L. Wang, H. Xing, S. Zhang, Q. Ren, L. Pan, K. Zhang, W. Bu, X. Zheng, L. Zhou, W. Peng, Y. Hua, J. Shi, A Gd-doped Mg-Al-LDH/Au nanocomposite for CT/MR bimodal imagings and simultaneous drug delivery, Biomaterials 34 (2013) 3390-3401. https://doi.org/10.1016/j.biomaterials.2013.01.070.

[177] S. Guan, Y. Weng, M. Li, R. Liang, C. Sun, X. Qu, S. Zhou, An NIR-sensitive layered supramolecular nanovehicle for combined dual-modal imaging and synergistic therapy, Nanoscale 9 (2017) 10367-10374. https://doi.org/10.1039/c7nr01771e.

[178] X. Mei, W. Wang, L. Yan, T. Hu, R. Liang, D. Yan, M. Wei, D.G. Evans, X. Duan, Hydrotalcite monolayer toward high performance synergistic dual-modal imaging and cancer therapy, Biomaterials 165 (2018) 14-24. https://doi.org/10.1016/j.biomaterials.2018.02.032.

[179] A.R. Reddi, L.T. Jensen, V.C. Culotta, Manganese homeostasis in saccharomyces cerevisiae, Chem. Rev. 109 (2009)

4722-4732. https://doi.org/10.1021/cr900031u.
[180] E.M. Gale, I.P. Atanasova, F. Blasi, I. Ay, P. Caravan, A manganese alternative to gadolinium for MRI contrast, J. Am. Chem. Soc. 137 (2015) 15548-15557. https://doi.org/10.1021/jacs.5b10748.
[181] B. Li, Z. Gu, N. Kurniawan, W. Chen, Z.P. Xu, Manganese-based layered double hydroxide nanoparticles as a T1 - MRI contrast agent with ultrasensitive pH response and high relaxivity, Adv. Mater. 29 (2017) 1700373. https://doi.org/10.1002/adma.201700373.
[182] B. Li, J. Tang, W. Chen, G. Hao, N. Kurniawan, Z. Gu, Z.P. Xu, Novel theranostic nanoplatform for complete mice tumor elimination via MR imaging-guided acid-enhanced photothermo-/chemo-therapy, Biomaterials 177 (2018) 40-51. https://doi.org/10.1016/j.biomaterials.2018.05.055.
[183] Y. Zhao, Y. Chen, W. Wang, Z. Zhou, S. Shi, W. Li, M. Chen, Z. Li, One-step *in situ* synthesis of nano silver-hydrotalcite coating for enhanced antibacterial and degradation property of magnesium alloys, Mater. Lett. 265 (2020) 127349-127352. https://doi.org/10.1016/j.matlet.2020.127349.
[184] G. Mishra, B. Dash, S. Pandey, P.P. Mohanty, Antibacterial actions of silver nanoparticles incorporated Zn–Al layered double hydroxide and its spinel, J. Environ. Chem. Eng. 1 (2013) 1124-1130. https://doi.org/10.1016/j.jece.2013.08.031.
[185] Y. Zhao, C.J. Wang, W. Gao, B. Li, Q. Wang, L. Zheng, M. Wei, D.G. Evans, X. Duan, D. O'Hare, Synthesis and antimicrobial activity of ZnTi-layered double hydroxide nanosheets, J Mater. Chem. B 1 (2013) 5988-5994. https://doi.org/10.1039/c3tb21059f.